Calix[4]arenes as Molecular Platforms in Magnetic Resonance Imaging

Daniel Schühle

Calix[4]arenes as Molecular Platforms in Magnetic Resonance Imaging

Proefschrift

ter verkrijging van de graad van doctor
aan de Technische Universiteit Delft,
op gezag van de Rector Magnificus prof. dr. ir. J. T. Fokkema,
voorzitter van het College voor Promoties,
in het openbaar te verdedigen

op vrijdag 9 oktober 2009 om 10.00 uur

door

Daniel Schühle

Diplomchemiker, Universität Ulm
geboren te Biberach an der Riß (Duitsland)

Dit proefschrift is goedgekeurd door de promotoren:

Prof. dr. R. A. Sheldon

Prof. Dr. J. Schatz

Copromotor: Dr. ir. J. A. Peters

Samenstelling promotiecommissie:

Rector Magnificus	voorzitter
Prof. dr. R. A. Sheldon	Technische Universiteit Delft, promotor
Prof. Dr. J. Schatz	Universiteit van Erlangen-Nürnberg, Duitsland, promotor
Dr. ir. J. A. Peters	Technische Universiteit Delft, copromotor
Prof. Dr. I. Lukeš	Charles Universiteit Praag, Tsjechië
Prof. dr. J. H. van Esch	Technische Universiteit Delft
Dr. U. Hanefeld	Technische Universiteit Delft
Dr. K. Djanashvili	Technische Universiteit Delft
Prof. dr. ir. H. van Bekkum	Technische Universiteit Delft, reserve lid

The research described in this thesis was supported by the EU COST Action D38 ("Metal-Based Systems for Molecular Imaging Applications"), by the Marie Curie Mobility Program of the EU (MEST-CT-2004-007442), the EU Network of Excellence 'European Molecular Imaging Laboratory' (EMIL, LSHC-2004-503569) and the "Daden voor Delft" program of the Delft University Fund and the Alumni Association.

ISBN: 978-90-9024668-0

Copyright © 2009 by Daniel Schühle

All rights reserved. No part of the material protected by this copyright notice may be reproduced or utilized in any form or by any other means, electronic or mechanical, including photocopying, recording or by any information storage and retrieval system, without written permission from the author.

Printed in the Netherlands

To my parents

Meinen Eltern

If we knew what it was we were doing, it would not be called research, would it?

Albert Einstein (1879-1955)

CONTENTS

CHAPTER 1

BIOLOGICAL APPLICATIONS OF METAL BINDING CALIXARENES **1**

INTRODUCTION 2

ARTIFICIAL ION CHANNELS 4
Na^+ Channels 4
K^+ Channels 7

METALLOENZYME MIMICS 8
Calix[4]arenes 9
Calix[6]arenes 18

METALLOENZYME INHIBITORS 25

AGENTS FOR RADIOTHERAPY AND MEDICAL IMAGING 26

OTHER APPLICATIONS 31

CONCLUSIONS/OUTLOOK 32

OUTLINE OF THE THESIS 32

REFERENCES 34

CHAPTER 2

KINETIC ACIDITY OF SUPRAMOLECULAR IMIDAZOLIUM SALTS — EFFECTS OF SUBSTITUENTS, PRE-ORIENTATION AND COUNTER IONS ONTO H/D EXCHANGE RATES **39**

INTRODUCTION 40

RESULTS AND DISCUSSION 41

CONCLUSIONS 45

EXPERIMENTAL 45

APPENDIX 49

ADDITIONAL COMMENTS 51

REFERENCES 52

CHAPTER 3

INFORMATION TRANSFER IN CALIX[4]ARENES: INFLUENCE OF *UPPER RIM* SUBSTITUTION ON ALKALINE METAL COMPLEXATION AT THE *LOWER RIM* **55**

INTRODUCTION 56

RESULTS AND DISCUSSION 58
Synthesis 58
Extraction Studies 59

CONCLUSIONS 62

EXPERIMENTAL 62

REFERENCES 68

CHAPTER 4

CALIX[4]ARENES AS MOLECULAR PLATFORMS FOR MRI CONTRAST AGENTS 71

INTRODUCTION 72

RESULTS AND DISCUSSION 73
Synthesis 73
Aggregation 74
Variable temperature ^{17}O NMR measurements 76
Nuclear Magnetic Relaxation Dispersion (^{1}H NMRD) 78
Interaction with HSA 81

CONCLUSIONS 83

EXPERIMENTAL 83
Sample preparation 83
Methods 83
Synthesis 84

REFERENCES 86

CHAPTER 5

DENSELY PACKED GD(III)-CHELATES WITH FAST WATER EXCHANGE ON A CALIX[4]ARENE SCAFFOLD: A POTENTIAL MRI CONTRAST AGENT 89

INTRODUCTION 90

RESULTS AND DISCUSSION 91
Synthesis 91
Aggregation 93
Water exchange 94
Relaxivity 96
Interaction with Bovine Serum Albumin 99

CONCLUSIONS 101

EXPERIMENTAL 102
Sample preparation 102
Methods 102
Synthesis 103

REFERENCES 105

CHAPTER 6

CALIX[4]ARENE BASED PARAMAGNETIC LIPOSOMES AS MRI CONTRAST AGENTS **107**

INTRODUCTION 108

RESULTS AND DISCUSSION 110
Synthesis 110
Self-Aggregation 112
Liposome formulations 115
NMR characterization of the calixarene based liposomes 119

CONCLUSIONS 121

EXPERIMENTAL 122
Methods 122
Preparation of liposomes 123
Synthesis 124

REFERENCES 129

SUMMARY 131

SAMENVATTING 135

LIST OF PUBLICATIONS 139

ACKNOWLEDGEMENTS 145

CURRICULUM VITAE 147

Biological Applications of Metal Binding Calixarenes

1

Introduction

The later Nobel Prize laureate Adolph von Baeyer, after reporting the condensation of phenol and formaldehyde to yield a resinous tar, decided to change his field of research. He could not foresee that some decades later, a whole generation of chemists in the then emerging field of supramolecular chemistry would revive this 'simple' chemistry on a new class of compounds, the calixarenes.[1-4] The main achievements of these early scientists are the elucidation of the chemical structure of the cyclic condensation products of 4-*tert*-butylphenol and formaldehyde and even more importantly the fine-tuning of the reaction conditions. Today, calix[4,6 or 8]arenes can be synthesized in high yield and with excellent purity.[5-7]

One of the early pioneers, David Gutsche, became interested in calixarenes because he wanted to mimic an aldolase with a completely artificial molecule and was looking for rigid molecular platforms.[1] After calixarenes were discovered and reproducible procedures to synthesize them were established, he developed methods to functionalize them and baptized these molecules with the name they have today (*calix crater* is the Latin word for certain ancient Greek vases, see Figure 1.1). His work also stimulated other research groups to spend some efforts in this new field of chemistry. Unfortunately, after almost 30 years of pioneering research in calixarene chemistry, the potential enzyme mimic that was synthesized by Gutsche and co-workers turned out not to be what the quest was about: an aldolase model system.

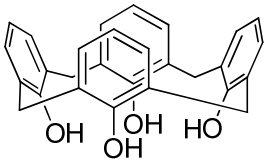

Figure 1.1. A calix crater and the three-dimensional structure of a calix[4]arene.

But happily, some twenty years after this early work, there are not only enzyme mimics based on the calixarene core, but also many more applications for this class of compounds in chemistry, physics, biology, medicine and in many interdisciplinary fields.[8-10]

Calix[*n*]arenes enable the synthetic introduction of at least *n* identical binding sites in the same molecule and offer an additional binding site *per se*, namely their hydrophobic cavity. Therefore, multivalent targeting is possible by attaching various (identical or different) binding motifs to the same calixarene scaffold.[11] Other small scaffolds such as benzene derivatives, cyclodextrins, monosaccharides, metal complexes or azamacrocycles quite often have the drawback that their selective functionalization is difficult and that they do not enable the arrangement of receptors on the same scaffold in various conformations (Figure 1.2). Furthermore, the larger calix[6 or 8]arenes are more mobile and can adjust their conformation to a geometry that is required for an efficient binding of the target/substrate (induced fit).

At the same time, especially the smaller calix[4]arenes are rather rigid molecules. This allows preorientation of functional groups in a three-dimensional space. These properties are almost unique in organic chemistry and predestine calixarenes for use as artificial receptors, substrates or enzyme mimics. In this chapter, recent developments (since about 1999) in the biological and medical chemistry of metal binding calixarenes are highlighted.

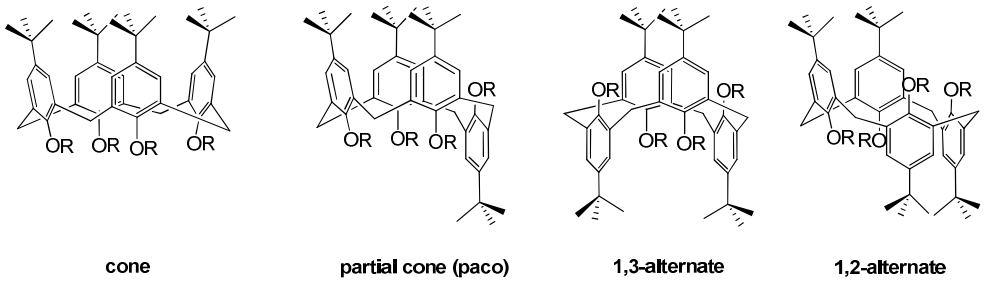

Figure 1.2. The four possible conformations of calix[4]arenes.

Artificial Ion Channels

The intra- and extracellular concentrations of physiologically relevant metal ions differ very often. One way how nature controls those concentration gradients is by the so-called channel mechanism.[8] Ion channels exist in every mammalian cell and allow the passage of typically 10^8 or more ions per second. In general, these channels provide a hydrophilic path inside the hydrophobic cell membrane. Malfunctioning of these systems can lead to severe diseases. Therefore there is a general interest to better understand transport processes of metal cations across phospholipid bilayers. A major challenge in the design of model systems is to develop compounds that do not only allow charged metal ions to pass a hydrophobic bilayer but that also show selectivity for a particular cation.[12] Especially the alkaline metal cations Na^+ and K^+ are of great interest for studies on such model systems since the ratio of their concentrations in- and outside cells is important for the proper functioning of signal transduction in nerves.

Calixarenes and their derivatives are very suitable models for ion channels.[12,13] In addition to their relatively simple synthetic accessibility, they are able to span phospholipid bilayers and can bind metal ions selectively. Furthermore, there are strong indications that, as a result of the size and the hydrophobicity of the calix[4]arene backbone, the potassium aquo ion is partly dehydrated prior to its transport through the cavity towards metal binding functions on the *lower rim*. This dehydration capability occurs in natural ion channels as well and is of utmost importance for a successful mimic.[12]

Na^+ Channels

In a systematic study on the selectivity of the transport of alkaline metal ions through a phospholipid bilayer model by calixarenes **1** of various sizes (from calix[4 to 8]arenes, Figure 1.3), Jin et al. demonstrated that the tetramer transports Na^+ ions twenty times better than all other metal ions tested.[14] Probably, this calixarene forms a dimer within the bilayer thus allowing efficient Na^+ transport. The calix[5]arene has some selectivity for K^+ ions, whereas calix[6 and 7]arenes transport Cs^+ ions with some selectivity. However, the octamer does not facilitate the transmembranal ion transport. The selectivies for certain

alkaline metal ions can be rationalized by the different distances spanned by the chelating ester and phenol ether groups: the small calix[4]arene shows a preference for complexation of the small Na^+ ion, whereas the larger calixarenes complex the larger alkaline metal ions better.

In studies of the parameters determining the metal ion flux through artificial cell membranes, it may be useful to have a possibility to block this transport. Therefore, the photo-switchable artificial Na^+ channel was formed by **2**.[15] This compound has a similar Na^+-selectivity to **1**. Upon irradiation with UV-light (> 310 nm) the anthroyl units dimerize and then block the way for diffusing metal ions. Upon switching off the UV-light, the dimer slowly falls apart and ion transport becomes possible again.

The ionophores **3a-e** bearing cholic acid moieties (Figure 1.4) were prepared and their ability to transport protons and Na^+ ions through liposomes was investigated.[16] The compounds in *1,3-alternate* conformation (**3a-c**) are much more effective in ion transport than the *cone*-conformers. This indicates that **3d** and **3e** form dimers in the membrane whereas the *1,3-alternate* ionophores can span the bilayer providing a much better channel. Acylation of the steroid moieties has only a minor influence on the transport efficiency.

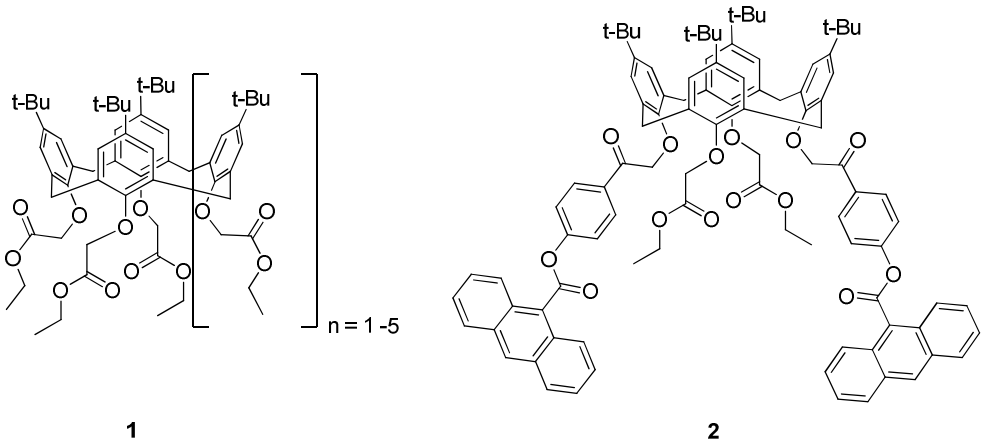

1 **2**

Figure 1.3. Na^+ selective calixarenes.

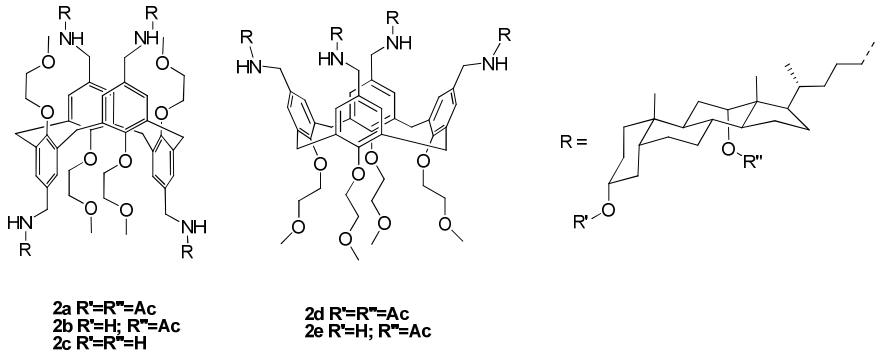

Figure 1.4. Cholic acid containing ionophores **3a-e**.

Triton (Figure 1.5) is a well-known non-ionic surfactant that is widely used to destroy liposomes and cell membranes. Its ability to penetrate such bilayers was the inspiration to synthesise **4**.[17] Unfortunately, **4** did not show any activity, whereas its calix[6]arene analogue bearing methylated phenolic groups is a good Na^+ channel mimic. Selectivities over other alkaline metal ions have not yet been reported.

Compounds of type **5** showed poor or no activity, which was ascribed to their inability to completely span the phospholipid bilayer.[18] Another reason could be that the long alkyl-spacers do not provide a hydrophobic channel within the lipid bilayer.

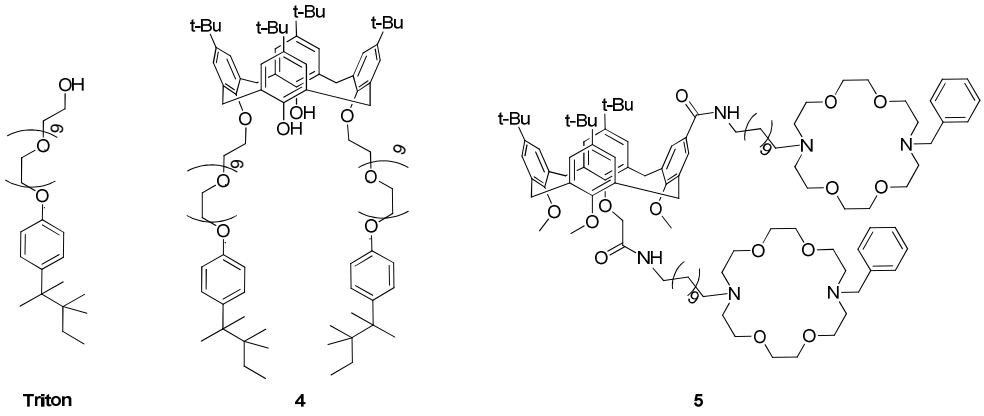

Figure 1.5. Calix[4]arene based ionophores.

K^+ Channels

The control of the Na^+/K^+ ratio inside artificial cells, requires not only Na^+ but also K^+ channels. Only a few reports on selective K^+ ionophores have been published and only little is reported about the K^+ transport ability through phospholipids bilayers. A promising approach to mimic K^+ transport was reported by Arduini et al., who showed that the tubular **6** (Figure 1.6) forms channels with about the length that is required to span such a bilayer.[19]

A four-fold symmetric arrangement of thr-val-gly-tyr-gly polypeptides forms the selectivity filter of the K^+ channel in *Streptomyces lividans*. Compounds **7** are mimics of this system and were used to learn more about the mechanism of cation transport and about the origin of the selectivity of this system.[20] Initially, the K^+ ion is bound by the phenolic and the valine carbonyl oxygens of all compounds studied. Hydrogen bonding was found to be crucial in this system: for the tripeptide, the N_{val}-H···O=C_{val} bonds are much stronger than for the shorter peptides. This effect stabilizes this species and as a result the metal binding is relatively weak. This might facilitate the release of the ion and therefore, the ion translocation.

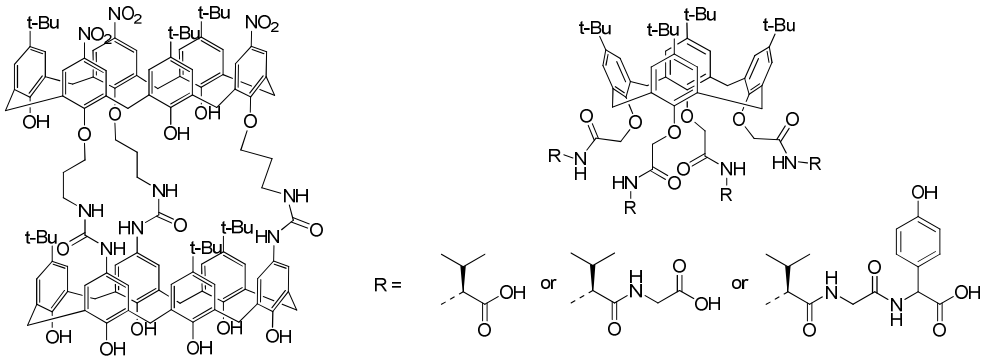

Figure 1.6. Synthetic K^+ channels.

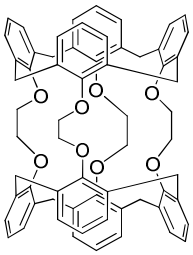

8

Figure 1.7. A K^+ selective calix[4]arene dimer.

A further possibility to span the bilayer by calix[4]arene dimers is with compounds similar to **8** (Figure 1.8) reported by Beer and co-workers.[21] The elongation of the bridges between the calixarene units of **8**, by insertion of more ethylene glycol moieties, may be expected to provide a channel for K^+ cation transportation that spans the bilayer.

Metalloenzyme Mimics

Enzymes are amongst the most selective catalysts available. Their active sites provide a variety of non-covalent interactions with substrates that control the recognition process and therefore, the selectivity of the enzyme. These include hydrogen bonding, charge/charge, CH/π and cation/π interactions. In order to learn from nature and to obtain an insight into how enzymes work, simpler low molecular weight model systems are used. Many enzymes contain metal ions that play a key role in the structural organization of the peptide, in the recognition processes of substrates or even as the catalytic centers in the active site. In the latter case, the enzyme does not only act as a very large ligand with preorganised metal binding sites, but it also provides a cavity and a corridor that control the access of the substrate and, therefore, the selectivity and the reactivity of the metal ion site.[1] Enzymes are complex systems that are not easy to study. Therefore, there is a need for good mimics of which the characterization is simpler. It is not surprising that calixarenes can be used as building blocks for such metalloenzyme mimics. They are not only easy to functionalize

but they also offer the possibility to prearrange chelating groups or bound metal ions in a three-dimensional space. Furthermore, they can adopt different conformations (induced fit or dynamic preorganisation) and can coordinate other molecules to mimic hydrophobic pockets of enzymes.[3]

Calix[4]arenes

Zn^{2+}-Based phosphodiesterase and lipase mimics

Many metal containing phosphodiesterases use one, two or three divalent metal centers such as Zn^{2+} for the activation of the substrate.[22,23] The prearrangement of the metal centers using synthetic spacers is crucial in mimics of such enzymes since the tetrahedrally coordinated Zn^{2+} centers are assumed to activate the phosphate group and a nucleophilic water molecule, to stabilize the pentacoordinate phosphorus transition state and possibly the leaving group by cooperative action.[24] In studies of phosphatase activity, 2-hydroxypropyl-*p*-nitrophenyl phosphate (HPNP, Figure 1.8) is used as RNA model substrate, the intramolecular cyclisation reaction and the release of *p*-nitrophenolate being the driving forces of the reaction. Reinhoudt and co-workers investigated the performance of calix[4]arenes **10** - **13** as enzyme mimics. Although Zn^{2+} is chelated by non-natural chelating units and the catalysis was performed in a MeCN/aqueous buffer mixture, the results gave information about the mode of action of the enzymes (Figure 1.8). The chelating units were chosen because they are easily accessible and are able to complex a variety of divalent transition metal ions.[23]

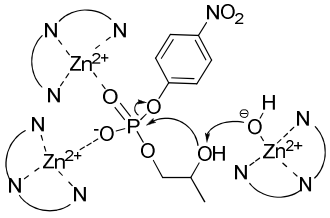

Figure 1.8. Possible mechanism for HPNP cleavage by trinuclear phosphatase models.

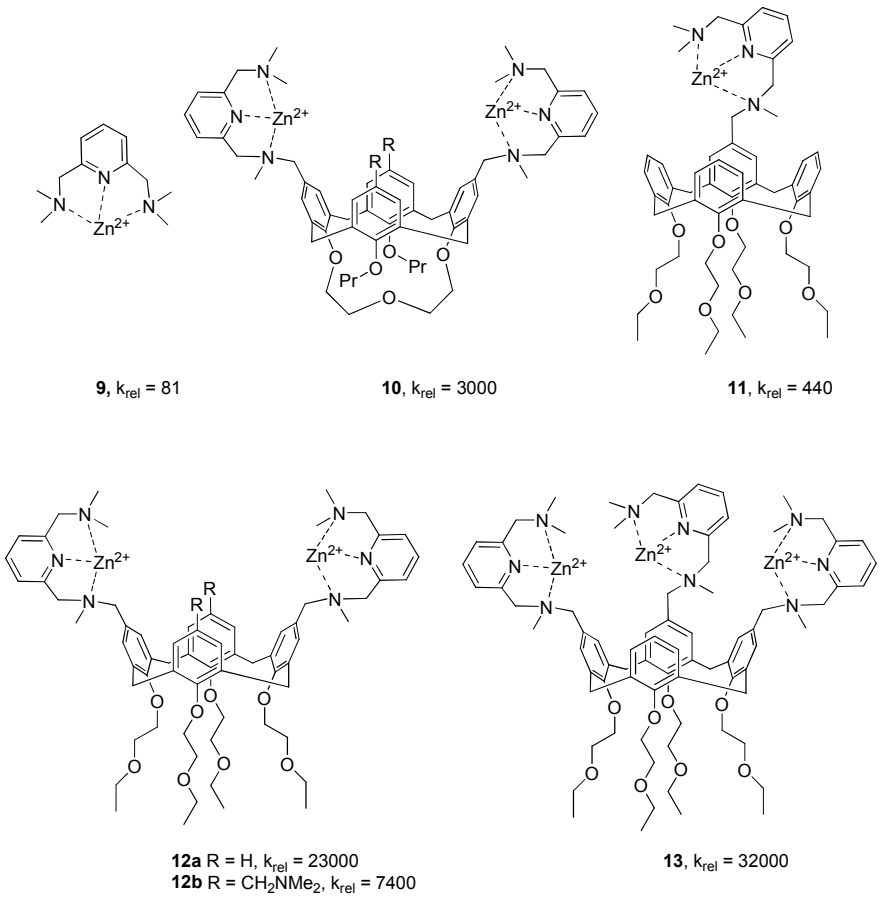

Figure 1.9. Mono-, di- and trinuclear Zn(II) phosphatase mimics and relative rate acceleration factors k_{rel}.

The relative rate acceleration factors k_{rel}, which are defined as the ratio of the observed rate constant of the reaction in the presence of the catalyst and the rate constant of the uncatalysed reaction, can be used to directly compare the activity of catalysts. The nonmacrocyclic **9,** for example, has a much lower catalytic activity than the mononuclear calixarene based **11**. This is a direct proof that the calixarene backbone itself is involved in the catalysis, probably by binding the substrate inside the hydrophobic pocket.[24] The dinuclear complex **12a** shows a rate acceleration of 23000 in the transesterification of HPNP over the uncatalyzed reaction, whereas the mononuclear **11** analogue is 50 times less active. This suggests that the metal centers have cooperative action and that the hydro-

phobic cavity is involved in the binding of the substrate. On the basis of extensive kinetic studies, the high catalytic activity of **12a** was ascribed to the high affinity of the substrate to the binding site. It should be noted that the rate of conversion was moderate, the high catalytic activity being a consequence of the high stability of the intermediate Michaelis-Menten like substrate/receptor complex. The mechanism is analogous to that depicted in Figure 1.8, but now the phosphate function is bound by a single metal ion. A more rigid calixcrown model compound **10** exhibits a smaller substrate affinity and a lower catalytic activity, which demonstrates the need for some flexibility within the calixarene to enable cooperative effects between the metal centers (induced fit). The trinuclear complex **13** induces a rate acceleration of 32000, which is rationalized by the activation of the nucleophile (water) by the third metal center. The vicinal analogue of **12a**, **14**, shows less activity probably due to weaker binding of the substrate.[25] In a later study, it was found that the trinuclear complex based on **13** containing two Zn^{2+} and one Cu^{2+} ion accelerates the reaction even more and shows high selectivities for certain RNA nucleotides.[26] Probably, this is caused by the synergy of the metal ions: Zn^{2+} leads to good substrate binding, Cu^{2+} to high conversion.

The comparison with the natural system, where basic histidine units often support the catalysis by providing hydroxide ions, led to the development of **12b**.[22] Rather than activation of water by a third metal ion in the form of a hydroxo complex, hydroxide was generated by one of the tertiary amine groups in proximity of the bound substrate. The decrease in catalytic activity with respect to **12a** is caused by the weaker binding of HPNP due to the partially blocked access to the hydrophobic cavity as well as a slower conversion. This can be ascribed to a less favorable binding geometry of the substrate. Both facts can be explained by the steric demands of the dimethylamino groups that hamper the binding of the substrate and therefore, the simultaneous binding of HPNP to both Zn-centers.

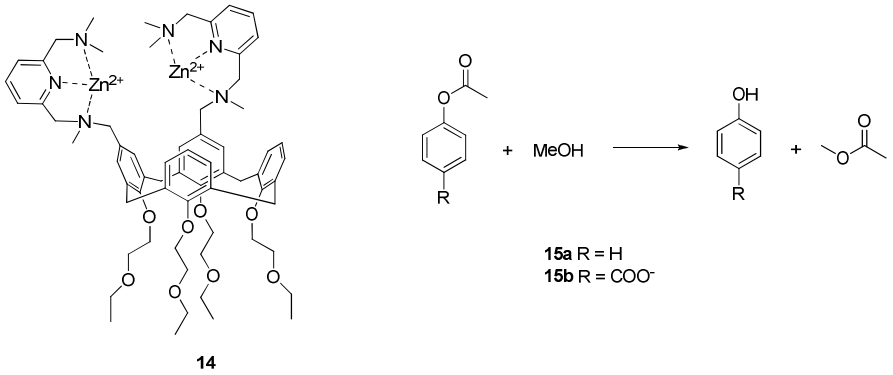

Figure 1.10. Vicinal Zn^{2+} complex **14** and solvolysis reaction tested.

The ability of complexes **9**, **12a**, **13** and **14** to cleave esters was investigated by solvolysis experiments in methanol (Figure 1.10).[25] Potentiometric titrations performed on the model compound **9** showed that the complex behaves as a weak acid with a pK_a of 9.5 which corresponds to the deprotonation of a metal bound solvent molecule. This means that for the di- and trimetallic Zn-complexes, one Zn-unit binds a solvent molecule as its methoxide whereas the second one is able to bind **15b** via its COO^--function. As a result, in dinuclear complexes, one metal ion preorganises the substrate for the nucleophilic attack of the activated solvent molecule that is provided by the other metal. At the same time, the binding of the carboxylate by the Zn^{2+} center activates the substrate for nucleophilic attack through the electron withdrawing effect of the charged metal ion. If **15a** is used as the substrate, the conversion is much slower since the lack of a carboxylate group leads to less efficient binding to the catalyst. Interestingly, and opposite to what was found in the studies with HPNP, the vicinal Zn_2-**14** is the much more active catalyst compared to its analogous geminal Zn_2-**12a** isomer. The relatively high catalytic activity of the vicinal isomer may be caused by either better substrate binding or different conformation or hydration of the catalyst in the different solvent systems (MeCN/buffer for transesterification of HPNP and methanol for methanolysis). The general superiority of vicinal compared to geminal isomers in the solvolysis of phenol esters was also found in a later study.[27] Similar pyridine based calixarenes have been proposed as metalloenzyme mimics but no experimental evidence has been given.[28]

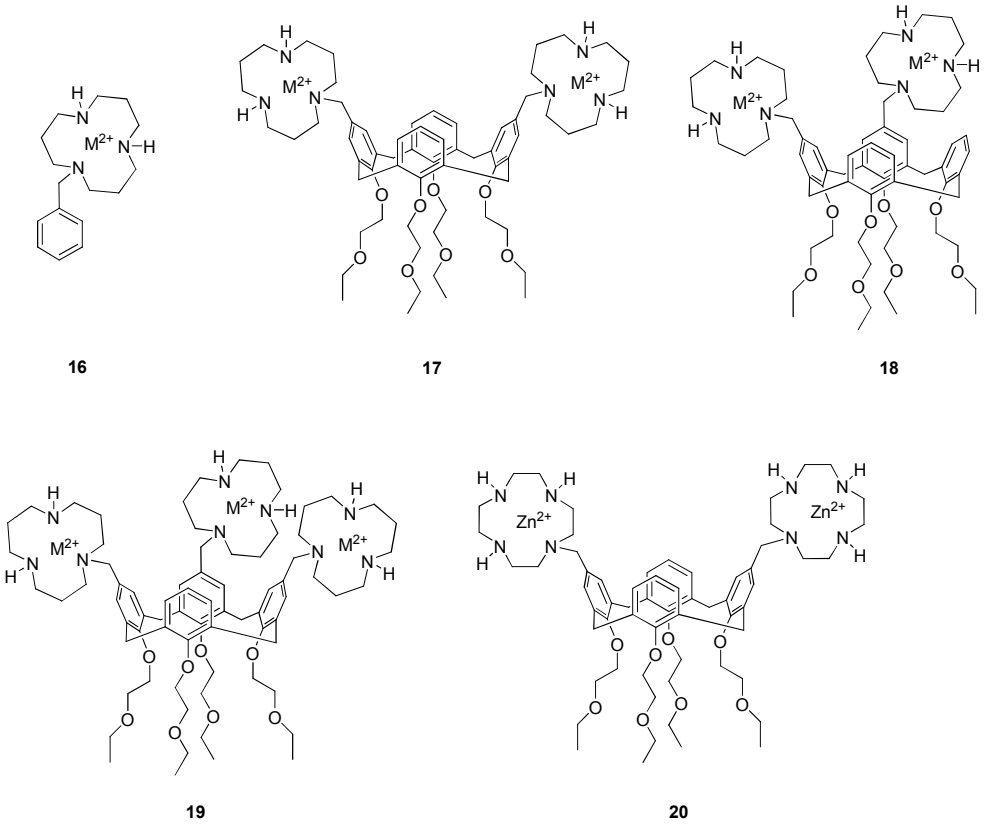

Figure 1.11. Azacrownether based metalloenzyme mimics.

Various azacrownethers attached to the *upper rim* of calix[4]arenes were used to chelate Zn^{2+}.[29] 1,5,9-Triazacyclododecane has three binding sites for metal coordination and, therefore, is favorable for tetrahedral coordination of Zn^{2+}. Since the mononuclear analogue was not soluble in the solvent applied (MeCN/aqueous buffer pH 7), compound **16** was chosen as a mononuclear reference. These compounds showed only low catalytic activities in the cleavage of HPNP. The fact that the activities of the bimetallic complexes **17** and **18** after correction for the different metal concentrations are not much superior to those of the monomeric **16** means that there is a lack of cooperation between the metal centers.[29] Nonetheless, the solvolysis of various phenol esters by methanol using these complexes was more successful.[30] As for the dimetallic complex **14**, one Zn^{2+} binds a methoxide,

which can act as a nucleophile in the solvolysis reaction of the coordinated substrate. Phenol esters containing carboxylate functions were again found to be good substrates since they provide a binding site for the second metal center and are activated upon binding to the metal (see above).

The strong chelator 1,4,7,10-tetraazacyclododecane (cyclen) complexes Zn^{2+} resulting in a rigid and bulky substituent attached to the calixarene core.[31] The steric demands of the two chelates in **20** hamper the binding of the substrate and reduce the catalytic activity very efficiently. By contrast to the systems described above, the mononuclear analogue of **20** shows superior catalytic activity over the dinuclear **20** due to the reduced steric hindrance.

Cu^{2+}-Based phosphatase mimics

The replacement of Zn^{2+} by Cu^{2+} in ligands **17**, **18** and **19** (Figure 1.11) leads to complexes that are sufficiently soluble in water to study transesterification without the need of applying organic co-solvents.[29] Although these complexes are less active than their Zn-analogues, they have the advantage over other Cu^{2+}-based enzyme mimics that there is no dimerisation of the copper centers leading to catalytically inactive species.[29] Model reactions with HPNP revealed that there is no cooperative action of the distally arranged Cu-atoms in **17** but a strong synergistic effect in the vicinal isomer **18**. The trimetallic **19** shows slightly less catalytic activity than **18**, which indicates that two vicinal copper centers perform the catalysis, whereas the binding of the substrate is slightly hampered by the third chelate. Especially the trimetallic Cu_3-**19** catalyst shows remarkable selectivities for certain diribonucleoside-2',3'-monophosphates, which represent better models for RNA than HPNP and which enable to detect specific cleavage, if any. These compounds appeared to be also very selective in the phosphodiester cleavage of single-stranded RNA oligonucleotides.[32] The catalyst is highly efficient under close to physiological conditions and resembles the natural RNAses A in their selectivity.

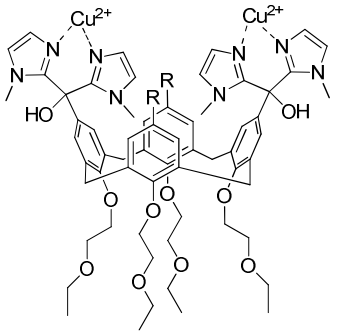

21a R = H
21b R = CH_2OH
21c R = CH_2NH_2

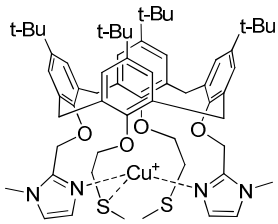

22

Figure 1.12. Bisimidazolyl-Cu-calixarenes.

Attempts to mimic metal enzymes more closely using methyl-imidazole as histidine analogue showed successfully that a cooperative effect of functional groups attached adjacent to the metal centers can play an important role in catalysis.[33] The general mechanism is similar to that shown in Figure 1.8, the difference being that the hydroxide is not provided by a third metal center but by the coordination sphere of a Cu^{2+}-center. When the amino function in **21c** is protonated, it can assist in the binding and stabilization of the transition state. The corresponding Zn^{2+}-**21c** shows poor catalytic activity.

Mimic for Cu^+ containing enzymes

In the reduced type 1 site (T1PR) in human ceruloplasmin, a permanently reduced Cu^+ is bound close to the active site although it probably does not participate in any catalysis. To elucidate the role of the metal center, the binding environment of the metal was mimicked by attaching two histidine analogues and two cysteine models to the *lower rim* of calixarene **22**. The metal is complexed by two imidazoles and one sulfur atom leaving one coordination site for a potential substrate. Unfortunately, apart from some structural details, no further information on the performance of this compound as enzyme mimic was provided.[34] Nevertheless, the fact that the metal is oxygen stable is very promising for future investigations.

Ba^{2+} complexes as acylase mimics

Many enzyme catalysed transacylation reactions proceed via a double-displacement mechanism. This means that first an acylated enzyme intermediate is generated, which acts as acylation agent for the nucleophilic substrate.[35] This principle is known to organic chemists for example from the pyridine catalysed esterification of activated carboxylic acids. In such reactions, first the pyridine reacts with the acylation agent creating a highly active species that subsequently transfers the acyl group to an attacking nucleophile. In mimics, the challenge is to achieve an efficient transfer of the activated acyl to the nucleophile. Efficient acyl transfer can be reached by using phenolic alcoholates due to their better leaving group character in comparison to alkoxides. In calixarene **23**, the phenolic groups can thus act as acyl-acceptors/acyl-donors, whereas the complexed Ba^{2+} acts as activating Lewis acid. The protonated ammonium function acts as intramolecular proton donor that protonates the leaving group (phenolate) that is released in the first acylation reaction. In comparison to derivatives that do not contain the amino functionalities, **23** does not show better catalytic activity, which was ascribed to the steric demands of the diethylamino groups.

In a later study, two Ba^{2+}-ions were complexed by crown ether moieties on the *upper rim* of calixarenes **24** and **25** (Figure 1.12).[36] In ethanolysis studies of different phenol esters, it was found that the distance between the metal ions determines the substrate specificity of the catalyst. A similar reaction mechanism as depicted in Figure 1.8 might also be operative in these reactions.

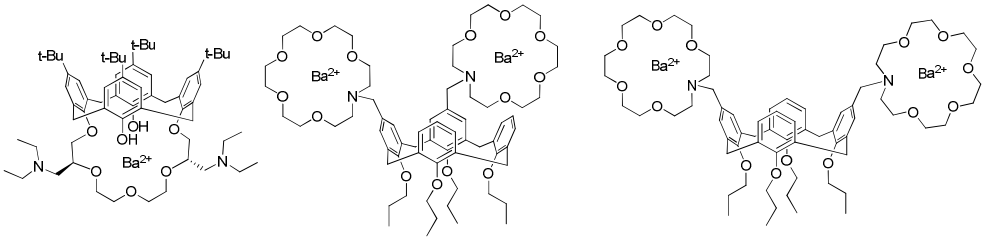

23 **24** **25**

Figure 1.12. Ba^{2+} containing artificial acyl-transferase **23** and acylases **24** and **25**.

Self-assembling supramolecular enzyme mimics

Many natural enzymatic systems consist of several self-aggregated subunits. Therefore, there is a general interest in combining several building blocks to artificial assemblies that have properties that neither of the single components has. This approach is rarely undertaken but there are some examples demonstrating that calixarenes can be very usefull in the design of such aggregates. A supramolecular heme mimic could be obtained by the formation of a complex between *p*-sulfonato calixarene **26a** and porphyrins (Scheme 1.1).[37] The strong charge/charge interactions lead to association constants of 10^5 M^{-1} in water, sufficient water solubility being provided by the amide side chains. The formation of ternary complexes with nitrogen containing compounds depends on the size of the base. Whereas small bases like 4-methylpyridine are bound inside the cavity spanned between the calixarene and the porphyrin, larger molecules like caffeine are bound on the surface of the assembly. The self-assembled Co^{2+} complex shows a modest but significant facilitated O_2-transport through membranes due to the reversible binding of oxygen to the complex.

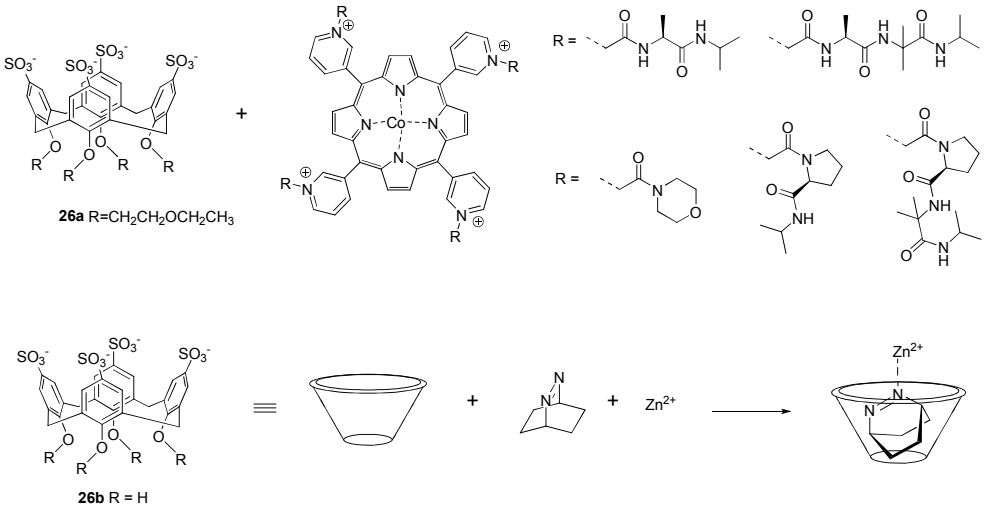

Scheme 1.1. Self-assembling metallo-enzyme mimics.

An interesting approach towards self-assembled enzyme mimics was described by Nau and coworkers.[38] The dynamic self-assembly of *p*-sulfonato calix[4]arene **26b** with an organic guest and a divalent metal ion shows cooperativity in the binding (host-assisted metal-ligand bond formation). This means that the apolar guest provides an additional binding site for the metal, which stabilizes its interaction with the ligand. This proof of concept might lead to the development of a new generation of metal enzyme mimics.

Calix[6]arenes

Enzyme mimics based on the calix[4]arene core are, as shown above, very well suitable to study the effects of multinuclearity, the distance between the metal ions, and the flexibility of the linker on the catalytic activity and the selectivity. For monometallic enzymes, calix[6]arenes are better platforms since they do not only allow the binding of the metal in a polydentate way, but they also provide a hydrophobic channel that is similar to the hydrophobic pocket in enzyme active sites.[1] Calix[6]arenes are in general less rigid than calix[4]arenes and it is much more difficult to freeze them in a particular conformation. On the other hand, they provide six phenolic oxygen atoms that can be functionalized in a defined way and a hydrophobic cavity that is larger than that in calix[4]arenes, which thus enables the complexation of larger guests. Calix[6]arenes can be methylated at three distal positions leaving the three remaining positions for the attachment of chelating groups. Therefore, metal ions with coordination number four are ideal candidates to be complexed since they can be bound very efficiently and still exhibit one free binding site for e.g. substrate binding. No catalytically active calix[6]arene system has been reported yet.

There are three generations of calix[6]arene based enzyme mimics which are called funnel complexes or calix-zymes, too.[1] A way to fix the calix[6]arene platform in the *cone* conformation that is best suited for metal and guest complexation is by the complexation itself. These so-called first generation ligands (Figure 1.14) were designed for this purpose and allowed detailed investigations of coordination chemistry, substrate binding and redox activity of the metal.[1,39] The second generation provides an additional binding site for metal complexation at the *lower rim*. These ligands are able to complex divalent metal ions

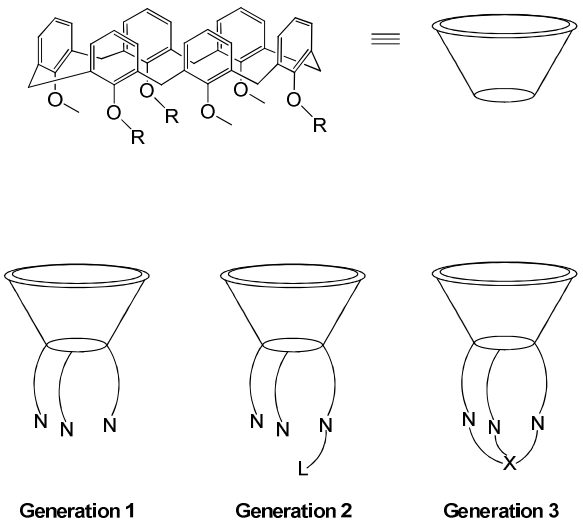

Figure 1.14. The three generations of calix[6]arene funnel complexes.

more efficiently than the first generation, blocking possible dimerisation and substrate binding outside the cavity. Furthermore, they provide the possibility to attach redox active ligands that are important in controlling the redox behaviour of the complexed metal.

The most prominent limitations of the two first generation complexes are the relatively weak binding of the metal ions due to the flexible calixarene core and the long distances between the donor atoms.[1] Furthermore, oligonuclear species can be formed in the presence of, for example, bridging anions. In the third generation ligands, the calix[6]azacryptands, the donor sites are connected to each other by a fourth coordinating atom, which at the same time rigidifies the calixarene core in the *cone* conformation.

Cu^{+}/Cu^{2+}-Metalloprotein mimics

The pyridine based ligands **27** show poor binding of Zn^{2+} but are very good ligands for Cu^{+}.[1] The steric protection of the metal centers and the coordination of a nitrile guest stabilizes Cu^{+} in this low oxidation state thus avoiding the oxidation to Cu^{2+} by molecular oxygen and the dimerization of the metal ions.[40] The Cu^{+} ion is tetrahedrally coordinated by the three pyridine units and e.g. a solvent molecule inside the cavity in a bicapped

trigonal pyramidal coordination geometry.[41] The redox potential from Cu^{+} to Cu^{2+} as well as the substrate binding is controlled by the ligand as in the natural enzyme.[41,42] Due to the transmission of the chiral coordination geometry to the calixarene backbone, Cu^{+}-**27** exists as two different helical enantiomers at lower temperatures.[43] Effects of *upper rim* substitution on the binding and exchange of guest molecules (MeCN, PhCN) were investigated using **27a** and **27b**.[44] The steric demands of the six *tert*-butyl groups in **27a** lead to a preference for binding the smaller MeCN over PhCN. The opposite holds for **27b** since the cavity becomes larger upon removal of three *tert*-butyl groups. The rate of MeCN exchange is greatly enhanced for **27b** since there is no 'closing of the door' by the bulky substituents.

The polyimidazole binding sites of peptides can be mimicked by compounds **28**. The coordination geometry of their Cu^{2+} complexes is similar to that in **27**.[45] The water molecule located inside the cavity can selectively be exchanged by guest molecules like nitriles. In the absence of coordinated solvent molecules or a guest, di-, tri- and tetranuclear clusters are formed.[46-48] Cu^{+}-**28a** is able to bind CO inside its cavity, the C≡O stretch vibration being a very sensitive tool to determine changes in the supramolecular environment like in copper proteins.[49] The properties of complexes of **28a** with Co^{2+} and Ni^{2+} are in line with these findings.[50] The water soluble Cu^{+}-**28b** is not only a stable Cu^{+}

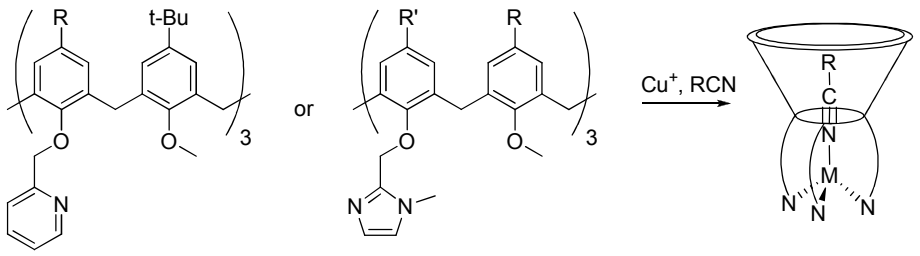

27a R = ^{t}Bu
27b R = H

28a R = R' = ^{t}Bu
28b R = Br, R' = SO_3^-

Figure 1.15. Pyridine and imidazole based Cu^{+} funnel complexes of the first generation.

complex in water that does not undergo oxidation or dimerization, it is also a rare example of three-coordinate Cu^{+}-species.[51]

The second generation ligand **29** has an additional phenolic oxygen atom for metal binding.[52] This model for a tyrosine binding site can be oxidized into the phenoxyl radical and therefore play an important role in mimicking enzyme catalysis. Indeed, Cu^{+}-**29** undergoes fully reversible oxidation at low temperatures and is able to oxidize benzyl alcohol to benzaldehyde. The corresponding Zn^{2+}-bound tyrosinyl radical mimic is stable for hours and does not undergo reaction with benzyl alcohol.

The successful application of the generation three Cu^{2+}-**30** complex to enzyme mimicry by Izzet, Reinaud and co-workers is a clear highlight in this field of research.[53] This compound exhibits a remarkable stability and a very high affinity towards small neutral guests such as water, EtOH, DMF, and MeCN. The cuprous center undergoes defined and reversible redox chemistry. Thanks to the different affinities of Cu^{2+}/Cu^{+} to different guests, an electrochemically controlled ligand exchange could be performed: Cu^{2+}-bound DMF is expelled from the metal upon its oxidation and replaced by MeCN, which remains metal bound even after reduction. This may be considered as 'antithermodynamical' electro-driven ligand exhange.

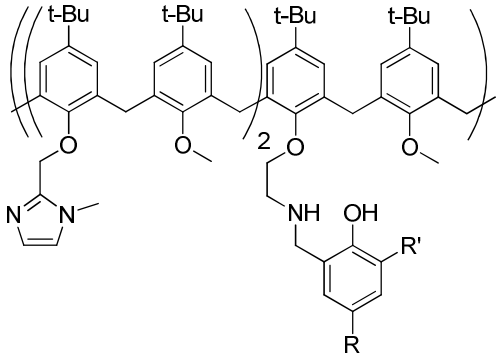

29a R = NO_2, R' = H
29b R = R' = ^{t}Bu

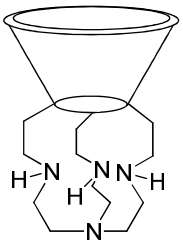

30

Figure 1.16. Second and third generation ligands.

Cu^{+}-**30** is able to activate molecular oxygen forming a Cu^{2+}-superoxide complex in a fast and irreversible way.[54] In a coordinating solvent like MeCN, the superoxide is released into the solution and substituted by a solvent molecule, whereas in the non-coordinating methylene chloride, the superoxide leads to oxygen insertion into the triethylene triamine (tren) ligand. Density functional theory (DFT) calculations using the B3LYP basis set performed on such systems were used to attribute the experimental IR data to the corresponding oxygen species bound to the metal ion and to gain insight into mechanistic details of the superoxide decomposition.[55,56]

The coordination of anionic guests was not possible with the third generation tren complex **30**. The pyridine analogue Cu^{+}-**31** is able to bind anions such as fluoride, azide, chloride, hydroxide, or alkoxide very efficiently.[57] This can be attributed to steric differences between the complexes. Whereas in **30**, the phenolic oxygen atoms point towards the free coordination site of the metal and hamper the binding of anions by charge-dipole interactions, this is not the case in **31,** which consequently offers better access of the guest to the binding site.

The replacement of the bridging N-atom in **31** by a phosphorous donor results in a very special complex **32** with a P-atom in axial trans-position to the binding guest.[58,59] This leads to a higher selectivity for binding of the π-accepting DMF over MeCN or EtOH as compared to **31**.

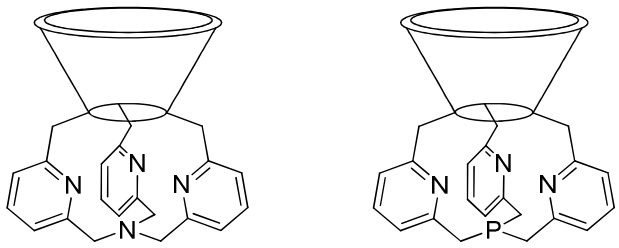

31 **32**

Figure 1.17. Pyridine based third generation ligands.

Mononuclear Zn^{2+}-metalloprotein mimics

Pyrazole, benzimidazole, or methylimidazole attached to the calix[6]arene platform can form very stable, mononuclear complexes with tetrahedrally coordinated Zn^{2+}.[60,61] However, attached tertiary amines are too basic and lead to hydroxide precipitation, whereas pyridine forms very weak complexes.[61] The Zn^{2+} complex of **28a** exists as its aquo ion with the water molecule complexed inside the cavity.[62] A second water molecule is held inside the cavity by hydrogen bonds with the metal bonded water molecule and a phenolic oxygen of the calixarene core and by OH/π stabilization. The two water molecules can be simultaneously replaced by amines, alcohols, nitriles or amides.[60,63,64] The sharp lines in ^1H NMR spectra for the encapsulated guest indicate that the exchange between free and encapsulated guest is slow on the NMR time scale.

The replacement of three *tert*-butyl groups on the *upper rim* by primary amine functions to give the water soluble **33** opens the possibility for further coordination of a) a second Zn^{2+}-atom or b) the encapsulated host leading to better specificity.[64-66]

When **33** is complexed with two Zn^{2+} atoms, a binuclear complex is formed that entraps an $(H_3O_2)^-$ ion as a kind of a bridging motif. The mononuclear Zn^{2+}-**33**, where the imidazole units inside the cavity bind the metal, is able to bind larger guests than its hexa-

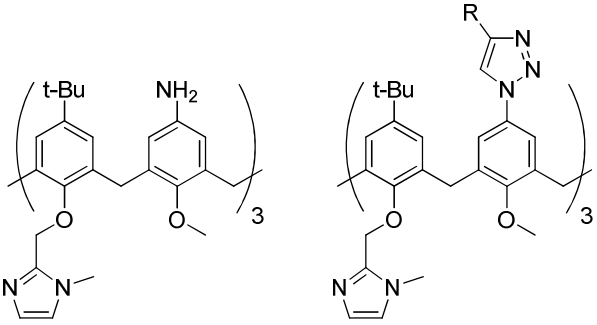

33 **34**

Figure 1.18. Ditopic ligands of the first generation.

tert-butyl derivative **28a,** and complexes only a single water molecule. The aniline nitrogen atoms point towards the entrance of the cavity, thus blocking its access for other guests. Upon addition of a bulky guest, the cavity opens and the encapsulated water molecule is exchanged by for example benzylamine resulting in a large induced fit, whereas small guests induce only a small induced fit of the conformation. Hydrogen bonding between the aniline units in a MeCN complex leads to an increase of aniline basicity with about three pK_a units thus providing, in addition to the metal center and the hydrophobic cavity, a third recognition unit within the molecule.

The triazole containing **34** is able to bind a first Zn^{2+} ion inside the cavity through the imidazole units, whereas a second equivalent of metal ion can be bound to the triazoles.[67] Despite the closed cavity in the binuclear complex, a nitrile guest can be bound by the imidazole-bound Zn^{2+}. In contrast to Zn_2-**33,** where the free coordination sites of the metals point to each other, the second Zn in **34** points outwards from the cavity and is able to bind a second guest on the periphery of the complex.

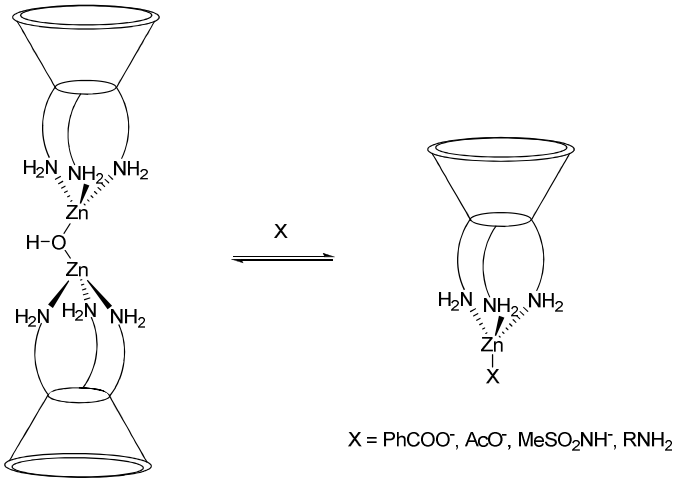

35

Figure 1.19. Coordination driven disassembly of the dimeric complex **35**.

A bimetallic complex is obtained by coordination of the primary amino groups attached to the calix[6]arene **35** core with stoichiometric amounts of Zn^{2+} under the formation of a μ-hydroxo-bridge.[68] The coordination of a guest outside the cavity is possible because the primary amines are sterically less demanding and thus allow coordination of the metal outside of the basket. The hydroxo-dimer can be converted into monomeric complexes using e.g. carboxylic acids, sulfonamides or primary amines. Guest binding studies of the different dimer/monomers revealed that the selectivity for guests can be efficiently controlled by the charge of the resulting complex. The second generation ligand **29b** forms three different monomeric Zn^{2+} complexes.[69] The dicationic complex is formed by complexation of the metal ion by the two imidazole units and the phenolic hydroxide. The latter can be deprotonated to yield the monocationic phenolate complex. The third species can be obtained by addition of hydroxide or chloride that coordinate to the metal center from the outside of the cavity. In this neutral compound the normally 5-coordinate metal center undergoes a change of coordination number from five to four by release of an imidazole pendant arm. The affinity for the guest decreases in the order dicationic > monocationic > neutral.

The third generation Zn-**30** is stabilized by a coordinating MeCN molecule.[70] This ternary compound is stable against anion coordination under basic conditions due to the strong chelate effect of the tren unit.

Metalloenzyme Inhibitors

As decribed above, some phosphatases have two Zn^{2+} ions in their active site. Compounds that have high affinities to the metal centers and block the access of the substrate can achieve an efficient inhibition of these enzymes. This is why calixarenes **36** and **37** are good inhibitors for calf intestine alkaline phosphatase.[71,72] The methylenebisphosphonates are able to interact with the enzyme's active site by complex formation. The hydrophobic calix[4]arene could provide additional interactions with the pocket of the enzyme. Amino functionalisation of the phosphonate pendant arms leads to chiral isomers that show different activity depending on the absolute stereochemistry.

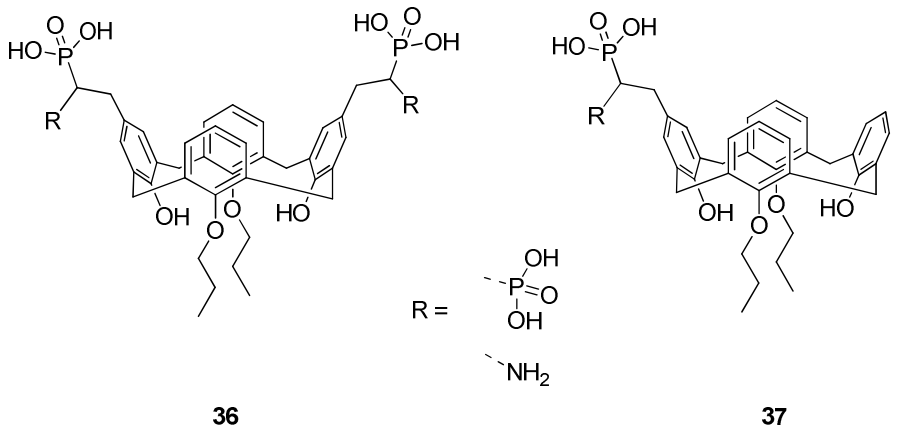

36 **37**

Figure 1.19. Alkaline phosphatase inhibitors.

Agents for Radiotherapy and Medical Imaging

As already mentioned before, calix[4]arene derivatives are able to form stable complexes with metal ions. For some medical purposes, lanthanides or actinides are of great interest. Already in the early days of calixarene chemistry, it was found that calixarenes can bind those trivalent cations very efficiently.[73]

Radiotherapy

Ionizing radiation can be used effectively in the treatment of cancer. To minimize the damage of healthy cells, the radioactive metal ions are complexed by strong chelators, which are coupled to e.g antibodies or specific peptides. Crucial for a successful application of such systems are bifunctional ligands that can be attached to a targeting vector and form very stable complexes with radionuclides. An attractive isotope for radiotherapy is the α-emitter $^{225}Ac^{3+}$ which has a half-life time of 10 days. Calixarenes of type **38** were prepared and their Ac^{3+} coordination was studied. Immunoreactivity and immunogenicity of these complexes were reported.[74]

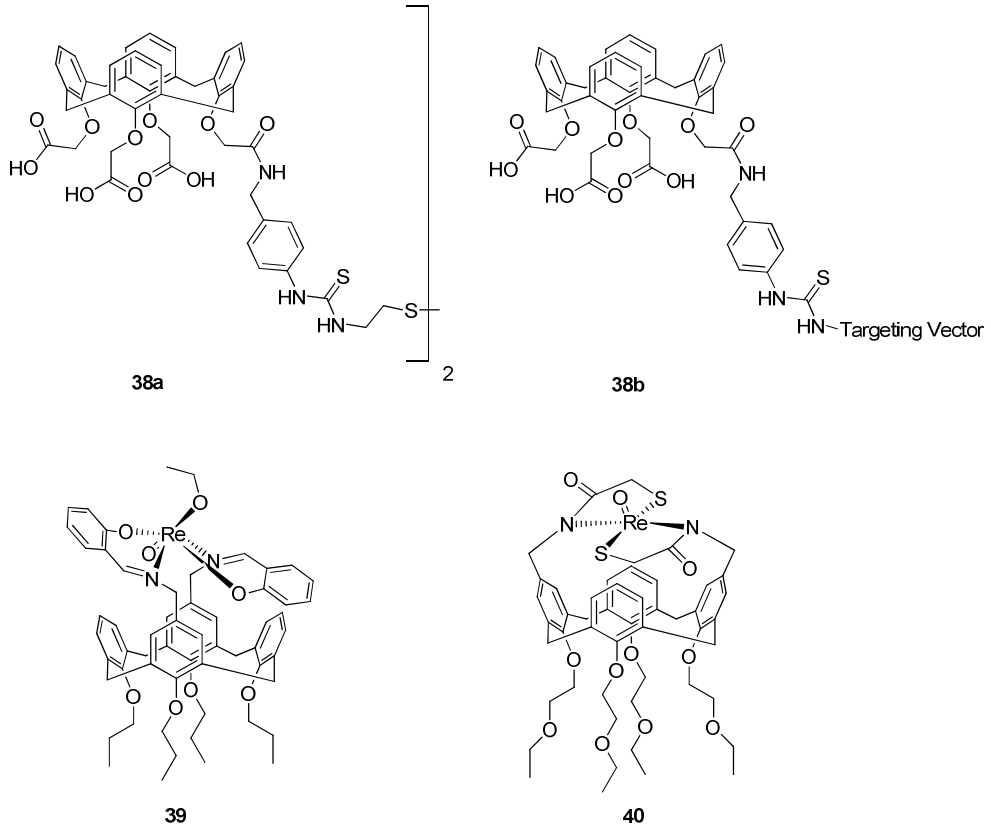
HO
O
O
O

Unfortunally, apart from the information that **40** is stable in PBS, no further characterization towards possible applications was performed.

Luminescent agents

The lanthanides Eu^{3+} and Tb^{3+} are widely used as luminescent probes. Because of their toxicity, they need to be complexed by strong chelators. The complexation is also necessary to shield the metal ions for coordination of water. To enhance their luminescent properties, organic antenna molecules that bind to the metal ions are used for effective sensitation. The advantage of the lanthanide based probes compared to organic agents is that the emission bands are extremely narrow and therefore, those agents are more sensitive than organic dyes.

Both the Eu^{3+} and Tb^{3+} complexes of the bipyridyl containing **41 – 43** have very promising luminescence properties in acetonitrile, whereas their solubility in water is not sufficient.[76] It needs to be stressed that when a water molecule is bound to a luminescent ion, it quenches its luminescence rather efficiently. Therefore, studies need to be performed in water to know whether these systems are suitable for bioimaging. Attachment of two bipyridyl groups to a di-iminodiacetic acid calix[4]arene backbone resulted in chelators **44** and **45** that form very stable, strongly luminescent complexes especially with Tb^{3+}.[77] These compounds are still not sufficiently water soluble but the results of luminescence studies performed in methanol, that has a quenching effect similar to water, are very promising. These studies also showed that the quantum yield is independent on whether the bipyridyl units are attached to the calixarene via their 3- or 4-position.

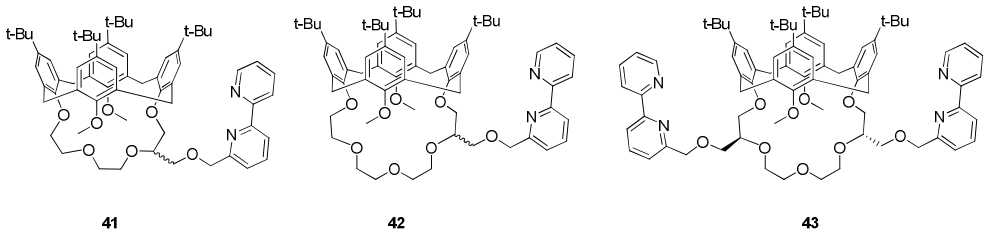

41 **42** **43**

Figure 1.22. Lanthanide chelators for luminescence studies.

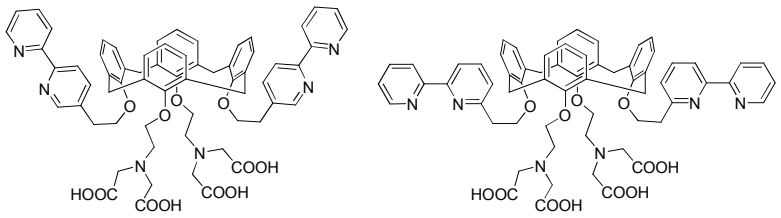

44 **45**

Figure 1.23. Strong chelators for luminescent lanthanide ions.

Magnetic resonance imaging (MRI)

The dose of a magnetic resonance imaging (MRI) contrast agent required to obtain good contrast is much higher than for luminescence probes. The majority of these agents contain Gd^{3+}-ions that are able to shorten the T_1 relaxation times of surrounding water molecules very efficiently.[78] This ability is expressed as longitudinal proton relaxivity (r_1), which is the relaxation rate enhancement of water protons in s^{-1} mM^{-1} Gd^{3+}. The thermodynamic and kinetic inertness of the complexes is of utmost importance to prevent adverse side effects to the patient. Therefore, there is a need to develop chelators that are able to bind Gd^{3+} very effectively.

In a first study towards calixarene based MRI contrast agents, calix[4]arene tetraamide **46** was used to chelate Gd^{3+}.[79] The relaxivity of this complex in a dmso/water mix (9:1) at 20 °C and 400 MHz is 3.40 $s^{-1}mM^{-1}$, the stability constant is about 1000 M^{-1}. For practical applications, the stability and the water solubility are much too low and, therefore, no further studies on this compound were performed.

A more stable Gd-complex is formed with **47**.[80] The additional presence of four chelating groups results in the formation of an octa-coordinated metal ion and an increase of the stability constant to $2 \cdot 10^5$ M^{-1}, which is still too low for practical applications. This compound interacts with human serum albumin (HSA) and, therefore, opens the way to the development of new, water soluble calixarene based MR angiography agents.

Casnati, Botta and co-workers used a di-imidodiacetic acid functionalized calixarene **48** for Gd^{3+} complexation and found a stability constant of at least 10^{13} M^{-1}.[81] The

relaxivity of the free complex is 9.6 $s^{-1}mM^{-1}$ at 20 MHz and 25 °C. The HSA-adduct is rather stable ($K_A = 2.4 \cdot 10^4\ M^{-1}$) and has a relaxivity of as high as 60 $s^{-1}mM^{-1}$. Interestingly, the compound has three inner-sphere water molecules (q = 3), whereas its HSA-adduct has only one. This can be explained by the fact that in the free form, the amide groups do not participate in the metal binding whereas in the complex with albumin, for example aspartate or glutamate binds to the metal and thus, increases the stability of the protein binding.

A probably very stable Gd^{3+} complex can be formed with **49**.[82] This compound is also highly soluble in water, which makes it the only calixarene based MRI contrast agent so far reported that could be used for *in vivo* studies. Unfortunately, no parameters describing the suitability of this compound as a contrast agent were given.

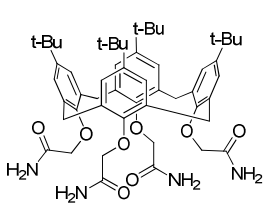

46

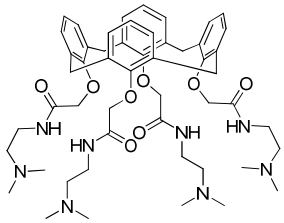

47

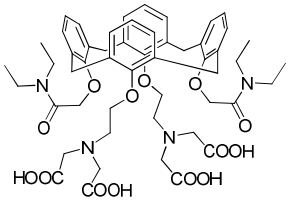

48

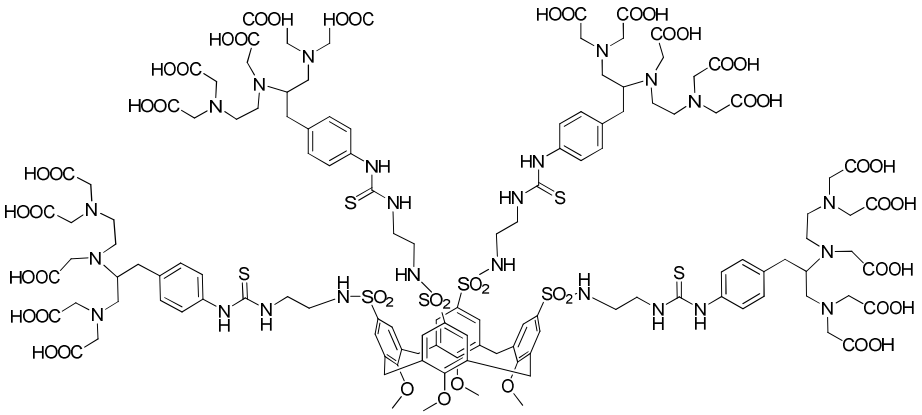

49

Figure 1.24. Calixarene based chelators for MRI contrast agents.

Other Applications

Carboxylic acid based di- and tetranuclear Sn(IV) complexes and their anticancer and antibacterial activity are well documented in the literature.[83] In a recent paper, the beneficial effect of such compounds **50** on the suppression of blood and tissue oxidative stress caused by lead in male albino Wistar rats was investigated.[84] The positive effect was attributed to the binding of **50** to cysteine moieties in peptides, which then hampers the binding of lead.

One of the most prominent chemotherapeutics is cisplatinum.[85] Compared to cis-platinum, **51** is less cytotoxic in human ovarian cancer cell lines. Sulfonatocalix[4]arene **26b** was tested as a drug delivery agent of **51** and for a possible activity enhancement.[86] Compound **51** interacts with the calixarene via ionic interactions as well as hydrogen bonding between its amino groups and the sulfonato moieties of **26b**, whereas, the hydrophobic dipyrazolylmethane part is complexed by the calixarene cavity. No change in activity of **51** in the presence of **26b** was observed which is caused by the low stability of the complex *in vitro*.

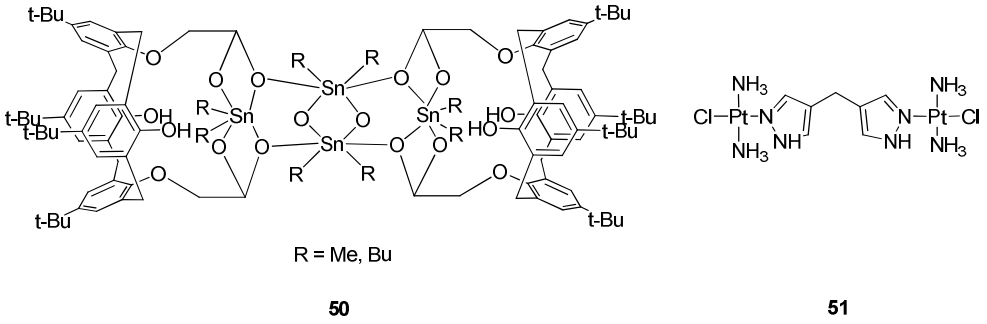

Figure 1.25. Structures of a Sn(IV) based anti-lead agent and of a cisplatinum derivative.

Conclusions/Outlook

In summary, calixarenes are multifunctional building blocks for many (biological) applications. They show very good properties as artificial ion channels, metallo-enzyme mimics/inhibitors and can be used in radiotherapy and medical imaging. In many applications, calixarenes are only used as synthetic platforms to prearrange functional groups in a three-dimensional space. The ion transport through artificial cell membranes (partial dehydration of the ion) directly benefits from the presence of the hydrophobic basket. In some cases, this is also beneficial for the substrate binding in enzyme mimics. Even though calixarene based ion channels are already quite sophisticated, there are still many challenges to be addressed by the enzyme mimics. In the case of calix[4]arene based mimics, the catalytic properties of the complexes are good but there are only a few cases where the calixarene is more than a spacer between functional groups. Calix[6]arenes are the more promising mimics since they show a direct use of the calixarene itself with surprising similarities to natural systems. To achieve real catalysis with these systems is a challenge that remains to be tackled. In radiotherapy and medical imaging, calixarenes will likely never become more than synthetic platforms. Nevertheless, they have a great potential to be used efficiently in these fields since they are able to carry a high payload of metal ions and thus, to multiply the desired properties of mononuclear analogues.

Outline of the Thesis

In this thesis, the versatility of calix[4]arenes with respect to biological applications are exploited. These compounds were used as synthetic backbones of potential organo-catalysts, artificial ion-channels and MRI contrast agents.

In Chapter 2, the kinetic acidity of imidazolium bearing calix[4]arenes is evaluated by H/D exchange measurements. The effect of the supramolecular environement, the counter-ion as well as the substitution pattern on the acidity of the C^2-proton is discussed. The knowledge gained in this work can help to explain the performance of the salts as precursors in catalysis as well as the formation of side products when imidazolium based ionic liquids are used as solvents.

In Chapter 3, a possibility is shown how to increase the Na^+ selectivity of calixarene tetra amides. Substituents on the *upper rim* are varied and the binding of alkaline metal ions on the *lower rim* is studied by liquid-liquid extraction. The potential use of this approach is in the design of Na^+ selective artificial ion channels.

Chapters 4 to 6 highlight the use of calixarene based MRI contrast agents. A first model compound along with its synthesis, purification, supramolecular chemistry and relaxometric characterization is presented in Chapter 4. In Chapter 5, the aim was to optimize the relaxivity of this model by acceleration of the water exchange. Therefore, the chelating units based on DOTA-monoamides were substituted with a pyridine-*N*-oxide based DOTA analogue. The self-aggregation and the interaction with bovine serum albumin of this conjugate is described and full characterization of the compound concerning its suitability as contrast agent in angiography is provided. The supramolecular chemistry of calixarene based MRI contrast agents is investigated in more detail in Chapter 6. The incorporation of a hydrophobic, non-charged Gd(III)-binding calixarene into the bilayer of liposomes and the effect on the morphology of the resulting aggregates is described. These systems have the perspective to be studied in human clinical trials with regard to tumor imaging since such liposomes accumulate in tumors.

References

1 Vicens, J.; Harrowfield, J.; Baklouti, L. *Calixarenes in the Nanoworld*, Springer, Dordrecht **2007**.

2 Von Baeyer, A. *Chem. Ber.* **1872**, *25*, 280.

3 Mandolini, L.; Ungaro, R. *Calixarenes in Action*, Imperial College Press, London **2000**.

4 Vicens, J.; Böhmer, V. *Calixarenes, a Versatile Class of Macrocyclic Compounds*, Kluwer, Dordrecht **1991**.

5 Gutsche, C. D.; Dhawan, B.; Leonis, M.; Stewart, D. *Org. Synth.* **1990**, *68*, 238.

6 Munch, J. H.; Gutsche, C. D. *Org. Synth.* **1990**, *68*, 243.

7 Gutsche, C. D.; Iqbal, M. *Org. Synth.* **1990**, *8*, 234.

8 Rodik, R. V.; Boyko, V. I.; Kalchenko, V. I. *Curr. Med. Chem.* **2009**, *16*, 1630.

9 Creaven, B. S.; Donlon, D. F.; McGinley, J. *Coord. Chem. Rev.* **2009**, *253*, 893.

10 Agrarwal, Y. K.; Bhatt, H. *Bioinorg. Chem. Appl.* **2004**, *2*, 237.

11 Baldini, L.; Casnati, A.; Sansone, F.; Ungaro, R. *Chem. Soc. Rev.* **2007**, *36*, 254.

12 Iqbal, K. S. J.; Cragg, P. J. *Dalton Trans.* **2007**, 26.

13 Mutihac, L. *Curr. Drug Disc. Techn.* **2008**, *5*, 98.

14 Jin, T.; Kinjo, M.; Kobayashi, Y.; Hirata, H. *Faraday Trans.* **1998**, *94*, 3135.

15 Jin, T. *Chem. Commun.* **2000**, 1379.

16 Maulucci, N.; Riccardis, F. D.; Botta, C. B.; Casapullo, A.; Cressina, E.; Fregonese, M.; Tecilla, P.; Izzo, I. *Chem. Commun.* **2005**, 1354.

17 Iqbal, K. S. J.; Allen, M. C.; Fucassi, F.; Cragg, P. J. *Chem. Commun.* **2007**, 3951.

18 Iglesias-Sánchez, J. C.; Wang, W.; Ferdani, R.; Prados, P.; Mendoza, J. D.; Gokel, G. W. *New J. Chem.* **2008**, *32*, 878.

19 Arduini, A.; Credi, A.; Faimani, G.; Massera, C.; Pochini, A.; Secchi, A.; Semeraro, M.; Silvi, S.; Ugozzoli, F. *Chem. Eur. J.* **2008**, *14*, 98.

20 Mareque Rivas, J. C.; Schwalbe, H.; Lippard, S. J. *Proc. Natl. Acad. Sci.* **2001**, *98*, 9478.

21 Matthews, S. E.; Schmitt, P.; Felix, V.; Drew, M. G. B.; Beer, P. D. *J. Am. Chem. Soc.* **2002**, *124*, 1341.

22 Molenveld, P.; Engbersen, J. F. J.; Reinhoudt, D. N. *Eur. J. Org. Chem.* **1999**, *12*, 3269.

23 Molenveld, P.; Engbersen, J. F. J.; Reinhoudt, D. N. *Chem. Soc. Rev.* **2000**, *29*, 75.

24 Molenveld, P.; Stikvoort, W. M. G.; Kooijman, H.; Spek, A. L.; Engbersen, J. F. J.; Reinhoudt, D. N. *J. Org. Chem.* **1999**, *64*, 3896.

25 Cacciapaglia, R.; Casnati, A.; Mandolini, L.; Reinhoudt, D. N.; Salvio, R.; Sartori, A.; Ungaro, R. *J. Org. Chem.* **2005**, *70*, 624.

26 Molenveld, P.; Engbersen, J. F. J.; Reinhoudt, D. N. *Angew. Chem. Int. Ed.* **1999**, *38*, 3189.

27 Cacciapaglia, R.; Casnati, A.; Mandolini, L.; Reinhoudt, D. N.; Salvio, R.; Sartori, A.; Ungaro, R. *J. Org. Chem.* **2005**, *70*, 5398.

28 Spencer, D. J. E.; Johnson, B. J.; Johnson, B. J.; Tolman, W. B. *Org. Lett.* **2002**, *4*, 1391.

29 Cacciapaglia, R.; Casnati, A.; Mandolini, L.; Reinhoudt, D. N.; Salvio, R.; Sartori, A.; Ungaro, R. *J. Am. Chem. Soc.* **2006**, *128*, 12322.

30 Cacciapaglia, R.; Casnati, A.; Mandolini, L.; Reinhoudt, D. N.; Salvio, R.; Sartori, A.; Ungaro, R. *Inorg. Chim. Acta* **2007**, *360*, 981.

31 Ozturk, G.; Akkaya, E. U. *Org. Lett.* **2004**, *6*, 241.

32 Cacciapaglia, R.; Casnati, A.; Mandolini, L.; Peracchi, A.; Reinhoudt, D. N.; Salvio, R.; Sartori, A.; Ungaro, R. *J. Am. Chem. Soc.* **2007**, *129*, 12512.

33 Molenveld, P.; Engbersen, J. F. J.; Reinhoudt, D. N. *J. Org. Chem.* **1999**, *64*, 6337.

34 Cao, Y.; Zheng, Q.; Chen, C.; Hu, H.; Huang, Z. *Inorg. Chim. Acta* **2004**, *357*, 316.

35 Baldini, L.; Bracchini, C.; Cacciapaglia, R.; Casnati, A.; Mandolini, L.; Ungaro, R. *Chem. Eur. J.* **2000**, *6*, 1322.

36 Cacciapaglia, R.; Casnati, A.; Stefano, S. D.; Mandolini, L.; Paolemili, D.; Reinhoudt, D. N.; Sartori, A.; Ungaro, R. *Chem. Eur. J.* **2004**, *10*, 4436.

37 Fiammengo, R.; Wojciechowski, K.; Crego-Calama, M.; Timmerman, P.; Figoli, A.; Wessling, M.; Reinhoudt, D. N. *Org. Lett.* **2003**, *5*, 3367.

38 Bakirci, H.; Koner, A. L.; Dickman, M. H.; Kortz, U.; Nau, W. M. *Angew. Chem. Int. Ed.* **2006**, *45*, 7400.

39 Blanchard, S.; Clainche, L. L.; Rager, M.; Chansou, B.; Tuchagues, J.; Duprat, A. F.; Mest, Y. L.; Reinaud, O. *Angew. Chem. Int. Ed.* **1998**, *37*, 2732.

40 Le Poul, N.; Campion, M.; Douziech, B.; Rondelez, Y.; Le Clainche, L.; Reinaud, O.; Le Mest, Y. *J. Am. Chem. Soc.* **2007**, *129*, 8801.

41 Le Poul, N.; Campion, M.; Izzet, G.; Douziech, B.; Reinaud, O.; Le Mest, Y. *J. Am. Chem. Soc.* **2005**, *127*, 5280.

42 Blanchard, S.; Rager, M.; Duprat, A. F.; Reinaud, O. *New J. Chem.* **1998**, *22*, 1143.

43 Rondelez, Y.; Rager, M.; Duprat, A.; Reinaud, O. *J. Am. Chem. Soc.* **2002**, *124*, 1334.

44 Le Clainche, L.; Giorgi, M.; Reinaud, O. *Inorg. Chem.* **2000**, *39*, 3436.

45 Izzet, G.; Frapart, Y. M.; Prangé, T.; Provost, K.; Michalowicz, A.; Reinaud, O. *Inorg. Chem.* **2005**, *44*, 9743.

46 Izzet, G.; Akdas, H.; Hucher, N.; Giorgi, M.; Prangé, T.; Reinaud, O. *Inorg. Chem.* **2006**, *45*, 1069.

47 Sénèque, O.; Campion, M.; Douziech, B.; Giorgi, M.; Rivière, E.; Journaux, Y.; Mest, Y.; Reinaud, O. *Eur. J. Inorg. Chem.* **2002**, *8*, 2007.

48 Rondelez, Y.; Sénèque, O.; Rager, M.; Duprat, A.; Reinaud, O. *Chem. Eur. J.* **2000**, *6*, 4218.

49 Sénèque, O.; Campion, M.; Giorgi, M.; Mest, Y. L.; Reinaud, O. *Eur. J. Inorg. Chem.* **2004**, *9*, 1817.

50 Rondelez, Y.; Bertho, G.; Reinaud, O. *Angew. Chem. Int. Ed.* **2002**, *41*, 1044.

51 Sénèque, O.; Campion, M.; Douziech, B.; Giorgi, M.; Mest, Y. L.; Reinaud, O. *Dalton Trans.* **2003**, 4216.

52 Izzet, G.; Douziech, B.; Prangé, T.; Tomas, A.; Jabin, I.; Le Mest, Y.; Reinaud, O. *Proc. Natl. Acad. Sci.* **2005**, *102*, 6831.

53 Izzet, G.; Zeitouny, J.; Akdas-Killig, H.; Frapart, Y.; Ménage, S.; Douziech, B.; Jabin, I.; Le Mest, Y.; Reinaud, O. *J. Am. Chem. Soc.* **2008**, *130*, 9514.

54 De la Lande, A.; Gérard, H.; Moliner, V.; Izzet, G.; Reinaud, O.; Parisel, O. *J. Biol. Inorg. Chem.* **2006**, *11*, 593.

55 De la Lande, A.; Parisel, O.; Gérard, H.; Moliner, V.; Reinaud, O. C*hem. Eur. J.* **2008**, *14*, 6465.

56 Izzet, G.; Zeng, X.; Akdas, H.; Marrot, J.; Reinaud, O. *Chem. Commun.* **2007**, 810.

57 Izzet, G.; Zeng, X.; Over, D.; Douziech, B.; Zeitouny, J.; Giorgi, M.; Jabin, I.; Le Mest, Y.; Reinaud, O. *Inorg. Chem.* **2007**, *46*, 375.

58 Over, D.; de la Lande, A.; Zeng, X.; Parisel, O.; Reinaud, O. *Inorg. Chem.* **2009**, *48*, 4317.

59 Sénèque, O.; Rager, M.; Giorgi, M.; Reinaud, O. *J. Am. Chem. Soc.* **2000**, *122*, 6183.

60 Sénèque, O.; Rondelez, Y.; Le Clainche, L.; Inisan, C.; Rager, M.; Giorgi, M.; Reinaud, O. *Eur. J. Inorg. Chem.* **2001**, *10*, 2597.

61 Sénèque, O.; Rager, M.; Giorgi, M.; Reinaud, O. *J. Am. Chem. Soc.* **2001**, *123*, 8442.

62 Sénèque, O.; Giorgi, M.; Reinaud, O. *Supramol. Chem.* **2003**, *15*, 573.

63 Sénèque, O.; Reinaud, O.; Giorgi, M. *Chem. Commun.* **2001**, 984.

64 Coquière, D.; Marrot, J.; Reinaud, O. *Chem. Commun.* **2006**, 3924.

65 Coquière, D.; Marrot, J.; Reinaud, O. *Org. Biomol. Chem.* **2008**, *6*, 3930.

66 Coquière, D.; de la Lande, A.; Marti, S.; Parisel, O.; Prangé, T.; Reinaud, O. *Proc. Natl. Acad. Sci.* **2009,** *106*, 10449.

67 Colasson, B.; Save, M.; Milko, P.; Roithová, J.; Schröder, D.; Reinaud, O. *Org. Lett.* **2007**, *9*, 4987.

68 Darbost, U.; Sénèque, O.; Li, Y.; Bertho, G.; Marrot, J.; Rager, M.; Reinaud, O.; Jabin, I. *Chem. Eur. J.* **2007**, *13*, 2078.

69 Sénèque, O.; Rager, M.; Giorgi, M.; Prangé, T.; Tomas, A.; Reinaud, O. *J. Am. Chem. Soc.* **2005**, *127*, 14833.

70 Darbost, U.; Zeng, X.; Rager, M.; Giorgi, M.; Jabin, I.; Reinaud, O. *Eur. J. Inorg. Chem.* **2004**, *22*, 4371.

71 Vovk, A. I.; Kalchenko, V. I.; Cherenok, S. A.; Kukhar, V. P.; Muzychka, O. V.; Lozynsky, M. O. *Org. Biomol. Chem.* **2004**, *2*, 3162.

72 Cherenok, S.; Vovk, A.; Muravyova, I.; Shivanyuk, A.; Kukhar, V.; Lipkowski, J.; Kalchenko, V. *Org. Lett.* **2006**, *8*, 549.

73 Steemers, F. J.; Meuris, H. G.; Verboom, W.; Reinhoudt, D. N.; van der Tol, E. B.; Verhoeven, J. W. *J. Org. Chem.* **1997**, *62*, 4229.

74 Grote Gansey, M. H. B.; De Haan, A. S.; Bos, E. S.; Verboom, W.; Reinhoudt, D. N. *Bioconj. Chem.* **1999**, *10*, 613.

75 Van Bommel, K. J. C.; Verboom, W.; Hulst, R.; Kooijman, H.; Spek, A. L.; Reinhoudt, D. N. *Inorg. Chem.* **2000**, *39*, 4099.

76 Fischer, C.; Sarti, G.; Casnati, A.; Carrettoni, B.; Manet, I.; Schuurman, R.; Guardigli, M.; Sabbatini, N.; Ungaro, R. *Chem. Eur. J.* **2000,** *6*, 1026.

77 Casnati, A.; Baldini, L.; Sansone, F.; Ungaro, R.; Armaroli, N.; Pompei, D.; Barigelletti, F. *Supramol. Chem.* **2002**, *14*, 281.

78 Tóth, É.; Merbach, A. *The Chemistry of Contrast Agents in Medical Magnetic Resonance Imaging*, Wiley, New York **2001**.

79 Georgiev, E. M.; Roundhill, D. M. *Inorg. Chim. Acta* **1997**, *258*, 93.

80 Bryant, L. H., Jr; Yordanov, A. T.; Linnoila, J. J.; Brechbiel, M. W.; Frank, J. A. *Angew. Chem. Int. Ed.* **2000**, *39*, 1641.

81 Aime, S.; Barge, A.; Botta, M.; Casnati, A.; Fragai, M.; Luchinat, C.; Ungaro, R. *Angew. Chem. Int. Ed.* **2001**, *40*, 4737.

82 Krishnan, A. M.; Lohrmann, R. *WO96/14876* **1996**.

83 Nath, M.; Pokharia, S.; Yadav, R. *Coord. Chem. Rev.* **2001**, *215*, 99.

84 Ali, A.; Flora, S. J.; Saxena, G.; Kolehmainen, E.; Mahieu, B.; Rao, C. P. *J. Inorg. Biochem.* **2006**, *100*, 206.

85 Kelland, L. *Nature Rev. Cancer* **2007**, *7*, 573.

86 Wheate, N. J.; Abbott, G. M.; Tate, R. J.; Clements, C. J.; Edrada-Ebel, R.; Johnston, B. F. *J. Inorg. Biochem.* **2009**, *103*, 448.

2 Kinetic Acidity of Supramolecular Imidazolium Salts — Effects of Substituents, Pre-Orientation and Counter Ions onto H/D Exchange Rates

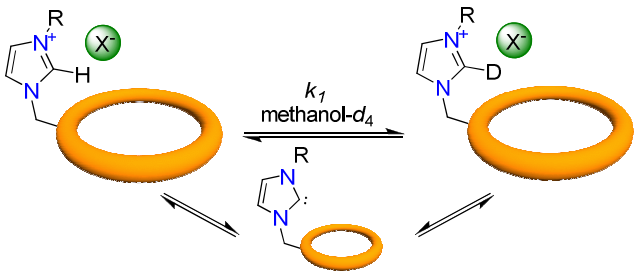

The contents of this chapter have been adapted from:
Fahlbusch, T.; Frank, M.; Schatz, J.; Schühle, D. T. *J. Org Chem.* **2006**, *71*, 1688.

Introduction

In 1958, Breslow was the first to postulate uncharged nucleophilic carbenes stemming from the corresponding thiazolium salts as the active catalysts in Stetter-type reactions.[1] Only two years later, Wanzlick introduced cognate *N*-heterocyclic carbenes (NHC) by trapping the intermediate carbene.[2] The inspiring idea that stable nucleophilic carbenes could be formed easily by dissociation of the C^2–proton was strongly supported by Olofson and others who could prove the facile H/D exchange of both thiazolium and imidazolium salts.[3,4] This early work came back into focus since the characterization of a stable crystalline NHC in 1991.[5] Since then, a considerable amount of work has been invested in the preparation and use of novel NHCs mainly as ligands in transition-metal-catalyzed reactions such as the Suzuki-Miyaura reaction or as umpolung catalysts in organo catalytic processes.[6,7]

The formation of the NHC starting from a salt precursor is often a decisive step in catalytic reactions (Scheme 2.1). Despite the plethora of reports which exploit this basic reaction scheme in catalytic applications considerably less information is available about fundamental properties. Both experimental and theoretical investigations characterize nucleophilic carbenes as strong bases (pK_a ~ 20–30) with high proton affinities above 1 kJ mol^{-1}.[8] Additionally, the rate of the formation of the active catalyst might indicate the suitability of an imidazolium salt in catalysis. Because protonation of the NHC is fast compared to the formation of the NHC, the H/D-exchange rates of the C^2–H give an indirect estimate for the reaction rate of its formation.

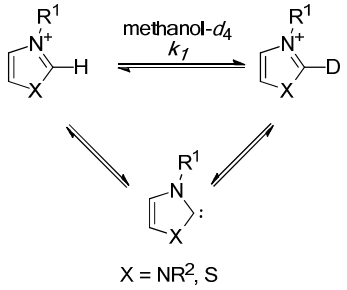

Scheme 2.1. *N*-Heterocyclic carbenes as intermediates in H/D exchange reactions.

Amyes et al. determined the rate constants of the H/D exchange of some imidazolium salts in D_2O in the presence of OD^--ions, and Diederich and Lutter measured this exchange of thiazolium cyclophanes in different buffers.[9,10] In contrast to these works, we decided not to study the exchange rates in solutions with constant ion strengths and various pD-values but instead to determine rate constants under conditions usually used for preparative applications of NHCs in organo-catalytic or transition-metal-catalyzed reactions.

Results and Discussion

Besides the simple structures **1** and **6** (Figure 2.1), calix[4]arene–based imidazolium salts **2**–**5** (Figure 2.1) have been synthesized to investigate the influence of preorientation and cooperativity of the imidazolium units.[11] In all experiments, we chose a 0.155 molar solution of the imidazolium salt, in terms of imidazolium units, in methanol–d_4 containing 3% water without any further additives as the reaction medium. The exchange was followed by ^{1}H NMR spectroscopy over a period of 24 h at 300 K by the disappearance of the C^2–proton. The rate constants were deduced from standard pseudo first-order-plots. The mean values of the rate constants of all compounds are shown in Table 2.1 and some remarkable trends are discussed.

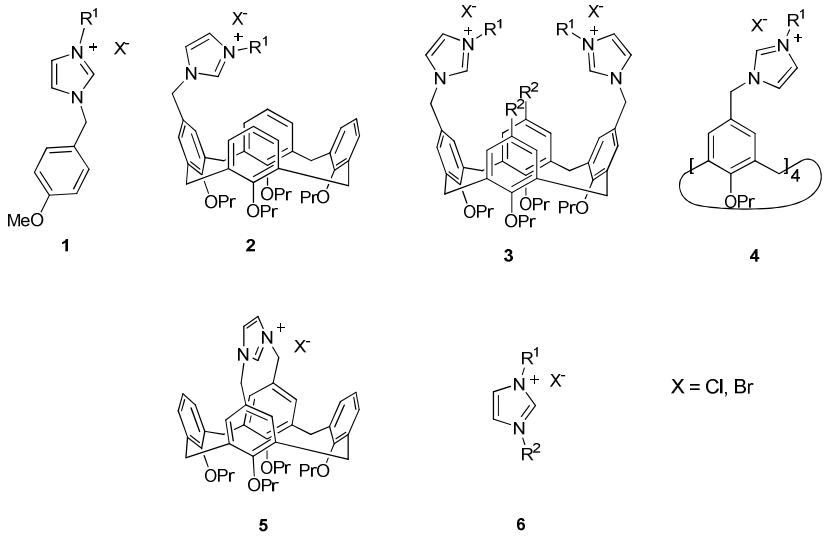

Figure 2.1. Imidazolium salts studied in this work.

Table 2.1. Rate constants of the H/D exchange in MeOD-d_4 containing 3% of water at 300 K.

	$R^{1, a)}$	R^2	X	k_1 / d^{-1}	k_x / k_{1a}
1a	mes	—	Cl	1.060 ± 0.150	≡ 1
1b	^{i}pr	—	Cl	0.553 ± 0.061	0.52
1c	cy	—	Cl	<< 0.001	0
1d	^{t}bu	—	Cl	<< 0.001	0
1e	dip	—	Cl	2.850 ± 0.430	2.69
1f	mes	—	Br	0.176 ± 0.008	0.17
1g	^{i}pr	—	Br	<< 0.001	0
1h	cy	—	Br	0.246 ± 0.009	0.23
1i	^{t}bu	—	Br	0.158 ± 0.014	0.15
2a	mes	—	Cl	0.603 ± 0.009	0.57
2b	CH_3	—	Cl	<< 0.001	0
3a	mes	H	Cl	5.938 ± 0.390	5.60
3b	CH_3	H	Cl	<< 0.001	0
3c	^{i}pr	H	Cl	0.629 ± 0.043	0.59
3d	cy	H	Cl	0.241 ± 0.024	0.23
3e	^{t}bu	H	Cl	<< 0.001	0
3f	dip	H	Cl	<< 0.001	0
3g	mes	CH_2OMe	Cl	<< 0.001	0
3h	^{i}pr	CH_2OMe	Cl	<< 0.001	0
3i	mes	^{t}bu	Cl	3.903 ± 0.326	3.68
3j	CH_3	^{t}bu	Cl	<< 0.001	0
3k	dip	^{t}bu	Cl	0.784 ± 0.130	0.74
4	mes	—	Cl	12.4 ± 0.8 / 1.03 ± 0.03	
5	—	—	Cl	<< 0.001	0
6a	mes	mes	Cl	>> 10	>>9.4
6b	dip	dip	Cl	<< 0.001	0

[a)] dip=2,6-diisopropylphenyl; mes= mesityl; cy= cyclohexyl.

With the exception of the methoxymethyl substituted calix[4]arene **3g**, mesityl imidazolium salts (**1a**, **1f**, **2a**, **3a**, **3i**, **4**, and **6a**) undergo a relatively fast H/D exchange. This exception might be explained by the fact that, in the molecules **3g** and **3h**, intramolecular hydrogen bonds between C^2–H•••O(CH_2R)Me could be formed that stabilize the imidazolium salts and hinder the formation of a carbene. Such a structure is comparable with the adducts of NHCs with phenol, amines, boranes or the bis–carbene–proton complex.[12] It is obvious that the preorientation of imidazolium units on the calixarene backbone has a large influence on the exchange rate. Whereas the monomesitylimidazolium salt **2a** shows a moderate exchange, the bifunctional calixarene **3a** exhibits a tenfold higher rate. It is noticeable that calixarene–based imidazolium salts (**2a**, **3a**) exchange with significant different rates than the open chain analog **1a** presumably owing to a micro polarity effect.[10] For the mono substituted derivative **2a** the H/D exchange is retarded slightly (k_{2a}/k_{1a} ~ 0.6) and for **3a** accelerated (k_{3a}/k_{1a} ~ 5.6). For calixarenes **3**, not only the influence of substituents directly bound to the salt unit but also the influence of substitution in positions 5 and 17 (R^2) in the calixarene backbone could be studied. As discussed before, the hydrogen bond accepting CH_2OMe unit suppresses the exchange. In the case of **3k**, the *tert*-butyl groups increase (compared to **3f**), and in case of **3i** decrease the exchange rates (compared to **3a**). The capping of the calixarene backbone (**5**) with an imidazolium group shielded the C^2–proton in such a way that no H/D exchange could be observed.

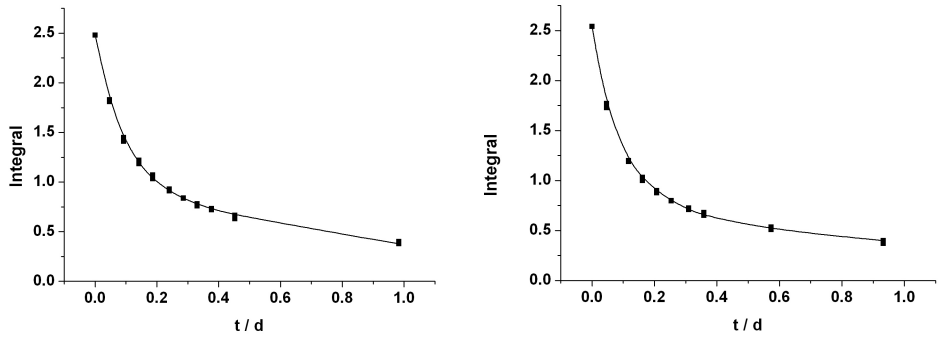

Figure 2.2. H/D Exchange kinetics of **4** for Exp 1 (left) and Exp 2 (right). The line represents the results from the fittings.

The H/D exchange of the tetraimidazolium calix[4]arene **4** did not obey simple pseudo-first-order kinetic rates (Figure 2.2). However, the observed data could be fitted by assuming two independent first order processes using Equations 2.1 and 2.2.

$$I_{obs} = I_1 + I_2 = I_1^0 \exp(-k_1 t) + I_2^0 \exp(-k_2 t) \quad 2.1$$

$$I_1^0 + I_2^0 = I_0 \quad 2.2$$

In Equations 2.1 and 2.2, I_{obs} stands for the observed integral, whereas I_1 is the integral resulting from the not exchanged imidazolium side 1, and I_2 of side 2, respectively. I_1^0 and I_2^0 are the starting integrals for each side. I_0 is the integral obtained from the first measurement (at time t=0) and was fixed to this value during the fittings. In Table 2.2, the results of two independent experiments (Exp 1 and Exp 2, see Figure 2.2) and fittings are presented.

Table 2.2. Parameters obtained from two independent fittings of two different measurements of the exchange kinetics of **4** using Equations 2.1 and 2.2.

	I^0	I_1^0	k_1 [d^{-1}]	k_2 [d^{-1}]
Exp 1	2.48[a)]	1.42 ± 0.07	11.6 ± 0.9	1.05 ± 0.13
Exp 2	2.54[a)]	1.59 ± 0.06	13.2 ± 0.89	1.01 ± 0.13

[a)] Fixed to the integral measured at t=0.

The first exchange rate is high (12.4 d^{-1}) indicating some kind of a cooperative action of two of the four imidazolium moieties. In contrast, the second exchange rate (1.03 d^{-1}) is similar to the one observed for monoimidazolium salts (**1a**, **2a**).

The influence of the counter ion on the H/D exchange was investigated for compounds **1**. In no case were similar rate constants for bromide and chloride found in methanol-d_4 containing 3% of water. The values differ by as much as a factor of 10. For the bromides **1f** and **1g** the exchange rate dropped significantly compared to the chlorides **1a** and **1b**. However, in case of bulky substituents (**1c**, **1h**, **1d** and **1i**) the bromide salts showed a higher exchange rate. A detailed investigation into the recognition properties of the studied imidazolium salts towards anions must clarify this matter because it is known that

imidazolium groups can be used as a recognition element in supramolecular anion receptors.[13]

Conclusions

The presented results show that the substitution of imidazolium salts at the distal 5- and 17-positions has a large influence on the H/D exchange rates in wet methanol-d_4. These rates play an important role in catalytic reactions, as observed for the Suzuki reaction. For example, the mesitylimidazolium salts show the fastest exchange and also the highest catalytic activity.[11] This is in agreement with the high exchange rate observed for the IMes ligand **6a** known for its good performance as ligand precursor in cross coupling reactions.[6c]

In summary, measuring fundamental physicochemical properties illuminated surprising differences in the kinetic acidities of a series of open-chain and macrocyclic imidazolium salts. Mesityl-substituted heterocycles showed the highest H/D exchange rates whereas alkyl substituents hampered this process. Additionally, the anion had a distinct influence on the exchange process.

Experimental

Compounds **1**, **3a–d**, **3f**, and **6** were synthesized according to literature procedures.[11,14] Melting points were determined in open capillaries and were not corrected. Infrared (IR) spectra were obtained from KBr pellets unless otherwise stated. Absorptions are given in wave numbers (cm^{-1}). NMR spectra were recorded at 400.13 MHz for ^1H and 100.62 MHz for ^{13}C, 2–dimensional experiments were measured at 500.14 MHz for ^1H and 125.76 MHz for ^{13}C. Tetramethylsilane was used for the ^1H NMR spectra as internal standard (δ = 0.00 ppm) and the solvent signals for the ^{13}C NMR spectra [δ ($CDCl_3$) = 77.0, δ (DMSO-d_6) = 39.5, δ (methanol-d_4) = 49.3 ppm]. Chemical shifts (δ) are given in ppm and coupling constants (J) in Hz.

General procedure for the reaction of benzyl halides with 1–substituted 1-imidazoles:
To a solution of the benzyl halide in dry $CHCl_3$ was added the corresponding 1–substituted imidazole. After heating the solution for 1–5 d, the solvent was removed under reduced pressure, diethyl ether was added, and the mixture was heated for 2–3 h. After cooling the

mixture, the formed colorless hygroscopic precipitate was collected by filtration, washed with several portions of Et_2O and dried in a desiccator.

5-(1-Mesitylimidazolium)methyl-25,26,27,28-tetrapropoxycalix[4]arene-chloride (2a): 5-Chloromethyl-25,26,27,28-tetrapropoxycalix[4]arene (2.00 g, 3.12 mmol), 1-mesitylimidazole (652 mg, 3.50 mmol), and $CHCl_{3(abs.)}$ (20 mL) were refluxed for 1 d. After stirring in boiling Et_2O (70 mL), a colorless product was obtained (708 mg, 0.86 mmol, 27%). Mp 153–155 °C. IR (KBr): $\tilde{\nu}_{max}$ 3147 (m), 2962 (s), 2932 (s), 2875 (s), 1587 (w), 1546 (m), 1457 (s), 1384 (m), 1302 (m), 1246 (m), 1203 (s), 1160 (m), 1087 (m), 1008 (s), 891 (w), 850 (w), 761 (s). ^{1}H NMR (400 MHz, $CDCl_3$): δ = 0.96 (t, *J* = 7.5 Hz, 6 H), 1.04 (t, *J* = 7.5 Hz, 3 H), 1.05 (t, *J* = 7.3 Hz, 3 H), 1.87–1.94 (m, 4 H), 1.96–2.04 (m, 4 H), 2.08 (s, 6 H), 2.34 (s, 3 H), 3.14 (d, *J* = 13.4 Hz, 2 H), 3.18 (d, *J* = 13.1 Hz, 2 H), 3.75 (t, *J* = 7.3 Hz, 2 H), 3.78 (t, *J* = 7.2 Hz, 2 H), 3.91–4.02 (m, 4 H), 4.46 (d, *J* = 13.3 Hz, 2 H), 4.47 (d, *J* = 13.0 Hz, 2 H), 5.45 (s, 2 H), 6.39 (s, 2 H), 6.43–6.47 (m, 2 H), 6.51–6.53 (m, 2 H), 6.67 (t, *J* = 7.5 Hz, 2 H), 6.77 (d, *J* = 7.6 Hz, 1 H), 6.78 (d, *J* = 7.5 Hz, 1 H), 6.85 (d, *J* = 7.5 Hz, 1 H), 6.86 (d, *J* = 7.5 Hz, 1 H), 6.93 (t, *J* = 1.8 Hz, 1 H), 7.00 (s, 2 H), 10.67 (s, 1 H). ^{13}C NMR (100 MHz, $CDCl_3$): δ = 9.9, 10.4, 17.6, 21.0, 23.0, 23.3, 30.8, 30.9, 53.3, 76.5, 77.1, 77.2, 121.4, 122.0, 122.1, 122.2, 125.8, 127.6, 128.1, 128.3, 128.5, 129.7, 130.7, 134.2, 134.5, 135.3, 135.4, 135.8, 138.7, 141.1, 156.1, 156.7, 156.8. MS (MALDI-TOF): Calcd for ($C_{53}H_{63}O_4N_2$): 791.5. Found: *m/z* 791.8 [$(M–Cl)^+$]. Anal. Calcd for ($C_{53}H_{63}O_4N_2Cl \times 1.1\ H_2O$): C 75.13%, H 7.76%, N 3.31%. Found: C 74.92%, H 7.65%, N 3.61%.

5-(3-Methylimidazolium)methyl-25,26,27,28-tetrapropoxycalix[4]arene-chloride (2b): 5-Chloromethyl-25,26,27,28-tetrapropoxycalix[4]arene (2.00 g, 3.12 mmol), 1-methylimidazole (276 µl, 3.50 mmol), and $CHCl_{3(abs.)}$ (20 mL) were refluxed for 1 d. After stirring in boiling Et_2O (70 mL), a colorless solid was obtained (1.08 g, 1.50 mmol, 48%). Mp 146 °C. IR (KBr): $\tilde{\nu}_{max}$ 3142 (m), 3060 (m), 2962 (s), 2932 (s), 2874 (s), 1725 (w), 1627 (w), 1586 (w), 1458 (s), 1385 (m), 1284 (m), 1247 (m), 1197 (s), 1163 (m), 1008 (s), 890 (w), 838 (w), 759 (m). ^{1}H NMR (400 MHz, $CDCl_3$): δ = 0.94 (t, *J* = 7.3, 6 H), 1.03 (t, *J* = 7.5 Hz, 3 H), 1.04 (t, *J* = 7.5 Hz, 3 H,), 1.85–2.01 (m, 8 H), 3.15 (pseudo t, *J* = 12.6 Hz, 4 H), 3.36 (d, *J* = 7.1 Hz, 2 H), 3.75 (d, *J* = 7.0 Hz, 2 H), 3.88–3.99 (m, 4 H), 4.05 (s, 3 H), 4.44 (d, *J* = 13.3 Hz, 2 H), 4.45 (d, *J* = 13.3 Hz, 2 H), 4.95 (s, 2 H), 6.32 (s, 2 H), 6.40

(dd, *J* = 2.3 Hz, 6.2 Hz, 1 H), 6.43 (t, *J* = 1.6 Hz, 1 H), 6.46–6.48 (m, 2 H), 6.73 (t, *J* = 7.3 Hz, 2 H), 6.81 (d, *J* = 7.5 Hz, 1 H), 6.82 (d, *J* = 7.5 Hz, 1 H), 6.87 (d, *J* = 7.5 Hz, 1 H), 6.88 (d, *J* = 7.5 Hz, 1 H), 7.19 (t, *J* = 1.5 Hz, 1 H), 10.28 (s, 1 H). ^{13}C NMR (100 MHz, $CDCl_3$): δ = 10.0, 10.4, 23.0, 23.2, 23.3, 30.8, 30.9, 36.6, 53.1, 76.5, 77.0, 121.1, 121.4, 122.2, 122.8, 125.2, 127.7, 128.2, 128.4, 128.7, 134.4, 135.3, 135.6, 135.9, 137.7, 156.0, 156.8, 156.9. MS (MALDI-TOF): Calcd for ($C_{45}H_{55}O_4N_2Cl$): 687.4. Found: *m/z* 687.4 [$(M–Cl)^+$]. Anal. Calcd for ($C_{45}H_{55}O_4N_2Cl \times 1.7\ H_2O$): C 71.68%, H 7.81%, N 3.72%. Found: C 71.61%, H 7.86%, N 3.69%.

5,17-Bis[(3-tert-butylimidazolium)methyl]-25,26,27,28-tetrapropoxycalix[4]arene-dichloride (3e):

5,17-Bis(chloromethyl)-25,26,27,28-tetrapropoxycalix[4]arene (2.00 g, 2.90 mmol), and 1-*tert*–butylimidazole (745 mg, 6.00 mmol) and $CHCl_{3(abs.)}$ (20 mL) were refluxed for 1 d. After stirring in boiling Et_2O (70 mL), the colorless product was obtained (2.59 g, 2.76 mmol, 95%). Mp 200–202 °C. IR (KBr): $\tilde{\nu}_{max}$ 3061 (m), 2963 (s), 2933 (s), 2875 (s), 1626 (w), 1586 (w), 1554 (m), 1463 (s), 1381 (m), 1283 (m), 1204 (s), 1133 (s), 1153 (m), 1008 (s), 889 (w), 836 (w), 758 (m). ^{1}H NMR (400 MHz, $CDCl_3$): δ = 0.89 (t, *J* = 7.6 Hz, 6 H), 1.11 (t, *J* = 7.3 Hz, 6 H), 1.70 (s, 18 H), 1.85–2.01 (m, 8 H), 3.17 (d, *J* = 13.6 Hz, 4 H), 3.70 (t, *J* = 6.8 Hz, 4 H), 4.02 (t, *J* = 7.8 Hz, 4 H), 4.46 (d, *J* = 13.4 Hz, 4 H), 4.93 (s, 4 H), 6.20 (s, 4 H), 6.69 (t, *J* = 1.8 Hz, 2 H), 6.95 (t, *J* = 7.3 Hz, 2 H), 7.13 (d, *J* = 7.6 Hz, 4 H), 7.86 (t, *J* = 2.0 Hz, 2 H), 10.51 (t, *J* = 1.5 Hz, 2 H). ^{13}C NMR (100 MHz, $CDCl_3$): δ = 9.6, 10.6, 22.7, 23.3, 29.9, 30.7, 52.7, 60.0, 76.4, 77.2, 120.2, 120.7, 122.5, 124.8, 128.6, 129.1, 134.8, 134.8, 136.2, 156.5, 157.3. MS (MALDI-TOF): Calcd for ($C_{56}H_{74}N_4O_4Cl$): 901.5. Found: *m/z* 901.7 [$(M–Cl)^+$]. Anal. Calcd for ($C_{56}H_{74}N_4O_4Cl_2 \times 2.6\ H_2O$): C 68.29%, H 8.10%, N 5.69%. Found: C 68.23%, H 8.00%, N 5.58%.

5,11,17,23-Tetrakis[(1-mesitylimidazolium)methyl]-25,26,27,28-tetrapropoxycalix[4]-arenetetrachloride (4):

5,11,17,23-Tetrakis(chloromethyl)-25,26,27,28-tetrapropoxycalix[4]arene (823 mg, 1.05 mmol), 1-mesitylimidazole (1.49 g, 8.00 mmol) and $CHCl_{3(abs.)}$ (10 mL) were refluxed for 2 d. After stirring in boiling Et_2O (30 mL), a light brown solid was obtained (1.56 g, 1.02 mmol, 97%). Mp > 220 °C (decomp.). IR (KBr): $\tilde{\nu}_{max}$ 2960 (s), 2926 (s), 2873 (s), 1607 (m), 1545 (s), 1464 (s), 1386 (w), 1289 (w), 1205 (s), 1157 (s), 1066 (m), 1007 (m), 854

(m), 754 (m), 669 (w). ^{1}H NMR (400 MHz, $CDCl_3$): δ = 1.00 (t, *J* = 7.5 Hz, 12 H), 1.88–2.00 (m, 8 H), 1.97 (s, 24 H), 2.31 (s, 12 H), 3.24 (d, *J* = 13.0 Hz, 4 H), 3.82 (t, *J* = 7.5 Hz, 8 H), 4.42 (d, *J* = 13.0 Hz, 4 H), 5.61 (s, 8 H), 6.95 (s, 8 H), 7.09 (t, *J* = 1.8 Hz, 4 H), 7.26 (s, 8 H), 8.41 (t, *J* = 1.7 Hz, 4 H), 10.34 (t, *J* = 1.5 Hz, 4 H). ^{13}C NMR (100 MHz, $CDCl_3$): δ = 10.2, 17.5, 21.0, 23.2, 30.4, 52.8, 76.9, 122.8, 124.2, 128.2, 129.3, 129.7, 130.9, 134.2, 135.6, 137.4, 140.9, 156.8. MS (MALDI-TOF): Calcd for ($C_{92}H_{108}O_4N_8$): 1389.9. Found: *m/z* 1390.5 [$(M - 4\ Cl)^+$]. Anal. Calcd for ($C_{92}H_{108}O_4Cl_4N_8 \times 5\ H_2O$): C 68.13%, H 7.33%, N 6.91%. Found: C 68.03%, H 7.25%, N 6.67%.

Distal bridged imidazoliumcalix[4]arene-chloride (5):

A solution of 5,17-bis(chloromethyl)-25,26,27,28-tetrapropoxycalix[4]arene (2.00 g, 2.90 mmol) in $CHCl_3$ (10 mL) was added slowly to a solution of imidazole (1.97 g, 29.0 mmol) in $CHCl_3$ (50 mL). After stirring for 4 h at rt the mixture was heated under reflux for an additional hour. The organic layer was separated and washed (50 mL 3 N NaOH, 4 × 50 mL H_2O). The obtained solid was suspended for 4 h in refluxing EtOAc, isolated by filtration, and dried in vacuo (1.40 g, 1.94 mmol, 67%). Mp > 280 °C (decomp.). IR (KBr): $\tilde{\nu}_{max}$ 3160 (m), 3069 (m), 2960 (s), 2932 (s), 2873 (s), 1614 (m), 1586 (w), 1564 (m), 1464 (s), 1385 (m), 1326 (w), 1281 (m), 1218 (s), 1174 (m), 1133 (s), 1008 (s), 891 (w), 835 (w), 778 (m). ^{1}H NMR (400 MHz, $CDCl_3$): δ = 0.93 (t, *J* = 7.5 Hz, 6 H), 1.12 (t, *J* = 7.3 Hz, 6 H), 1.88–1.97 (m, 4 H), 2.00–2.10 (m, 4 H), 3.22 (d, *J* = 13.4 Hz, 4 H), 3.70 (t, *J* = 7.0 Hz, 4 H), 4.12 (t, *J* = 8.5 Hz, 4 H), 4.51 (d, *J* = 13.1 Hz, 4 H), 4.85 (s, 4 H), 5.00 (s, 1 H), 6.37 (s, 4 H), 6.92 (t, *J* = 7.5 Hz, 2 H), 7.13 (d, *J* = 7.6 Hz, 4 H), 8.12 (d, *J* = 1.5 Hz, 2 H). ^{13}C NMR (100 MHz, $CDCl_3$): δ = 9.7, 10.6, 22.8, 23.4, 30.8, 53.1, 76.6, 77.7, 123.2, 123.8, 124.2, 129.2, 129.9, 131.1, 135.6, 136.2, 156.4, 156.8. MS (MALDI-TOF): Calcd for ($C_{45}H_{53}N_2O_4$): 685.4. Found: *m/z* 685.6 [$(M - Cl)^+$]. Anal. Calcd for ($C_{45}H_{53}N_2O_4Cl \times 1.9\ H_2O$): C 71.53%, H 7.58%, N 3.71%; found: C 71.51%, H 7.63%, N 3.74%.

Appendix

With the exception of imidazolium salt **4**, all compounds studied exchange with pseudo-first-order kinetics according to Equation 2.3.

$$v = -\frac{d[I]}{dt} = k[I] \qquad 2.3$$

In Equation 2.3, *v* is the reaction rate, *k* the rate constant and *[I]* the integral of the C^2-proton. To determine rate constants k, Equation 2.3 was solved as follows:

$$\int_{[I]_0}^{[I]} \frac{d[I]}{[I]} = -\int_0^t k dt \qquad 2.4$$

$$\ln[I] = -kt + \ln[I]_0 \qquad 2.5$$

$$[I] = [I]_0 * e^{-kt} \qquad 2.6$$

The experimental data were fit using Equation 2.6 with $[I]_0$ fixed to the experimental value at t=0.

The rate constants for each salt were determined by at least three independent measurements of a 0.155 M solution of the salt (concerning imidazolium units). Some examples for the determination of *k*-values are given in Figure 2.3 and Figure 2.4.

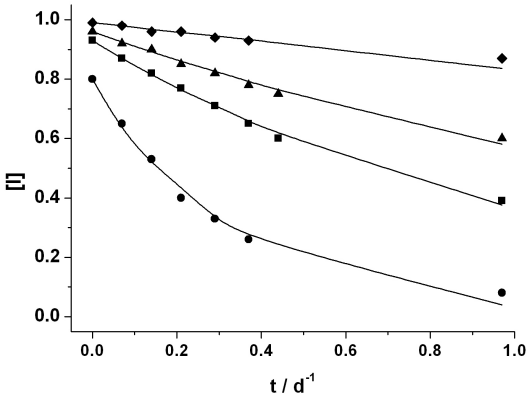

Figure 2.3. Examples for the H/D exchange of the open-chain imidazolium salts **1a** (squares), **1b** (triangles), **1e** (dots) and **1f** (diamonds). The solid lines were obtained by a pseudo-first-order non-linear curve fit with Equation 2.6.

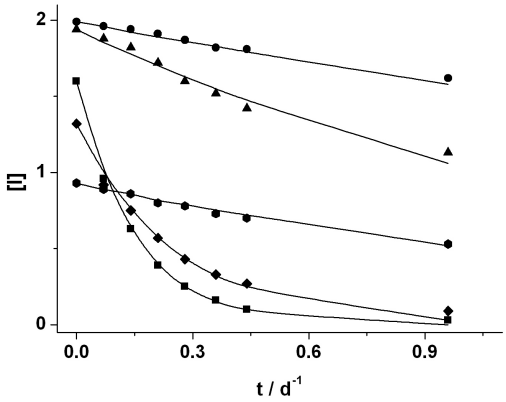

Figure 2.4. Examples for the H/D exchange of the calixarene-based imidazolium salts **2a** (hexagons), **3a** (squares), **3c** (triangles), **3d** (dots) and **3i** (diamonds). The solid lines were obtained by a pseudo-first- order non-linear curve fit with Equation 2.6.

Additional Comments

The reasoning why certain imidazolium salts undergo faster H/D exchange than others is not trivial. Since the results presented in this paper were published, a series of other imidazolium salts was synthesized by Schatz and co-workers and their kinetic acidity was investigated. In many cases, aryl groups directly attached to the imidazolium backbone accelerate the exchange, whereas alkyl substitution in most cases has only a small or no influence on the exchange rates. The attachment of imidazolium units to other molecular platforms than calix[4]arenes, such as benzene rings, leads to dramatic changes in the kinetic acidity.

If we assume that the intermediate carbene is close to the transition state in the H/D exchange reaction (see Scheme 2.1), then the stabilization of this carbene should accelerate the reaction because of the decreased activation energy. That means that substituents on the imidazolium core that have a positive inductive or mesomeric effect lead to faster exchange compared to for example proton substituents which is reflected in Table 2.1. The mesomeric effect of aromatic substituents could also be supported by additional data collected in the Schatz group. The trend that *ortho*-substitution is less beneficial than *meta*- or *para*-substitution, especially in the case of bulky groups such as diisopropyl or nitro, indicates that the angle between the imidazolium ring and the aromatic group and therewith the mesomeric conjugation between the two changes with substitution as was already found in the solid state (phenyl ca. 30°, mesityl 60-75° and 2,6-diisopropylphenyl 80-90°). The finding that the supramolecular surrounding has a big influence on the rates can be reasoned for example by different solvation of the imidazolium salts or the complexation of the counter ion that might act as a base or hamper the interaction with solvent molecules that might be needed for the deprotonation.

In summary, some trends can be found for the different H/D exchange rates of imidazolium salts in methanol-d_4 but the number of exceptions is too large to enable a better understanding of the exchange process. Further investigations should be directed towards the understanding of e.g. a possible correlation between thermodynamic and kinetic acidity, the influence of the anion on the exchange and the validation of the assumption that the protonation of the carbene is fast compared to its formation.

References

1 Breslow, R. *J. Am. Chem. Soc*. **1958**, *80*, 3719.

2 Wanzlick, H.-W.; Schikora, E. *Angew. Chem.* **1960**, *72*, 494.

3 Olofson, R. A.; Thompson, W. R.; Michelman, J. S. *J. Am. Chem. Soc.* **1964**, *86*, 1865.

4 a) Vaughan, J. D.; Mughrabi, Z.; Chung Wu, E. *J. Org. Chem.* **1970**, *35*, 1141; b) Haake, P.; Bausher, L. P.; Miller W. B. *J. Am. Chem. Soc* **1969**, *91*, 1113.

5 Arduengo III, A. J.; Harlow, R. L.; Kline, M. *J. Am. Chem. Soc.* **1991**, *113*, 361.

6 a) Miyaura, N.; Suzuki, A. *Chem. Rev.* **1995**, *95*, 2457; b) Bourissou, D.; Guerret, O.; Gabbai, F.; Bertrand, G. *Chem. Rev.* **2000**, *100*, 39; c) Hillier, A. C.; Nolan, S. P. *Platinum Metals Rev.* **2002**, *46*, 50; d) Littke, A. F.; Fu, G. C. *Angew. Chem. Int. Ed.* **2002**, *41*, 4176.

7 a) Enders, D.; Balensiefer, T. *Acc. Chem. Res.* **2004**, *37*, 534; b) Singh, R.; Kissling, R. M.; Letellier, M.-A.; Nolan, S. P. *J. Org. Chem.* **2004**, *69*, 209; c) Nair, V.; Bindu, S.; Sreekumar, V. *Angew. Chem.* **2004**, 116, 5340; *Angew. Chem. Int. Ed*. **2004**, *43*, 5130.

8 a) Alder, R. W.; Allen, P. R.; Williams, S. J. *J. Chem. Soc., Chem. Commun*. **1995**, 1267; b) Kim, Y.-J.; Streitwieser, A. *J. Am. Chem. Soc.* **2002**, *124*, 5757; c) Chen, H.; Justes, D. R.; Cooks, R. G. *Org. Lett.* **2005**, *7*, 3949; d) Magill, A. M.; Cavell, K. J.; Yates, B. F. *J. Am. Chem. Soc*. **2004**, *126*, 8717.

9 Amyes, T. L.; Diver, S. T.; Richard, J. P.; Rivas, F. M.; Toth, K. *J. Am. Chem. Soc.* **2004**, *126*, 4366.

10 Diederich, F.; Lutter, H.-D. *J. Am. Chem. Soc.* **1989**, *111*, 8438.

11 Frank, M.; Maas, G.; Schatz, J. *Eur. J. Org. Chem.* **2004**, 607.

12 a) Cowan, J. A.; Clyburne, J. A. C.; Davidson, M. G.; Harris, R. L. W.; Howard, J. A. K.; Küpper, P. L. M. A.; Richards, S. P. *Angew. Chem.* **2002**, *114*, 1490; b) Ramnial, T.; Jong, H.; McKenzie, I. D.; Jennings, M.; Jason, A. C. *Chem. Commun.* **2003**, 1722; c) Arduengo III, A. J.; Gamper, S. F.; Tamm, M.; Calabrese, J. C.; Davidson, F.; Craig, H. A. *J. Am. Chem. Soc.* **1995**, *117*, 572.

13 a) Ramos, S.; Alcade, E.; Doddi, G.; Mencarelli, P.; Luisa, P.-G. *J. Org. Chem.* **2002**, *67*, 8463; b) Sunggoo, Y.; Ihm, H.; Kim, H. G.; Lee, C.-W.; Indrajit, B.; Oh,

K. S.; Gong, Y. J.; Lee, J. W.; Yoon, J.; Lee, H. C.; Kim, K. S. *J. Org. Chem* **2003**, *68*, 2467; c) Kim, S. K., Kang, B.-G, Koh, H. S., Yoon, Y. J., Jung, S. J., Jeong, B., Lee, K.-D, Yoon, J. *Org. Lett.* **2004**, *6*, 4655.

14 a) Brendgen, T.; Frank, M.; Schatz, J. *Eur. J. Org. Chem.* **2006**, 2378; b) Huang, J.; Nolan, S. P. J. *J. Am. Chem. Soc.* **1999**, *121*, 9889; c) Arduengo III, A. J.; Krafczyk, R.; Schmutzler, R. *Tetrahedron* **1999**, *55*, 14523.

3 Information Transfer in Calix[4]arenes: Influence of *Upper Rim* Substitution on Alkaline Metal Complexation at the *Lower Rim*

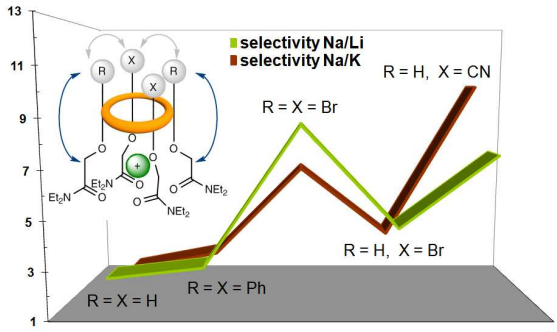

The contents of this chapter have been adapted from:
Schühle, D. T.; Klimosch, S.; Schatz, J.; *Tetrahedron Lett.* **2008**, *49*, 5800.

Introduction

Ion channels play a key role in the transport of ions across cell membranes. The best known result of such transport is the difference in concentration of alkaline metal ions between the inside and the outside of cells: the extracellular concentrations of Na^+ and K^+ are 140 mM and 5 mM, respectively, whereas the intracellular concentrations in humans have about the opposite magnitude (5 mM and 150 mM).[1] Nature has developed very effective strategies to control this concentration difference in order to ensure a proper functioning of cells.

To gain more insight into the mechanism of how these natural systems function, supramolecular chemists try to develop artificial model systems mimicking the action of ion channels or ion transportation systems. Some of the major challenges are the design of synthetic channels with high metal binding selectivity, the possibility to include these compounds into artificial bilayers and the need to completely span this bilayer (~40 Å).[1] An approach to fulfil these requirements is to include molecules that have proven to bind ions with good selectivity into liposomal bilayers that serve as model compounds for cell membranes.[2] Amongst other good chelators such as crown ethers, some calix[4]arene derivatives are known to bind ions while maintaining their hydrophobicity and thus their ability to be included into bilayers. Therefore, it is not surprising that this class of compounds found some application in the design of artificial transmembrane ion transporters.[1,3]

Previously, it has been shown that *cone*-calix[4]areneamides are able to complex metal ions and therefore, they found applications in various fields.[4-14] Especially, calix[4]arenetetraamides (Figure 3.1) show interesting features in the complexation of Li^+, Na^+ and K^+ ions and therefore, they were used as lead structures in artificial transmembrane ion transport systems.[1,15,16]

An easy and fast way to screen the binding abilities of this type of compound is by performing extraction experiments of metal salts from an aqueous solution into a solution of the metal binding compound in an organic solvent. The absolute values of the extraction efficiency are of minor importance for application as ion transporters whereas the selectivity factors for certain ions are of big interest for this application. The preference of

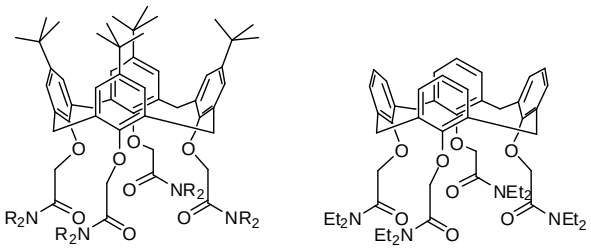

1 a R = Et
b R = $(CH_2)_4$
c R = Pr
d R = Bu
e R = Allyl
f R = Propargyl
g R = Benzyl

2

Figure 3.1. Structures of some metal chelators based on calix[4]arenes.

compounds for particular metal ions can be expressed by selectivity factors S. For example, the selectivity for alkaline metal ions by **1** (see Figure 3.1) can be given by the ratio of the mole percent extraction Na^+/mole percent extraction M^+ (M = Li, K).[17] As shown in Table 3.1, variation of the *N*-substituents in **1** leads to significant changes in the selectivity in picrate extraction experiments.

Table 3.1. Selectivity factors S for picrate extraction of alkali picrates from H_2O into CH_2Cl_2 at 20 °C.

Chelator	S (Na^+/K^+)[a]	S (Na^+/Li^+)[a]
1a	1.3	1.5
1b	1.6	1.9
1c	1.2	1.3
1d	1.2	1.4
1e	1.4	2.3
1f	6.7	8.8
1g	1.4	2.2
2	1.7	2.5

[a] Values calculated from ref. [17,18]

The influence of *upper rim* substitution on the metal complexation at the *lower rim* is demonstrated by the selectivity factors of **2** compared to those of its alkylated derivative **1a**: both selectivity factors show that **2** has a higher selectivity for Na^+ than **1a**. This difference has been attributed to the larger conformational mobility of **2** and to its better solvation which decreases its binding ability towards alkaline metal cations.[18]

The finding that weaker complexation might lead to enhanced selectivity inspired us to synthesize new calix[4]arenetetraamides bearing different substituents on the *upper rim* of the molecule. We introduced electron-withdrawing groups (Br, CN) to decrease the electron density at the phenolic oxygen atoms or phenyl rings to mimic steric effects that might occur upon changing the substitution pattern.

Results and Discussion

Synthesis

Tetrabromo-calix[4]arene **3** was obtained by bromination of **2** using *N*-bromosuccinimide (NBS). The $Pd(PPh_3)_4$ catalyzed Suzuki reaction with phenylboronic acid in a toluene/methanol mixture yielded **4** (Scheme 3.1).

Bisprotected calix[4]arene **5** was prepared by bisbenzoylation of tetrahydroxycalix[4]arene in distal position (Scheme 3.2). During the subsequent bromination to the dibromo derivative **6**, it turned out that the excess of bromine in the reaction mixture could be more easily removed by cyclohexene than with the commonly applied sulfur based quenching agents. Deprotection in boiling ethanol/water proceeded smoothly and calixarene **7** was obtained after alkylation with *N*,*N*-diethylbromoacetamide in DMF/THF using a standard protocol.[19] *N*,*N*-Diethylbromoacetamide was prepared by a modified literature procedure with a change in the work-up enabling the synthesis of this compound on a large scale and with high purity.[20]

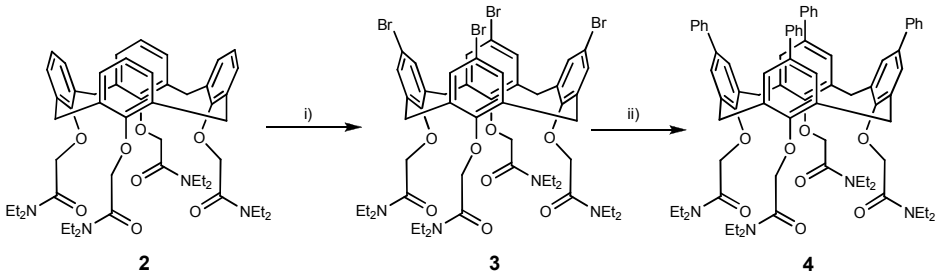

Scheme 3.1. Synthesis of **3** and **4**. i) NBS, butanone, 5 d, rt, 51%; ii) $PhB(OH)_2$, $Pd(PPh_3)_4$, Cs_2CO_3, $PhCH_3$, MeOH, 16 h, 70 ºC, 72%.

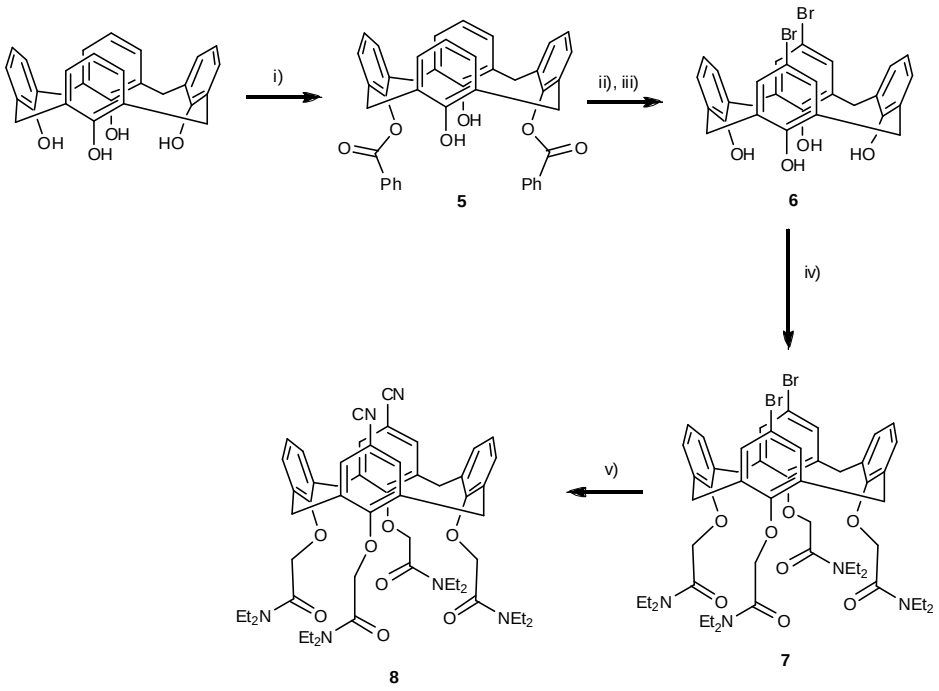

Scheme 3.2. Synthesis of **7** and **8**. i) PhCOCl, TEA, MeCN, 3 d, rt, 70%; ii) Br_2, $CHCl_3$, 1 d, rt, 85%; iii) NaOH, EtOH, H_2O, 95%; iv) $BrCH_2CONEt_2$, NaH, DMF, THF, 4 d, rt, 54%; v) CuCN, NMP, 22 h, 200 ºC, 11%.

While a previous attempt of another group to synthesize dicyano-calix[4]arene **8** by a palladium catalyzed reaction was not successful, we could obtain this compound using CuCN in NMP although the yield was rather poor.[19,21] This reaction was not optimized further since a sufficient amount of **8** could be obtained by this methodology.

Extraction Studies

Extraction of metal picrate salts from aqueous into organic solution is a powerful, fast, reliable and well-established method in supramolecular chemistry. From its early days until today, this technique has found many applications.[22,23]

Our main interest lies in the complexation of physiologically relevant alkaline metal ions. Therefore, the extraction experiments were performed with lithium, sodium and

potassium picrate. The extractions were performed from aqueous solution into dichloromethane at 20 °C (Table 3.2).[18]

The binding stoichiometry of the complex between the calixarenetetraamide and the metal ions is 1:1, which was exemplarily confirmed by a Job's plot analysis for **2** (data not shown) as well as by literature data.[16,21] The extraction percentages obtained for ligand **2** are consistent with the literature.[18]

Table 3.2. Mole percent extraction (%E)[a)] of alkali picrates from H_2O into CH_2Cl_2 at 20 °C.

Chelator	Li^+	Na^+	K^+	S (Na^+/Li^+)	S_{rel}	S (Na^+/K^+)	S_{rel}
2	38.5	91.4	55.2	2.4	=1	1.7	=1
3	6.3	54.7	8.5	8.7	3.6	6.4	3.8
4	31.0	87.7	36.5	2.8	1.2	2.4	1.4
7	17.5	78.1	23.3	4.5	1.9	3.4	2.0
8	5.6	41.8	4.1	7.5	3.1	10.2	6.0

[a)] Mean value of at least three independent experiments. Errors of %E generally ≤ 2%.

To the best of our knowledge, the influence of chemical modifications on one side of the calix[4]arene backbone on the guest binding on its other side has been rarely studied. An early example published by Ungaro and co-workers is the complexation of anions by **9** bearing a thiourea unit as a binding motif for anions and the tetraamide pattern also used in the present work.[21]

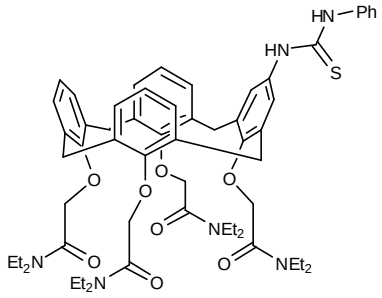

9

Figure 3.2. Anion receptor **9** as published by Ungaro et al.[21]

In the presence of Na^+-ions, **9** binds anions stronger and shows a lower selectivity towards e.g. acetate than in the absence of Na^+-ions. The authors attributed this to an electron-withdrawing effect and rigidification of the calixarene backbone upon complexation. Furthermore, changes in the solvation might contribute to the observed increase in binding capability.[18]

The changes in the extraction behavior as shown in Table 3.2 are a consequence of the same phenomena, which makes a quantitative evaluation impossible. Qualitatively, it can be concluded that also in **3**, **4**, **7** and **8** an 'information transfer' occurs between the two different rims of the calixarene backbone.

Comparison of the sodium ion selectivity of the benchmark ligand **2** with the functionalized ligands **3**, **4**, **7** and **8** shows that electron withdrawing substituents increase the sodium selectivities over K^+ and Li^+ roughly by a factor of 2–6 as expressed by the relative selectivity factors S_{rel}. This can be rationalized by the electron withdrawing effects of the bromo and cyano groups in **3**, **7** and **8**, which decrease the electron density at the phenolic oxygen atoms and therefore, weaken the binding ability of the receptors towards cations. The strong decrease in mainly Li^+- and K^+-binding leads to better selectivity in all cases. The selectivity for Na^+ is qualitatively correlated with the number of such electron-withdrawing groups. For example, dibromo ligand **7** exhibits only about twice the Na^+ selectivity compared to the unsubstituted ligand **2**, whereas tetrabromo-calixarene **3** has about fourfold selectivity. Comparison of ligands **7** and **8** clearly shows that the mesomeric effect of the nitrile groups on the binding abilities of the phenolic oxygen atoms is more effective than the inductive effects caused by bromo-substitution and leads to a better sodium selectivity compared to both, lithium and potassium. Dicyano-calixarene **8** is the only compound studied which shows a higher Na^+/K^+ than Na^+/Li^+ selectivity. This may be explained by additional steric reasons and possibly different solvation. The CN-groups exhibit a strong electron-withdrawing effect parallelled by less sterical demand compared to the bromo group. Therefore, the ligand sphere located at the *lower rim* is less distorted by the nitrile substituent and the general sodium selectivity resulting from an increasing electron-withdrawing effect can be deployed more effectively.

We explain the small differences between **2** and **4** by mainly steric interactions of the phenyl groups with each other leading to a change in the geometry of the ligand. The repulsion between the phenyl rings seems to lead to a reduced size of the cavity spanned by

the amide groups on the *lower rim* of calixarene **4**, since the biggest ion (K^+) experiences a significant decrease in affinity to **4**. Changes in solvation and minor electronic effects cannot be excluded.

Conclusions

In conclusion, we synthesized new calix[4]arene tetraamides and performed extraction experiments towards CH_2Cl_2 of biologically relevant alkaline metal ions in the form of their picrate salts in water. The decreased binding ability towards these cations leads to enhanced Na^+ selectivity over Li^+ and K^+ in extractions. This is attributed mainly to the more dramatic decrease in Li^+ or K^+ binding compared to Na^+. However, this general trend is fine-tuned by a subtle interplay between the electronic and steric effects exerted by the substituents located at the *upper rim* whose characteristics are transferred to the binding site at the *lower rim* by the calix[4]arene backbone acting as an electronic and steric "hinge". Besides, changes in the flexibility and solubilization of the various compounds can play an additional role in the metal ion binding. The new, more selective cation receptors or derivatives thereof have potential to be included into liposomes giving access to models for cation transportation across lipid bilayers.

Experimental

The extraction studies were performed according to Ungaro et al.[18] Equimolar solutions of calixarene in CH_2Cl_2 and picrate in water ($2.5 \cdot 10^{-4}$ M) were mechanically shaken for 3 min and then stirred vigorously for 30 min at 25 °C. The amount of picrate remaining in the aqueous phase was determined by UV measurements at 355 nm. Compound **2** was prepared using a literature procedure.[24] Tetrahydroxycalix[4]arene is readily available following a known method.[25]

***N*,*N*-Diethylbromoacetamide**.

A solution of bromoacetyl bromide (53.0 mL, 608 mmol) in CH_2Cl_2 (400 mL) was added to a solution of diethylamine (63.0 mL, 608 mmol) and triethylamine (85.0 mL, 608 mmol) in CH_2Cl_2 (800 mL) at 0 °C. After stirring for 2 h at ambient temperature, the solution was washed with 2 N HCl (250 mL) and brine (1.00 L). The solution was dried over anhydrous

Na_2SO_4 and the solvent was removed. The slightly yellow product (75.4 g, 388 mmol, 64%) was obtained by distillation (88 °C, 0.17 mbar). IR (KBr, $\tilde{\nu}_{max}$): 2975, 2935 (s) 1645 (s), 1463 (s), 1381 (m), 1362 (m), 1312 (m), 610 (s), 559 (m). ^{1}H NMR (400 MHz, $CDCl_3$): δ 1.15 (3 H, t, *J*= 7.1 Hz, CH_2CH_3), 1.27 (3 H, t, *J*= 7.2 Hz, CH_2CH_3), 3.40 (2 H, q, *J*= 7.1 Hz, CH_2CH_3), 3.41 (2 H, q, *J*= 7.2 Hz, CH_2CH_3), 3.89 (2 H, s, Br-CH_2).

^{13}C NMR (100 MHz, $CDCl_3$): δ 12.26, 14.13 (CH_2CH_3), 26.11 (Br-CH_2), 40.44, 42.84 (CH_2CH_3), 165.91 (C=O). MS *m/z* (CI): calcd. for ($C_6H_{12}BrNO$), 194, found 194 (M^+). Anal. calcd. for $C_6H_{12}BrNO$: C, 37.13%; H, 6.23%; N, 7.22%. Found: C, 37.10%; H, 6.22%; N, 7.19%.

5,11,17,23-Tetrabromo-25,26,27,28-tetrakis-(*N*,*N*-diethylamino-carbonylmethoxy)-calix[4]arene (3).

To a stirred solution of 25,26,27,28-tetrakis-(*N*,*N*-diethylaminocarbonylmethoxy)-calix[4]arene (**2**) (19.3 g, 22.0 mmol) in butanone (1.00 L), NBS (59.0 g, 331 mmol) was added. After stirring for 5 d at ambient temperature, cyclohexene (50 mL) was added and the solvent was partially removed. *n*-Hexane (500 mL) was added and the precipitated yellow solid was recrystallized from $CHCl_3$/MeOH to yield the product (13.2 g, 11.1 mmol, 51%) as a white solid. Mp. 251 – 260 °C. IR (KBr, $\tilde{\nu}_{max}$): 2973 (s), 2930 (s) (C-H); 1656 (s), 1461 (m) (C-H); 1379 (m), 1359 (m), 1304 (m), 1267 (m), 1203 (m), 1147 (m), 855 (w). ^{1}H NMR (400 MHz, $CDCl_3$): δ 1.07 (12 H, t, *J* = 6.9 Hz, CH_2-CH_3), 1.14 (12 H, t, *J* = 7.1 Hz, CH_2-CH_3), 3.15 (4 H, d, *J* = 13.6 Hz, Ar-CH_2^{eq}-Ar), 3.28 (8 H, q, *J* = 7.2. Hz, CH_2-CH_3), 3.32 (8 H, q, *J* = 6.9 Hz, CH_2-CH_3), 4.89 (8 H, s, O-CH_2), 5.29 (4 H, d, *J* = 13.6 Hz, Ar-CH_2^{ax}-Ar), 6.81 (8 H, s, Ar-*H*). ^{13}C NMR (100 MHz, $CDCl_3$): δ 13.02, 14.24 (CH_2-CH_3), 31.63 (Ar-CH_2-Ar), 39.96, 40.77 (CH_2-CH_3), 71.63 (O-CH_2), 115.40, 131.20, 136.35, 155.78 (Ar-*C*), 168.13 (*C*=O). MS *m/z* (MALDI-TOF): calcd. for ($C_{52}H_{64}Br_4N_4O_8$), 1192.7, found 1192.3 (M^+). Anal. calcd. for ($C_{52}H_{64}Br_4N_4O_8$): C, 52.37%; H, 5.41%; N, 4.70%. Found: C, 52.43%; H, 5.43%, N, 4.76%.

5,11,17,23-Tetraphenyl-25,26,27,28-tetrakis-(*N*,*N*-diethylamino-carbonylmethoxy)-calix[4]arene (4).

Under argon, 5,11,17,23-tetrabromo-25,26,27,28-tetrakis-(*N*,*N*-diethylamino-carbonyl-methoxy)-calix[4]arene (**3**) (1.50 g, 1.26 mmol) and Cs_2CO_3 (4.20 g, 12.6 mmol) were dissolved in dry toluene (25 mL) and $Pd(PPh_3)_4$ (152 mg, 0.13 mmol) was added. The

solution was degassed and phenylboronic acid (1.54 g, 12.6 mmol) dissolved in anhydrous MeOH (25 mL) was added. After stirring for 16 h at 70 °C, the suspension was cooled to ambient temperature. After filtration, the solvents were removed and the crude product was dissolved in $CHCl_3$ (60 mL). This solution was washed with 1 N HCl (2 × 60 mL) and H_2O (2 × 60 mL) and dried over anhydrous Na_2SO_4. The product 1.07 g (0.91 mmol, 72%) was obtained by treating the oil with boiling *n*-hexane, filtration and drying in vacuo. Mp. 224 – 226 °C. IR (KBr, $\tilde{\nu}_{max}$): 3028 (w), 2972 (m), 2929 (m), 1662 (s), 1467 (m), 1380 (w), 1359 (w), 1310 (m), 1266 (m), 1231 (m), 1180 (m), 1147 (m), 1082 (m), 1055 (m), 947 (w), 874 (w), 762 (m), 697 (m). ^{1}H NMR (400 MHz, $CDCl_3$): δ 1.11 (12 H, t, *J* = 7.2 Hz, CH_2-C*H*$_3$), 1.18 (12 H, t, *J* = 7.2 Hz, CH_2-C*H*$_3$), 3.33 – 3.40 (20 H, m, Ar-C*H*$_2^{eq}$-Ar and C*H*$_2$-CH_3), 5.07 (4 H, s, O-C*H*$_2$), 5.45 (4 H, d, *J* = 13.4 Hz, Ar-C*H*$_2^{ax}$-Ar), 6.95 (8 H, s, Ar-*H*), 7.08 – 7.12 (20 H, m, Ar-*H*). ^{13}C NMR (100 MHz, $CDCl_3$): δ 13.10, 14.31 (CH_2-*C*H_3), 32.30 (Ar-*C*H_2-Ar), 39.88, 40.83 (*C*H_2-CH_3), 71.73 (O-*C*H_2), 126.08, 126.61, 127.31, 128.23, 134.80, 135.34, 141.08, 156.31 (Ar-*C*), 168.74 (*C*=O). MS *m/z* (MALDI-TOF): calcd for ($C_{76}H_{84}N_4O_8$), 1181.5, found 1181.8 (M^+). Anal. calcd for ($C_{76}H_{84}N_4O_8$) 0.2·$CHCl_3$: C, 75.93%; H, 7.04%; N, 4.65%. Found: C, 76.02%; H, 7.09%, N, 4.47%.

25,27-Dibenzoyloxy-26,28-dihydroxycalix[4]aren (5).

Benzoyl chloride (17.7 mL, 152 mmol) was added to a suspension of tetrahydroxycalix[4]arene (25.0 g, 58.9 mmol) and triethylamine (81.8 mL, 587 mmol) in acetonitrile (1150 mL). After stirring for 3 d at ambient temperature, the precipitate was filtered off and recrystallized from $CHCl_3$/MeOH. The colorless solid was dried at 60 °C in high vacuo to give 26.2 g (41.5 mmol, 70%) of the bisprotected calix[4]arene. Mp 264.3 – 264.6 °C. IR (KBr, $\tilde{\nu}_{max}$): 3519 (br s), 3022 (m), 2926 (s), 2854 (s), 1739 (s), 1584 (m), 1462 (m), 1318 (m), 1265 (s), 1242 (s), 1204 (m), 1173 (s), 1146 (s), 1082 (m), 1048 (s), 1020 (s), 904 (w), 864 (w), 799 (m), 754 (s), 711 (s). ^{1}H NMR (400 MHz, $CDCl_3$): δ 3.53 (4 H, d, *J* = 14.1 Hz, Ar-C*H*$_2^{eq}$-Ar), 4.00 (4 H, d, *J* = 14.1 Hz, Ar-C*H*$_2^{ax}$-Ar), 5.50 (2 H, s, O*H*), 6.71 (2 H, t, *J* = 7.5 Hz, Ar-*H*), 6.79 – 6.83 (2 H, m, Ar-*H*), 6.89 (4 H, d, *J*= 7.5 Hz, Ar-*H*), 7.05 (4 H, d, *J* = 7.6 Hz, Ar-*H*), 7.54 (4 H, t, *J* = 8.0 Hz, Ar-*H*), 7.72 (2 H, tt, *J*= 7.5 Hz and 1.13 Hz, Ar-*H*), 8.38 (4 H, dd, *J* = 8.5 Hz and 1.4 Hz, Ar-*H*). ^{13}C NMR (100 MHz, $CDCl_3$): δ 32.48 (Ar-*C*H_2-Ar), 119.91, 126.66, 128.14, 128.93, 128.99, 129.14, 129.23, 130.55, 132.32, 133.88, 145.46, 152.83 (Ar-*C*), 164.82 (*C*=O). MS *m/z* (MALDI-TOF):

calcd. for ($C_{42}H_{32}O_6$), 632.7, found 632.3 (M^+). Anal. calcd. for $C_{42}H_{32}O_6 \cdot 0.05\ CHCl_3$: C, 79.08%; H, 5.06%. Found: C, 79.07%; H, 5.22%.

5,17-Dibromo-25,27-dibenzoyloxy-26,28-dihydroxycalix[4]arene.

To a solution of 25,27-dibenzoyloxy-26,28-dihydroxycalix[4]arene (**5**) (25.0 g, 39.5 mmol) in $CHCl_3$ (675 mL) bromine (32.5 mL, 639 mmol) was slowly added. After stirring for 1 h at ambient temperature, cyclohexene (300 mL) was added very slowly and stirred for another 15 min. This solution was washed with 1 N HCl (2 × 300 mL) and H_2O (2 × 300 mL). The organic solvent was evaporated to give the title compound (26.5 g, 33.6 mmol, 85%). Mp. 305 – 306 °C. IR (KBr, $\tilde{\nu}_{max}$): 3504 (br s), 3062 (m), 2916 (s), 1706 (s), 1599 (w), 1583 (w), 1454 (m), 1313 (m), 1270 (s), 1201 (m), 1170 (s), 1089 (m), 1064 (s), 1021 (s), 920 (w), 861 (m), 790 (m), 753 (m), 711 (s). ^{1}H NMR (400 MHz, $CDCl_3$): δ 3.53 (4 H, d, *J* = 14.4 Hz, Ar-C*H*$_2^{eq}$-Ar), 3.85 (4 H, d, *J* = 14.4 Hz, Ar-C*H*$_2^{ax}$-Ar), 5.20 (2 H, s, O*H*), 6.92 – 7.01 (2 H, m, Ar-*H*), 7.00 (4 H, d, *J* = 6.8 Hz, Ar-*H*), 7.11 (4 H, s, Ar-*H*), 7.62 (4 H, t, *J* = 7.8 Hz, Ar-*H*), 7.76 (2 H, t, *J* = 7.5 Hz, Ar-*H*), 8.25 (4 H, d, *J* = 8.1 Hz, Ar-*H*). ^{13}C NMR (100 MHz, $CDCl_3$): δ 33.07 (Ar-*C*H$_2$-Ar), 111.75, 126.72, 128.58, 129.26, 129.66, 129.84, 130.44, 131.73, 132.02, 134.00, 146.11, 152.02 (Ar-*C*), 164.52 (*C*=O). MS *m/z* (MALDI-TOF): calcd. for ($C_{42}H_{30}Br_2O_6$), 790.5, found 813.1 ((M+Na)$^+$). Anal. calcd. for ($C_{42}H_{30}Br_2O_6$)·0.3 $CHCl_3$: C, 61.49%; H, 3.70%. Found: C, 61.58%; H, 3.83%.

5,17-Dibromo-25,27,26,28-tetrahydroxycalix[4]arene (6)

A solution of 5,17-dibromo-25,27-dibenzoyloxy-26,28-dihydroxycalix[4]arene (22.7 g, 28.67 mmol) and NaOH (80 g, 2.00 mol) in EtOH (1.00 L) and H_2O (1.00 L) was stirred for 3 d at 70 °C. After the addition of 2 N HCl (1.50 L), the precipitate was collected, dissolved in $CHCl_3$ and dried over anhydrous Na_2SO_4. After the removal of the solvent, the deprotected calix[4]arene **6** (15.8 g, 27.2 mmol, 95%) was obtained as a colorless solid. Mp. 341 – 343 °C. IR (KBr, $\tilde{\nu}_{max}$): 3144 (br s), 2947 (s), 1468 (s), 1449 (s), 1400 (m), 1371 (m), 1262 (m), 1240 (m), 1210 (s), 1068 (w), 960 (s), 917 (w), 877 (m), 858 (m), 828 (m), 783 (m), 750 (m), 724 (m). ^{1}H NMR (400 MHz, $CDCl_3$): δ 3.49 (4 H, br s, Ar-C*H*$_2^{eq}$-Ar), 4.20 (4 H, br s, Ar-C*H*$_2^{ax}$-Ar), 6.79 (2 H, *J* = 7.6 Hz, Ar-*H*), 7.07 (4 H, d, *J* = 7.6 Hz, Ar-*H*), 7.15 (4 H, s, Ar-*H*), 10.04 (4 H, s, O*H*). ^{13}C NMR (100 MHz, $CDCl_3$): δ 31.44 (Ar-*C*H$_2$-Ar), 114.02, 122.50, 127.46, 129.30, 130.19, 131.57, 147.88, 148.77 (Ar-*C*). MS *m/z*

(MALDI-TOF): calcd. for ($C_{28}H_{22}Br_2O_4$), 582.3, found 582.0 (M^+). Anal. calcd. for ($C_{28}H_{22}Br_2O_4$): C, 57.76%; H, 3.81%. Found: C, 57.57%; H, 3.90%.

5,17-Dibromo-25,26,27,28-tetrakis-(*N*,*N*-diethylamino-carbonylmethoxy)-calix[4]arene (7).

To a stirred solution of 5,17-dibromo-25,26,27,28-tetrahydroxycalix[4]arene (**6**) (23.4 g, 40.3 mmol) in dry THF (730 mL) and DMF (150 mL), NaH (12.0 g, 304 mmol, 60% in mineral oil) was added and the suspension was stirred for 0.5 h at ambient temperature. *N*,*N*-Diethylbromoacetamid (47.8 g, 246 mmol) was slowly added. After stirring overnight at room temperature, another portion of NaH (5.00 g, 208 mmol) was added and the reaction was continued for 3 d. After the addition of 2 N HCl (1.00 L), the THF was removed by evaporation, the precipitate collected by filtration and dissolved in $CHCl_3$ (700 mL). The organic phase was washed with H_2O (3 × 500 mL) and dried over anhydrous Na_2SO_4. The resulting oil was treated with boiling Et_2O for 4 h. The product (23.7 g, 22.9 mmol, 57%) was obtained by filtration and dried in high vacuo to yield a colorless solid. Mp. 211 – 214 °C. IR (KBr, $\tilde{\nu}_{max}$): 2975 (s), 2928 (s) , 1661 (s), 1458 (m), 1379 (m), 1358 (m), 1305 (m), 1265 (m), 1201 (m), 1146 (m), 869 (w). ^{1}H NMR (400 MHz, $CDCl_3$): δ 1.07 (6 H, t, *J* = 7.1 Hz, CH_2-C*H*$_3$), 1.08 (6 H, t, *J* = 6.9 Hz, CH_2-C*H*$_3$), 1.13 (6 H, t, *J* = 7.1 Hz, CH_2-C*H*$_3$), 1.14 (6 H, t, *J* = 6.9 Hz, CH_2-C*H*$_3$), 3.19 (4 H, d, *J* = 13.6 Hz, Ar-C*H*$_2^{eq}$-Ar), 3.24 – 3.33 (16 H, m, C*H*$_2$-CH_3), 4.82 (4 H, s, O-C*H*$_2$), 4.99 (4 H, s, O-C*H*$_2$), 5.27 (4 H, d, *J* = 13.6 Hz, Ar-C*H*$_2^{ax}$-Ar), 6.54 (6 H, s, Ar-*H*), 6.91 (4 H, s,. Ar-*H*). ^{13}C NMR (100 MHz, $CDCl_3$): δ 13.04, 14.27 (CH_2-*C*H_3), 31.75 (Ar-*C*H_2-Ar), 39.85, 39.93, 40.74, 40.82 (*C*H_2-CH_3), 71.40, 71.66 (O-*C*H_2), 114.76, 122.74, 128.50, 131.10, 133.70, 137.45, 156.05, 156.24 (Ar-*C*), 168.20, 168.50 (*C*=O). MS *m/z* (MALDI-TOF): calcd. for ($C_{52}H_{66}Br_2N_4O_8$), 1034.9, found 1034.4 (M^+). Anal. calcd. for ($C_{52}H_{66}Br_2N_4O_8$): C, 60.35 H, 6.43%; N, 5.41%. Found: C, 60.22%; H, 6.35%, N, 5.36%.

5,17-Dicyano-25,26,27,28-tetrakis-(*N*,*N*-diethylamino-carbonylmethoxy)-calix[4]aren (8).

A suspension of 5,17-dibromo-25,26,27,28-tetrakis-(*N*,*N*-diethylamino-carbonylmethoxy)-calix[4]aren (**7**) (1.5 g, 1.93 mmol) and CuCN (552 mg, 7.16 mmol) in NMP (14 mL) was reacted for 22 h at 200 °C. After cooling to ambient temperature, $FeCl_3$ (880 mg, 5.4 mmol) dissolved in 2 N HCl (40 mL) was added. The resulting suspension was stirred for 2 h at rt

and the dark brown solid was removed by filtration. It was dissolved in $CHCl_3$, washed with H_2O and dried over anhydrous Na_2SO_4. The solvent was removed and the crude product was purified by column chromatography (EE/triethylamine 9:1) on silica. The purified oil was treated with boiling *n*-hexane. The white solid (200 mg, 0.22 mmol, 11%) could be obtained by filtration. Mp. 231 – 233 °C. IR (KBr, $\tilde{\nu}_{max}$): 2974 (s), 2932 (s), 2219 (s), 1661 (s), 1466 (m), 1380 (w), 1358 (w), 1306 (m), 1270 (m), 1223 (m), 1200 (m), 1134 (m), 1088 (m), 1052 (m), 947 (w), 897 (w), 802 (w), 771 (w), 751 (w). ^{1}H NMR (400 MHz, $CDCl_3$): δ 1.08 (12 H, t, *J* = 6.5 Hz, CH_2-C*H*$_3$), 1.15 (12 H, t, *J* = 7.2 Hz, CH_2-C*H*$_3$), 3.21 – 3.36 (20 H, m, Ar-C*H*$_2^{eq}$-Ar and C*H*$_2$-CH_3), 4.79 (4 H, s, O-C*H*$_2$), 5.13 (4 H, s, O-C*H*$_2$), 5.32 (4 H, d, *J* = 13.6 Hz, Ar-C*H*$_2^{ax}$-Ar), 6.47 (4 H, d, *J* = 7.3 Hz, Ar-*H*), 6.55 (2 H, dd, *J* = 8.3 and 6.6 Hz, Ar-*H*), 7.14 (4 H, s,. Ar-*H*). ^{13}C NMR (100 MHz, $CDCl_3$): δ 12.99, 14.23 (CH_2-*C*H_3), 31.61 (Ar-*C*H_2-Ar), 39.89, 40.01, 40.65, 40.78 (*C*H_2-CH_3), 71.60, 71.72 (O-*C*H_2), 105.49 (*C*N), 119.29, 123.09, 128.60, 132.52, 133.18, 136.95, 156.07, 160.81 (Ar-*C*), 167.86, 168.06 (*C*=O). MS *m/z* (MALDI-TOF): calcd. for ($C_{54}H_{66}N_6O_8$), 927.2, found 927.7 (M^+). Anal. calcd. for ($C_{54}H_{66}N_6O_8$)·0.05 $CHCl_3$: C, 69.57%; H, 7.13%; N, 9.01%. Found: 69.56%; H, 7.19%, N, 8.81%.

References

1 Iqbal, K. S. J; Cragg, P. J. *J. Chem. Soc., Dalton Trans.* **2007**, 26 and references therein.

2 Gokel, G. W. *J. Chem. Soc., Chem. Commun.* **2000**, 1.

3 Okunola, O. A.; Seganish, J. L.; Salimian, K. J.; Zavalij, P. Y.; Davis, J. T. *Tetrahedron* **2007**, *63*, 10743.

4 Zhang, H.; Rudkevich, D. M. *J. Chem. Soc., Chem. Commun.* **2007**, 4893.

5 Halouani, H.; Dumazet-Bonnamour, I.; Duchamp, C.; Bavoux, C.; Ehlinger, N.; Perrin, M.; Lamartine, R. *Eur. J. Org. Chem.* **2002**, 4202.

6 Cho, Y. L.; Rudkevich, D. M.; Rebek, J., Jr. *J. Am. Chem. Soc.* **2000**, 122, 9868.

7 Oueslati, I. *Tetrahedron* **2007**, *63*, 10840.

8 Casnati, A.; Sansone, F.; Sartori, A.; Prodi, L.; Montalti, M.; Zaccheroni, N.; Ugozzoli, F.; Ungaro, R. *Eur. J. Org. Chem.* **2003**, 1475.

9 Liu, J.-M.; Bu, J.-H.; Zheng, Q.-Z.; Chen, C.-F.; Huang, Z.-T. *Tetrahedron Lett.* **2006**, *47*, 1905.

10 Tu, C.; Liu, D.; Surowiec, K.; Purkiss, D. W.; Bartsch, R. A. *Org. Biomol. Chem.* **2006**, *4*, 2938.

11 Ji, H.-F.; Yang, Y.; Xu, X.; Brown, G. *Org. Biomol. Chem.* **2006**, *4*, 770.

12 Arduini, A.; Bozzoli, M.; Massera, C.; Pochini, A.; Secchi, A.; Ugozzoli, F. *Collect. Czech. Chem. Commun.* **2004**, *69*, 1309.

13 Matsumoto, H.; Ori, A.; Inokuchi, F.; Shinkai, S. *Chem. Lett.* **1996**, 301.

14 Lyskawa, J.; Sallé, M.; Balandier, J.-Y.; Le Derf, F.; Levillain, E.; Allain, M.; Viel, P.; Palacin, S. *J. Chem. Soc., Chem. Commun.* **2006**, 2233.

15 Calestani, G.; Ugozzoli, F.; Arduini, A.; Ghidini, E.; Ungaro, R. *J. Chem. Soc., Chem. Commun.* **1987**, 344.

16 Arduini, A.; Ghidini, E.; Pochini, A.; Ungaro, R.; Andreetti, G. D.; Calestani, G.; Ugozzoli, F. *J. Incl. Phenom.* **1988**, *6*, 119.

17 Arnaud-Neu, F.; Barrett, G.; Fanni, S.; Marrs, D.; McGregor, W.; McKervey, M.A.; Schwing-Weill, M.-J.; Vetrogon, V.; Wechsler, S. *J. Chem. Soc., Perkin Trans. 2* **1995**, 453.

18 Arnaud-Neu, F.; Barboso, S.; Berny, F.; Casnati, A.; Muzet, N.; Pinalli, A.; Ungaro, R.; Schwing-Weill, M.-J.; Wipff, G. *J. Chem. Soc., Perkin Trans. 2,* **1999**, 1727.

19 Hioki, H.; Nakaoka, R.; Maruyama, A.; Kodama, M. *J. Chem. Soc,. Perkin Trans. 1*, **2001**, 3265.

20 Aquino, C. J.; Armour, D. R.; Berman, J. M.; Birkemo, L. S.; Carr, R. A. E.; Croom, D. K.; Dezube, M.; Dougherty, R. W., Jr.; Ervin, G. N.; Grizzle, M. K.; Head, J. E.; Hirst, G. C.; James, M. K.; Johnson, M. F.; Miller, L. J.; Queen, K. L.; Rimele, T. J.; Smith, D. N.; Sugg, E. E. *J. Med. Chem.* **1996**, *39*, 562.

21 Pelizzi, N.; Casnati, A.; Friggeri, A.; Ungaro, R. J. *Chem. Soc,. Perkin Trans. 2*, **1998**, 1307.

22 Cram, D. *Fed. Proc. Fed. Am. Soc. Exp. Biol.* **1968**, *27*, 1305.

23 Wintergerst, M. P.; Levitskaia, T. G.; Moyer, B. A.; Sessler, J. L.; Delmau, L. H. *J. Am. Chem. Soc.* **2008**, *130*, 4129.

24 Casnati, A.; Ting, Y.; Berti, D.; Fabbi, M.; Pochini, A.; Ungaro, R.; Sciotto, D.; Lombardo, G. G.. *Tetrahedron* **1993**, *49*, 9815.

25 Gutsche, C. D.; Lin, L.-G. *Tetrahedron* **1986**, *42*, 1633.

Calix[4]arenes as Molecular Platforms for MRI Contrast Agents

4

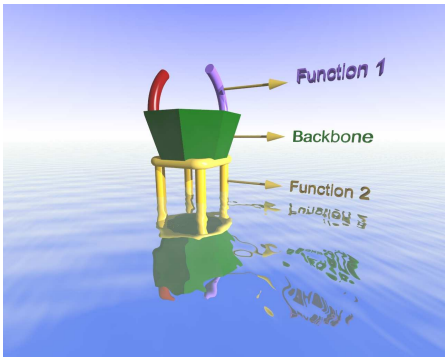

The contents of this chapter have been published in:
Schühle, D. T.; Schatz, J.; Laurent, S.; Vander Elst, L.; Muller, R. N.; Stuart, M. C. A.; Peters, J. A. *Chem. Eur. J.* **2009**, *15*, 3290.

Introduction

Magnetic resonance imaging (MRI) is one of the most important techniques in medical imaging. It is noninvasive, avoids problems occurring in other imaging techniques such as scattering (optical imaging) or high-energy radiation (computed tomography (CT) or X-ray), and enables the production of three-dimensional images of various tissues. The contrast is generated by differences in the proton density between tissues and differences in T_1 or T_2 relaxation times.[1-3] To enhance the contrast in T_1-weighted images, Gd(III)-complexes are often administered because the paramagnetic metal ion (Gd(III) has an f^7-configuration) accelerates the relaxation time of the water protons in its proximity very efficiently.[1-4] The challenge is to prepare complexes that do not release the toxic metal ion *in vivo* and yet are efficient contrast agents.[1,2] To achieve high stability of the complexes, mainly two different chelators and their derivatives are in use, namely diethylenetriaminepentaacetic acid (DTPA) and 1,4,7,10-tetra(carboxymethyl)-1,4,7,10-tetraazacyclododecane (DOTA).[1,2]

In general, the relaxivity as a function of the average water residence lifetime (τ_M^{298}) depends on the magnetic field and has, for instance, a sharp optimum at 20-40 ns at 60 MHz. Long rotational correlation times (τ_R) are favorable for enhanced relaxivities, which means that large rigid molecules have to be prepared. This has already been achieved by attaching low molecular weight chelators to, for example, dendrimers, nanoparticles, polysaccharides, or peptides giving rather rigid, slowly tumbling conjugates.[5] A noncovalent approach is to prepare amphiphilic compounds that form aggregates such as micelles, liposomes or adducts with, for example, the hydrophobic transport protein human serum albumin (HSA) or cyclodextrins.[6,7] Furthermore, targeted contrast agents usually have (besides other advantages such as lower required doses) higher relaxivities when interacting with the target due to the restriction of the rotational motion upon binding.[8]

In MRI, an ongoing trend is to apply higher magnetic field strengths (>1.5 T). However, common T_1 contrast agents do not perform optimally at these field strengths. Therefore, there is a quest to develop novel contrast agents for these applications. This can be achieved by optimizing the average water residence lifetime τ_M to even shorter values than that predicted of 20 - 40 ns for high molecular weight agents and the molecular

tumbling time τ_R to around 400 ps at 400 MHz.[9,10] To optimize τ_R, not only the slowing down of the motion of the molecule in solution but also the decrease of motion within the molecule itself is essential.[11] The practical consequence of these theoretical predictions is that for high-field applications, medium-sized and rigid contrast agents exhibiting a fast water exchange rate need to be designed.

One of our approaches to find systems with optimal τ_R is to use the rather rigid calix[4]arene core as a synthetic platform.[12] Calix[4]arenes have already been used in MRI with the aim of finding novel chelators for efficient complexation of Gd(III).[13-15] So far, complex stability and/or poor water solubility have been the limiting properties of compounds of this type. To the best of our knowledge, the only calix[4]arene based Gd-complex reported to have good stability and good water solubility has been described in a patent, but no information about its relaxivity was given.[16] To overcome the stability issue, we decided to bind DOTA-moieties, which are known to form highly stable complexes with lanthanide(III) ions, to the calix[4]arene core. At the same time, the hydrophilicity of these groups was expected to ensure that the corresponding conjugate had good water solubility.

Calixarenes generally enable the introduction of at least two different functions, one at the *upper* (*wide*) *rim* and the other one at the *lower* (*narrow*) *rim*. For synthetic and rigidity reasons, we attached the chelating units on the *upper rim*. In principle, all kinds of functions can be introduced to the other side of such conjugates enabling the control of physical, biological and pharmacological properties. For the first model compound **1** presented in this study (Scheme 4.1), propyl groups were attached to the *lower rim* to lock the calix[4]arene in the *cone* conformation.[17]

Results and Discussion

Synthesis

Amide coupling of calix[4]arene **2** with *tert*-butyl-DOTA monoacid **3** using 1-ethyl-3-(3-dimethylaminopropyl)carbodiimide hydrochloride (EDC) and a stoichiometric amount of 1-hydroxybenzotriazole (HOBt) resulted in the corresponding conjugate which was purified by ultrafiltration over a 1 kDa membrane (see Scheme 4.1).[18,19] The use of at least seven equivalents of **3** and long reaction times were found to be crucial for full conversion of **2** to

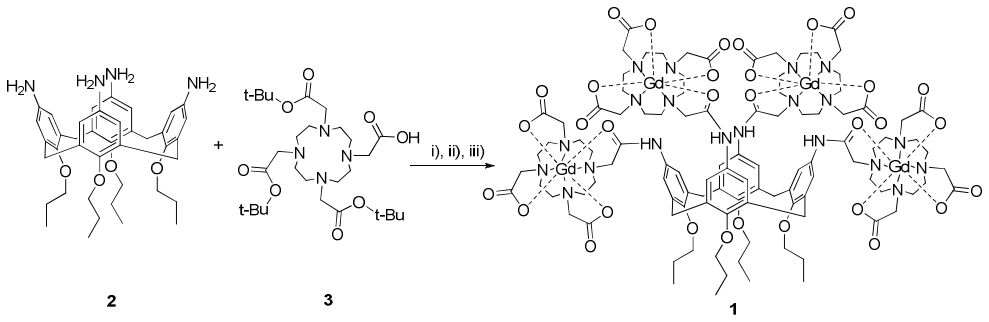

Scheme 4.1. Preparation of **1**. i) EDC, HOBt, DIPEA, DMF, 2d, rt, 71%, ii) TFA/CH_2Cl_2 50:50, overnight, rt, iii) $GdCl_3 \cdot 6H_2O$, pH 6, 57% over 2 steps.

the tetraamide. Cleavage of the protective *tert*-butyl-groups was achieved in a 1:1-mixture of TFA/CH_2Cl_2 at ambient temperature overnight. The complexation of the lanthanide was performed by portionwise addition of $GdCl_3 \cdot 6H_2O$ to an aqueous solution of the free ligand maintaining the pH at 6. The excess of the Gd salt and other inorganic salts formed during the complexation were removed by ultrafiltration. The yield for the diprotection/ complexation was limited to 57% as small amounts of **1** passed through the membrane used for the ultrafiltration.

Aggregation

Amphiphilic calix[4]arenes have a tendency to aggregate in water, so dynamic light scattering (DLS) and cryo-TEM were performed in aqueous solution.[20] The concentration of **1** (c_1) in this sample was 0.93 mM, which corresponds to a gadolinium concentration (c_{Gd}) of 3.73 mM. The presence of small aggregates (average hydrodynamic radius of 2.2 nm as determined by DLS, see Figure 4.1), the narrow size distribution and the cryo-TEM image strongly suggest the presence of spherical micelles under the conditions applied.

The self-association leads to an increase in τ_R of the paramagnetic complex, which according to the relaxation theory should be reflected in an increase in relaxivity. We exploited this phenomenon for the determination of the critical micelle concentration (*cmc*).[7a] The relaxometric data were acquired at 37 °C and 20 MHz by observing the effect of variation of c_{Gd} on the paramagnetic relaxation rate R_1 of the water protons (see Figure 4.1). The curve of R_1 as a function of c_{Gd} shows a clear change of slope around c_{Gd} = 1 mM,

which suggests that the *cmc* is about that value. Equation 4.1 describes R_1 as a function of c_{Gd} above the *cmc*, whereas Equation (4.2) is valid below it.[21,22]

$$\frac{1}{T_1} = \frac{1}{T_{1,obs}} - \frac{1}{T_{1,dia}} = R_1 = cmc * r_1^{n.a.} + (c_{Gd} - cmc) * r_1^{a} \tag{4.1}$$

$$R_1 = c_{Gd} * r_1^{n.a.} \tag{4.2}$$

In Equation 4.1, T_1 is the paramagnetic contribution to the longitudinal relaxation time, $T_{1,obs}$ is the measured longitudinal relaxation time and $T_{1,dia}$ is the diamagnetic contribution (the T_1 of pure water); $r_1^{n.a.}$ is the relaxivity of the nonaggregated compound whereas r_1^{a} is the relaxivity of the aggregates. Here, the relaxivity r_1 is defined as the longitudinal relaxation rate enhancement of the water protons per 1 mM concentration of the paramagnetic metal ion, compared to a diamagnetic medium (water).

From the relaxation rates of the initial part of the curve (see Figure 4.1), $r_1^{n.a.}$ was estimated to be 8.22 $s^{-1}mM^{-1}$. A fit of the experimental data with Equations 4.1 and 4.2 using the *cmc* and r_1^{a} as adjustable parameters gave an optimal fit for *cmc* = 0.84 ± 0.14 mM (concerning Gd, 0.21 mM concerning **1**) and r_1^{a} of 18.3 ± 0.8 $s^{-1}mM^{-1}$ at 37 °C and 20 MHz.

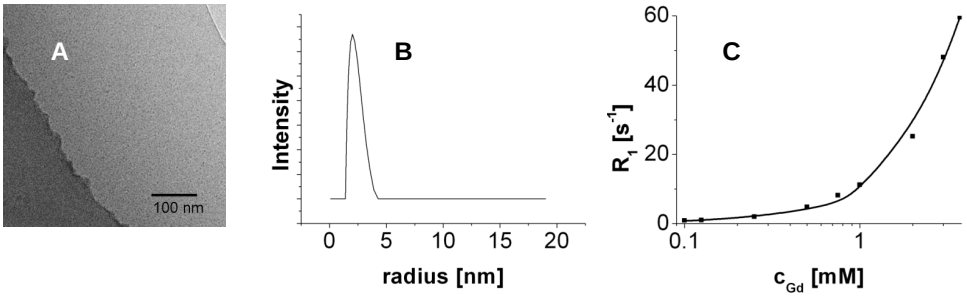

Figure 4.1. (A) Cryo-TEM image, (B) DLS curve and (C) dependence of R_1 on the c_{Gd} as determined at 37 °C and 20 MHz (the curve represents a fit of the experimental data with Equations 4.1 and 4.2).

During the fitting, $r_1^{n.a.}$ was fixed to 8.22 $s^{-1}mM^{-1}$ to improve the accuracy of the fit. This was justified, since the relaxivities determined for very low concentrations (c_{Gd} < 0.47 mM) were found to be identical within the error range. The *cmc* obtained is comparable with previously published values for calix[4]arenes in water.[22]

The dependence of R_1 on the concentration of **1** is not perfectly linear between c_{Gd} = 0.47 mM and the *cmc*, which suggests that the relaxivity of the sample changes already at concentrations below the *cmc*. This is most probably due to the formation of pre-aggregates such as dimers, trimers etc. which in this case cannot be observed by either DLS or cryo-TEM but leads to significant changes in the relaxation behavior due to increases in τ_R.[23] Nevertheless, the existence of such pre-aggregates might result in a different biodistribution than for the pure micellar system only.[24]

Variable temperature ^{17}O NMR measurements

The influence of the paramagnetic compound on the ^{17}O NMR reduced angular frequency ($\Delta\omega_r$) and the transverse relaxation rate ($1/T_{2r}$) at different temperatures was determined for an aqueous solution of **1** containing 74.5 mM of Gd (see Figure 4.2).

$$\frac{1}{T_{2r}} = \frac{1}{P_m}\left[\frac{1}{T_2} - \frac{1}{T_{2A}}\right] \tag{4.3}$$

$$\Delta\omega_r = \frac{1}{P_m}(\omega - \omega_A) \tag{4.4}$$

In Equations 4.3 and 4.4, the variables T_{2A} and ω_A stand for the corresponding values measured for the reference (acidified water) whereas T_2 and ω are the experimental values for the solution containing **1**. P_m is the mole fraction of bound water (P_m = mole fraction of Gd if q = 1, for which q = number of Gd-bound water molecules in the complex). Because the concentration of the sample was far above the *cmc*, it may be assumed that complex **1** is almost exclusively present as micelles. The data obtained (see Figure 4.2) contain information particularly on the hyperfine coupling constant ($A/\hbar$) and the average residence

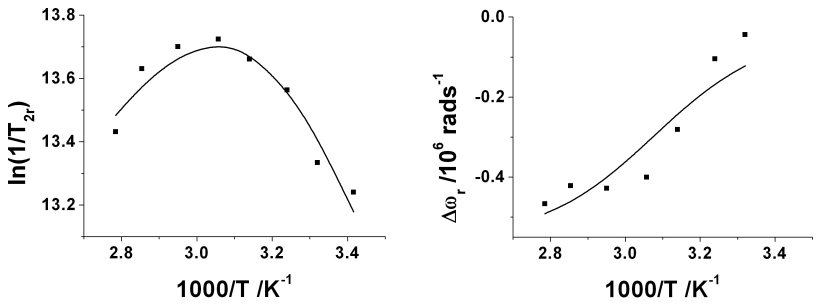

Figure 4.2. Temperature dependence of reduced transversal (T_{2r}) relaxation time and angular frequency ($\Delta\omega_r$) of a 74.5 mM aqueous solution of **1** at 7.5 T (curves represent results from the fittings).

life time at 298 K (τ_M^{298}). Under the assumption that q=1, these variable temperature ^{17}O NMR data give a good fit with the appropriate equations for the parameters compiled in Table 4.1.[21] The corresponding calculated curves are shown in Figure 4.2. τ_M^{298} was found to be in the expected range for DOTA-monoamides. This rate is rather different from the value for which an optimum relaxivity is predicted (20 to 40 ns at 60 MHz).[10] Within the experimental error, the hyperfine coupling constant is identical to commonly observed values for oxygen atoms directly coordinated to Gd. This indicates that the assumption of the number of first-sphere water molecules (q = 1) was correct; any deviation would have been reflected in a different best-fit value for $A/\hbar$.

Table 4.1. Parameters obtained from simultaneous fitting of the variable temperature ^{17}O NMR data of **1**.

parameter	Best-fit value
τ_M^{298} [μs]	1.20 ± 0.12
$\Delta H^{\neq}$ [kJ mol^{-1}][a]	29.4 ± 5.5
$A/\hbar$ [10^6 rads^{-1}]	-3.7 ± 0.6
$1/T_{2m}^{298}$ [10^6 s^{-1}]	0.46 ± 0.11
E_m [kJmol^{-1}]	16.2 ± 3.7

[a] $\Delta H^{\neq}$ is the enthalpy of activation of the exchange process.

Nuclear Magnetic Relaxation Dispersion (^{1}H NMRD)

Nuclear magnetic relaxation dispersion (NMRD) is a powerful technique for characterizing MRI contrast agents. The field dependence of the relaxivity (NMRD profile) gives important information on the extent to which parameters, such as electronic relaxation, rotational correlation time and water exchange rate contribute, to the relaxivity. To evaluate these parameters ^{1}H NMRD profiles were measured for samples with concentrations (c_{Gd}) of 0.47 and 3.73 mM (see Figure 4.3). At 0.47 mM, the non-aggregated **1** is present exclusively, whereas at concentrations above the *cmc* (c_{Gd} > 0.84 mM), both monomer and micelles contribute to the observed relaxivity. The sample at 0.47 mM was measured at 6, 15, 37, and 50 °C and the sample at 3.73 mM concentration at 37 °C.

In cases where internal motions influence the relaxivity, the Lipari-Szabo approach is applied to describe the rotational dynamics. This method separates the motions in global and local ones. An order parameter S^2 quantifies these contributions; S^2 =1 for an ideal rigid system, whereas S^2 =0 for a system where fast internal motions fully determine the relaxivity.[1] At first, we fitted the experimental data using this approach but we always found a value for S^2 of 1, which is consistent with the proposed high rigidity of the conjugates. Since local contributions to the rotational dynamics do not play a role in these systems, we could use the standard approach. Therefore, the NMRD profiles obtained were fitted with a set of equations based on the Solomon-Bloembergen-Morgan theory for the inner sphere contribution and those of Freed for the outer sphere. The average residence life time of a water molecule in the first coordination sphere (τ_M^{298}) and its activation energy $\Delta H^{\ddagger}$ were fixed at the value obtained from the ^{17}O NMR measurements in the case of the micellar and the HSA system, whereas they were allowed to vary during the fitting process for the monomeric **1**. This was done since the concentration used for the ^{17}O measurements was far above the *cmc* and to test whether the water exchange parameters change upon self-aggregation. A good fit was obtained for the parameters compiled in Table 4.2. The NMRD profiles calculated with these parameters are displayed as curves in Figure 4.3. The best fit

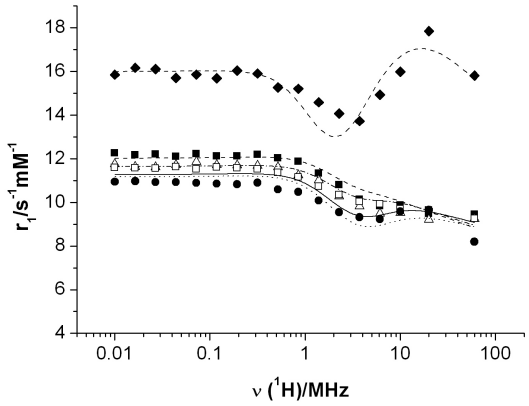

Figure 4.3. ^{1}H NMRD profiles of a c_{Gd} =0.47 mM solution at 6 °C (full squares, dashed), 15 °C (empty triangles, dashed-dotted), 37 °C (empty squares, full line) and 50 °C (dots, dotted line) as well as the calculated profile for the micellar **1** at 37 °C (diamonds). The curves indicate the results from the fittings.

values obtained for monomeric **1** show that τ_R is very close to the predicted optimal value of around 400 ps for high-field contrast agents.[10] The τ_R of **1** can be estimated by the Debye-Stokes-Einstein equation 4.5 (in which η is the microviscosity, k_B the Boltzmann constant and r_0 the effective radius) to correspond with that of a spherical particle of a diameter of 1.66 nm.

$$\tau_R = \frac{4\pi\eta r_0^3}{3k_B T} \tag{4.5}$$

Molecular models show that **1** measures about 2.3 × 2.1 × 1.2 nm, which is in agreement with the size estimated from τ_R. This suggests that the molecule is very rigid and that the global motion of the molecule determines the rotational correlation time, so local motions do not play a role in the relaxation process.

The parameters determining the electronic relaxation, namely the mean square zero-field splitting energy (Δ^2), and the corresponding correlation time (τ_V) are in good agreement with values found for other DOTA-monoamide based contrast agents.[25] Intramolecular contributions to the electronic relaxation are negligible in the calix[4]arene

Table 4.2. Parameters obtained from fitting of ^{1}H NMRD profiles of the monomeric, micellar and HSA-bound **1**.

parameter	Monomer[a]	Micellar **1**[b]	HSA **1**[c]
τ_M^{310} [μs]	1.28 ± 0.11	0.72[d]	0.72[d]
$\Delta H^{\ddagger}$ [kJmol^{-1}]	17.7 ± 1.3	–	–
τ_R^{310} [ns]	0.39 ± 0.05	1.21 ± 0.11	8.84 ± 2.0
E_r [kJmol^{-1}]	8.58 ± 2.78	–	–
τ_v^{310} [ps]	45.9 ± 2.3	60.9 ± 2.2	60.4 ± 3.6
Δ^2 [10^{19} s^{-2}]	1.07 ± 0.10	0.51 ± 0.06	0.85 ± 0.05

[a] Values obtained by a simultaneous fit of the temperature dependent NMRD profiles (see Figure 4.3);

[b] Values obtained from a fit of the calculated profile for the micellar **1** at 37 ºC shown in Figure 4.3;

[c] Values obtained by a fit of the calculated profile for the HSA-bound **1** at 37 ºC shown in Figure 4.5;

[d] Fixed at the value calculated from the ^{17}O data in Table 4.1.

system studied, since inspection of molecular models show that all Gd-Gd-distances in **1** are at least 8 nm.[10] The average water residence lifetime obtained by ^{17}O NMR for the micellar system (τ_M^{298}=1.20±0.12, determined at high concentration) is consistent with the results of the fitting of the NMRD profiles of the monomer (τ_M^{298}=1.33±0.11, low concentration) indicating that there is only a negligible effect of self-aggregation on the water exchange dynamics.

In the profile for the 3.73 mM sample, there is a maximum in relaxivity at about 20 MHz, which is a characteristic for compounds with high τ_R values and therefore consistent with self-association at that concentration. Using Equation 4.1, we calculated the NMRD profile for the pure micelles at 37 ºC (Figure 4.3). The parameters obtained from the fittings are listed in Table 4.2.

The best-fit value for τ_R, which can be calculated using Equation 4.5 (see Table 4.2), corresponds with that for a sphere with a diameter of 2.4 nm in agreement with the diameter of the micelles as obtained from the DLS measurements (see above). This shows that also the micelles are rather rigid and that there are no internal motions that influence the relaxivity. Hirsch, Böttcher and co-workers have shown that a similar calix[4]arene forms

extremely stable micelles (radius approx. 3 nm) consisting of exactly seven molecules.[20d] Even when the solvent is evaporated, the micelles persist and can be visualized by TEM techniques. The strong interactions within micelles of this type and the uncommon aggregation geometry lead to the very rigid aggregates found for **1**.

Interaction with HSA

It has previously been shown that calix[4]arenes can interact with the hydrophobic transport protein human serum albumin (HSA) due to their apolar structure.[14,15] The affinity of hydrophobic compounds to HSA is an ongoing topic in modern MRI research since both, relaxivity and pharmacokinetics, can be controlled by non-covalent binding of contrast agents to HSA.[6a,29] We therefore investigated the binding of **1** (c_1 = 25 µmol, 37 ºC) to HSA by established methods involving variation of the concentration of HSA in a solution of **1** and observing the increase of the paramagnetic water proton relaxation rate R_1 after correction for the diamagnetic contribution of the protein (see Figure 4.4).[1,14]

The increase in relaxivity is caused by the slowing down of the rotational motion upon binding resulting in similar effects to those described above for the micelle formation (Equation 4.5). To compare our results with literature data on calixarene-based Gd-complexes interacting with HSA, we followed the procedure described for these systems and assumed that there is, effectively, only a single binding site in HSA (n was fixed to 1).[14,15] Thus we determined a binding constant K_A of (1.2±0.3)·10^3 M^{-1}, a relaxivity for the monomer (r_1^f) of 9.6±0.4 s^{-1}mmol^{-1} and a relaxivity of the adduct **1**·HSA (r_1^c) of 24.6±1.2 s^{-1}mmol^{-1} (corresponds to a relaxivity of 98.5±5.0 s^{-1}mmol^{-1} in terms of **1**) at 37 °C and 20 MHz using Equation 4.6.[6b]

$$R_1 = 1000\left[r_1^f c_1 + (r_1^c - r_1^f)\frac{n\cdot c_{HSA} + c_1 + K_A^{-1} - \sqrt{(n\cdot c_{HSA} + c_1 + K_A^{-1})^2 - 4c_1 c_{HSA}}}{2} \right] \qquad (4.6)$$

In Equation 4.6, r_1^f is the relaxivity of free (non-aggregated) **1** and n is the number of binding sites and c_{HSA} is the concentration of HSA.

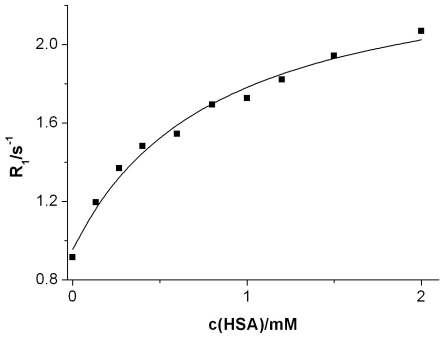

Figure 4.4. Changes in R_1 of a 25 μM solution of **1** upon variation of the concentration of HSA at 37 °C and 20 MHz (line represents the result from the fitting).

NMRD measurements at 37 ºC of a solution containing 4% HSA (0.6 mM) and 0.47 mM **1** were performed. Using the binding constant calculated earlier as well as the profile for the monomer alone, we calculated the NMRD profile for the HSA·**1** conjugate (Figure 4.5).[29c] For the parameters shown in Table 4.2, a good fit was obtained for this profile.

The electronic parameters are in the same range as those of the micellar aggregates and for the monomer. The deviations can be attributed to the insufficiencies in the model that is used to describe the electronic relaxation processes.[28] The rotational correlation time is in the range expected for conjugates with HSA.

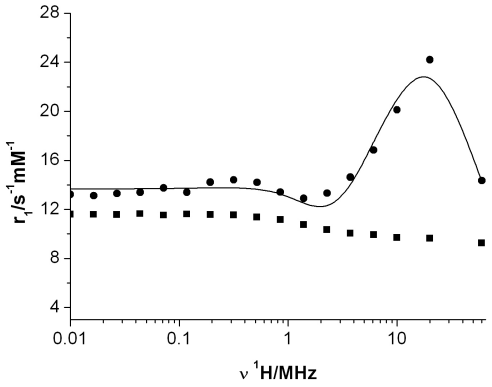

Figure 4.5. ^{1}H NMRD profiles of monomer **1** (squares) and HSA·**1** conjugate (circles) at 37 °C (line represents the result from the fittings).

Conclusions

The novel noncharged self-aggregating calix[4]arene based MRI contrast agent described here exhibits good relaxivities over a broad range of Lamor frequencies. Evaluation of the parameters governing the relaxivity shows that it is limited by the average residence time of water in the first coordination sphere of Gd(III). Both the conjugate and its micellar aggregates are highly rigid systems with a τ_R that is very close to the predicted optimal value for high-field contrast agents. Therefore, further optimization of this type of contrast agents is possible by changing the structure of the chelate in such a way that the rate of water exchange increases and the rigidity is maintained. Investigations to further improve the efficiency of calix[4]arene-based MRI contrast agents along these lines are in progress.

Experimental

Sample preparation

An aqueous solution of **1** was filtered with a syringe filter (0.2 μm). The exact concentration c_{Gd} of this solution was determined by measuring the bulk magnetic susceptibility shift (BMS) of *tert*-butanol compared to an external standard.[30]

Methods

DLS. Dynamic light scattering (DLS) was performed with a DLS/SLS/ALV-5000 apparatus using a 35 mW HeNe laser with a wavelength of 633 nm. The intensity autocorrelation function was measured at an angle of 90º and analysed with the CONTIN method. All samples were filtered through a syringe filter (pore size 0.2 μm) and centrifuged before the measurements in order to remove dust.

Cryo-TEM. A few microliters of a solution of **1** (c_{Gd} =3.73 mM) were placed on a quantifoil 3.5/1 holey carbon/coated grid (Quantifoil micro tools GmbH, Jena, Germany). The grids were automatically blotted and vitrified using the vitrobot (FEI, Eindhoven, The Netherlands). Frozen hydrated specimen were observed with a Gatan cryo-stage (Model 626, Gatan, Pleasanton, CA) in a Philips CM10 cryo/electron microscope (Philips,

Eindhoven, The Netherlands) operating at 100 keV. Images were recorded under low-dose conditions with a slow scan CCD camera (Gatan, Pleasanton, CA).

NMR. The ^{17}O NMR measurements were performed on a Varian Inova-300 spectrometer. The ^{1}H NMRD measurements were performed on a Stelar apparatus covering a range of 0.01 – 10 MHz, the T_1 measurements at 20 and 60 MHz on Bruker Minispec relaxometers (mq20 and mq60) and those at 300 MHz at a Varian Inova-300 spectrometer.

Fittings. For the fittings, the established equations were used.[7a,21] The least-squares fit of the ^{17}O NMR and ^{1}H NMRD data were performed by the MicroMath program Scientist using known equation sets.[26] For some of the parameters describing the NMRD profiles, commonly accepted values were used such as for the distance between Gd(III) and a proton of coordinated water (r_{GdH}) 0.31 nm and the distance of the closest approach of an outer sphere water proton to Gd(III) 0.35 nm. The activation energy for the electronic rotational correlation time (E_v) was fixed at 1 kJmol^{-1} and the parameter determining the spin rotation contribution (δg_L) at 0.021.[26] The diffusion coefficient and its activation energy were fixed to the values of pure water.[27]

Synthesis

Materials. All reagents and anhydrous solvents were of commercial quality. **2** and **3** were synthesised using slightly modified literature methodologies.[18,19]

5,11,17,23-Tetrakis(tris-4,7,10-*tert*-butoxycarbonylmethyl-1,4,7,10-tetraazacyclo-dodec-1-yl-acetamidyl)-25,26,27,28-tetrapropoxy-calix[4]arene.

Under inert atmosphere, a suspension of tris-1,4,7-*tert*-butoxycarbonylmethyl-10-carboxymethyl-1,4,7,10-tetraazacyclododecane (**3**) (1.55 g, 2.71 mmol), dry DIPEA (1.3 mL), HOBt (370 mg, 2.71 mmol) and EDC (520 mg, 2.71 mmol) in dry DMF (20 ml) was stirred for 0.5 h at ambient temperature. To the resulting mixture, a solution of 5,11,17,23-tetraamino-25,26,27,28-tetrapropoxy-calixarene (**2**) (252 mg, 387 μmol) in dry DMF (5 ml) was added and the mixture was stirred at ambient temperature for 2 d. After the solvent was removed in high vacuo, the residue was redissolved in DCM and washed twice with brine, once with 0.1 N NaOH, and then with water until the pH of the aqueous phase was neutral. The organic phase was dried over Na_2SO_4 and the solvent was evaporated. The product was purified by ultrafiltration in EtOH using a 1 kDa membrane to give 0.79 g (71%) of the title

compound. ^{1}H NMR (300 MHz, DMSO-d_6, 100 ˚C, TMS): δ = 0.98 (12 H, t, J = 5.2 Hz, CH_3), 1.42, 1.46 (108 H, 2 s, *tert*-Bu), 1.88 (8 H, sext, J = 5.2 Hz, CH_2CH$_3$), 2.74 – 3.30 (100 H, N-CH_2-CO, N-CH_2-CH_2, ArCH_2Ar), 3.87 (8 H, t, J = 5.2 Hz, OCH_2CH$_2$), 4.43 (4 H, d, J = 9.9 Hz, ArCH_2Ar), 6.86 (8 H, br. s, Ar-*H*), 9.27 (4 H, br. s, N*H*). ESI-HRMS: calc.: *m/z* = 718.7185 $(M+4H)^{4+}$, found: 718.7282.

5,11,17,23-Tetrakis(tris-4,7,10-carboxymethyl-1,4,7,10-tetraazacyclododec-1-yl-acetamidyl)-25,26,27,28-tetrapropoxy-calix[4]arene.

5,11,17,23-Tetrakis(tris-4,7,10-*tert*-butoxycarbonylmethyl-1,4,7,10-tetraazacyclododec-1-yl-acetamidylmethyl)-25,26,27,28-tetrapropoxy-calix[4]arene (481 mg, 167 μmol) was dissolved in DCM (10 ml) and TFA (10 ml) was added. After stirring at ambient temperature overnight, the liquids were removed with a rotary evaporator. The solid obtained in this way was not purified further. For the NMR characterization, a defined amount of pyridine was added to the solution in order to suppress protonation of the substrate. The content of product in the solid was determined to be 35%, by integration of the proton resonances of the substrate with respect to those of pyridine. The rest of the solid consisted of TFA and inorganic salts which could easily be removed after complexation (see below). Therefore, the title compound was used without further purification. ^{1}H NMR (300 MHz, DMSO-d_6, 100 ˚C, TMS): δ = 0.89 (12 H, t, J = 6.9 Hz, CH_3), 1.80 (8 H, sext, J = 6.9 Hz, CH_2CH$_3$), 3.01 – 3.61 (100 H, N-CH_2-CO, N-CH_2-CH_2, ArCH_2Ar), 3.76 (8 H, t, J = 6.9 Hz, OCH_2CH$_2$), 4.32 (4 H, d, J = 12.3 Hz, ArCH_2Ar), 6.91 (8 H, br. s, Ar-*H*), 9.53 (4 H, br. s, N*H*).

Gd(III)-complex of 5,11,17,23-tetrakis(tris-4,7,10-carboxymethyl-1,4,7,10-tetraaza-cyclo-dodec-1-yl-acetamidyl)-25,26,27,28-tetrapropoxy-calix[4]arene (1).

5,11,17,23-Tetrakis(tris-4,7,10-carboxymethyl-1,4,7,10-tetraazacyclododec-1-yl-acetamid-ylmethyl)-25,26,27,28-tetrapropoxy-calix[4]arene (**4**) (445.3 mg, ~69.7 μmol) (as obtained above) was dissolved in water (2.6 ml) and the pH was adjusted to 6. $GdCl_3$•$6H_2O$ (111.8 mg, 300 μmol) was added and the pH re-adjusted to 6. The complex was purified by ultrafiltration in water using a 1 kDa membrane to yield 108 mg (39.7 μmol, 57%) of the title compound after lyophilisation. ESI-HRMS: calc.: *m/z* = 1408.3631 $(M)^{2+}$, found 1408.3879.

References

1 Tóth, É.; Merbach, A. *The Chemistry of Contrast Agents in Medical Magnetic Resonance Imaging*, Wiley, Chichester, **2001**.

2 Caravan, P.; Ellison, J. J.; McMurry, T. J.; Lauffer, R. B. *Chem. Rev.* **1999**, *99*, 2293.

3 Aime, S.; Geninatti Crich, S.; Gianolio, E.; Giovenzana, G. B.; Tei, L.; Terreno, E. *Coord. Chem. Rev.* **2006**, *250*, 1562.

4 Bottrill, M.; Kwok, L.; Long, N. J. *Chem. Soc. Rev.* **2006**, *35*, 557.

5 a) Langereis, S.; Dirksen, A.; Hackeng, T. M.; van Genderen, M. H. P.; Meijer, E. W. *New J. Chem.* **2007**, *31*, 1152; b) Endres, P. J.; Paunesku, T.; Vogt, S.; Meade, T. J.; Woloschak, G. E. *J. Am. Chem. Soc.* **2007**, *129*, 15760; c) Corsi, D. M.; Vander Elst, L.; Muller, R. N.; van Bekkum, H.; Peters, J. A. *Chem. Eur. J.* **2001**, *7*, 64; d) Lebdušková, P.; Kotek, J.; Hermann, P.; Vander Elst, L.; Muller, R. N.; Lukeš, I.; Peters, J. A. *Bioconj. Chem.* **2004**, *15*, 881; e) Aime, S.; Botta, M.; Geninatti Crich, S.; Giovenzana, G.; Palmisano, G.; Sisti, M. *Bioconj. Chem.* **1999**, *10*, 192.

6 a) Caravan, P.; Cloutier, N. J.; Greenfield, M. T.; McDermid, A.; Dunham, U.; Bulte, J. W. M.; Amedio, Jr., J. C.; Looby, R. J.; Supkowski, R. M.; Horrocks, Jr., W. DeW.; McMurry, T. J.; Lauffer, R. B. *J. Am. Chem. Soc.* **2002**, *124*, 3152; b) Henrotte, V.; Vander Elst, L.; Laurent, S.; Muller, R. N. *J. Biol. Inorg. Chem.* **2007**, *12*, 929.

7 a) André, J. P.; Tóth, É.; Fischer, H.; Seelig, A.; Mäcke, H. R.; Merbach, A. E. *Chem. Eur. J.* **1999**, *5*, 2977; b) Mulder, W. J. M.; Strijkers, G. J.; van Tilborg, G. A. F.; Griffioen, A. W.; Nicolay, K. *NMR Biomed.* **2006**, *19*, 142; c) Aime, S.; Botta, M.; Fedeli, F.; Gianolio, E.; Terreno, E.; Anelli, P. *Chem. Eur. J.* **2001**, *7*, 5262; d) Accardo, A.; Tesauro, D.; Morelli, G.; Gianolio, E.; Aime, S.; Vaccaro, M.; Mangiapia, G.; Paduano, L.; Schillén, K. *J. Biol. Inorg. Chem.* **2007**, *12*, 267; e) Hovland, R.; Gløgård, C.; Aasen, A. J.; Klaveness, J. *Org. Biomol. Chem.* **2003**, *1*, 644; f) Gianolio, E.; Giovenzana, G. B.; Longo, D.; Longo, I.; Menegotto, I.; Aime, S. *Chem. Eur. J.* **2007**, *13*, 5785; g) Torres, S.; Martins, J. A.; André, J. P.; Pereira, G. A.; Kiraly, R.; Brücher, E.; Helm, L.; Tóth, É.; Geraldes, C. F. G. C.

Eur. J. Inorg. Chem. **2007**, 5489; h) Delli Castelli, D.; Gianolio, E.; Geninatti Crich, S.; Terreno, E.; Aime, S. *Coord. Chem. Rev.* **2008**, 2424.

8 Aime, S.; Botta, M.; Fasano, M.; Terreno, E. *Chem. Soc. Rev.* **1998**, *27*, 19.

9 Balogh, E.; Mato-Iglesias, M.; Platas-Iglesias, C.; Tóth, É.; Djanashvili, K.; Peters, J. A.; de Blas, A.; Rodríguez-Blas, T. *Inorg. Chem.* **2006**, *45*, 8719.

10 Livramento, J. B.; Helm, L.; Sour, A.; O'Neil, C.; Merbach, A. E.; Tóth, É. *Dalton Trans.* **2008**, 1195.

11 Caravan, P. *Chem. Soc. Rev.* **2006**, *35*, 512.

12 a) Vicens, J.; Böhmer, V. *Calixarenes, a Versatile Class of Macrocyclic Compounds* **1991**, Kluwer, Dordrecht; b) Mandolini, L.; Ungaro, R. *Calixarenes in Action 2000*, Imperial College Press, London; c) Vicens, J.; Harrowfield, J.; Baklouti, L. (eds.) *Calixarenes in the Nanoworld 2007*, Springer, Dordrecht.

13 Georgiev, E. M.; Roundhill, D. M. *Inorg. Chim. Acta* **1997**, *258*, 93.

14 Bryant, Jr., L. H.; Yordanov, A. T.; Linnoila, J. J.; Brechbiel, M. W.; Frank, J. A. *Angew. Chem. Int. Ed.* **2000**, *39*, 1641.

15 Aime, S.; Barge, A.; Botta, M.; Casnati, A.; Fragai, M.; Luchinat, C.; Ungaro, R. *Angew. Chem. Int. Ed.* **2001**, *40*, 4737.

16 Krishnan, A. M.; Lohrmann, R. *PCT Int. App.* **1996**, WO 96/14878.

17 Iwamoto, K.; Araki, K.; Shinkai, S. *J. Org. Chem.* **1991**, *56*, 4955.

18 Klimentová, J.; Vojtíšek, P. *J. Mol. Struct.* **2007**, *826*, 48.

19 Aarons, R. J.; Notta, J. K.; Meloni, M. M.; Feng, J.; Vidyasagar, R.; Narvainen, J.; Allan, S.; Spencer, N.; Kauppinen, R. A.; Snaith, J. S.; Faulkner, S. *Chem. Commun.* **2006**, 909.

20 a) Shinkai, S.; Arimura, T.; Araki, K.; Kawabata, H.; Satoh, H.; Tsubaki, T.; Manabe, O.; Sunamoto, J. *J. Chem. Soc. Perkin Trans. 1* **1989**, 2039; b) Arimori, S.; Nagasaki, T.; Shinkai, S. *J. Chem. Soc. Perkin Trans. 2* **1995**, 679; c) Lee, M.;. Lee, S.-J; Jiang, L.-H. *J. Am. Chem. Soc.* **2004**, *126*, 12724; d) Kellermann, M.; Bauer, W.; Schade, A. B.; Ludwig, K.; Böttcher, C. *Angew. Chem. Int. Ed.* **2004**, *43*, 2959.

21 Gaëlle, M. N.; Tóth, É.; Eisenwiener, K.-P.; Mäcke, H. R.; Merbach, A. E. *J. Biol. Inorg. Chem.* **2002**, *7*, 757.

22 Torres, S.; Martins, J. A.; André, J. P.; Geraldes, C. F. G. C.; Merbach, A. E.; Tóth, É. *Chem. Eur. J.* **2006**, *12*, 940.

23 Fatin-Rouge, N.; Tóth, É.; Perret, D.; Backer, R. H.; Merbach, A. E.; Bünzli, J.-C. G. *J. Am. Chem. Soc.* **2000**, *122*, 10810.

24 Torres, S.; Prata, M. I. M.; Santos, A. C.; André, J. P.; Martins, J. A.; Helm, L.; Tóth, É.; García-Martín, M. L.; Rodrigues, T. B.; López-Larrubia, P.; Cerdán, S.; Geraldes, C. F. G. C. *NMR Biomed.* **2008**, *21*, 322.

25 Jászberényi, Z.; Moriggi, L.; Schmidt, P.; Weidensteiner, C.; Kneuer, R.; Merbach, A. E.; Helm, L.; Tóth, É. *J. Biol. Inorg. Chem.* **2007**, *12*, 406.

26 Powell, D. H.; Ni Dhubhghaill, O. M.; Pubanz, D.; Helm, L.; Lebedev, Y. S.; Schlaepfer, W.; Merbach, A. E. *J. Am. Chem. Soc.* **1996**, *118*, 9333.

27 Vander Elst, L.; Sessoye, A.; Laurent, S.; Muller, R. N. *Helv. Chim. Acta.* **2005**, *88*, 574.

28 a) Helm, L. *Prog. Nucl. Magn. Reson. Spectrosc.* **2006**, *49*, 45; b) Fries, P. H.; Richardi, J.; Rast, S.; Belorizky, E. *Pure Appl. Chem.* **2001**, *73*, 1689; c) Rast, S.; Borel, A.; Helm, L.; Belorizky, E.; Fries, P. H.; Merbach, A. E. *J. Am. Chem. Soc.* **2001**, *123*, 2637.

29 a) Zhang, Z.; Greenfield, M. T.; Spiller, M.; McMurry, T. J.; Lauffer, R. B.; Caravan, P. *Angew. Chem. Int. Ed.* **2005**, *44*, 6766; b) Avedano, S.; Tei, L.; Lombardi, A.; Giovenzana, G. B.; Aime, S.; Longo, D.; Botta, M. *Chem. Commun.* **2007**, 4726; c) Aime, S.; Botta, M.; Geninatti Crich, S.; Giovenzana, G. B.; Pagliarin, R.; Piccinini, M.; Sisti, M.; Terreno, E. *J. Biol. Inorg. Chem.* **1997**, *2*, 470; d) Parac-Vogt, T. N.; Kimpe, K.; Laurent, S.; Vander Elst, L.; Burtea, C.; Chen, F.; Muller, R. N.; Ni, Y.; Verbruggen, A.; Binnemans, K. *Chem. Eur. J.* **2005**, *11*, 3077.

30 Corsi, D. M.; Platas-Iglesias, C.; van Bekkum, H.; Peters, J. A. *Magn. Reson. Chem.* **2001**, *39*, 723.

Densely packed Gd(III)-chelates with fast water exchange on a calix[4]arene scaffold: a potential MRI contrast agent

5

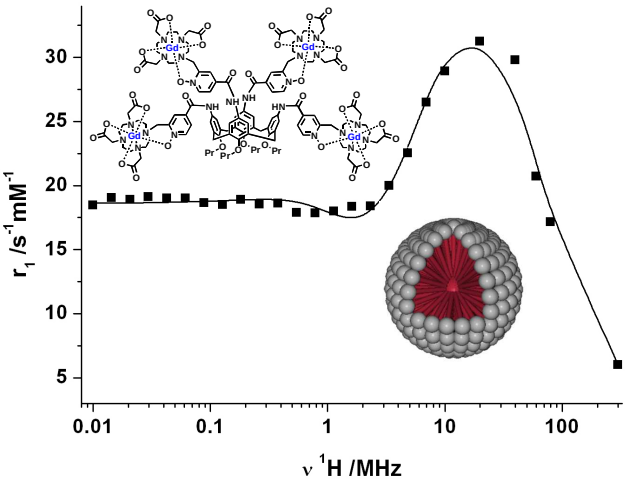

The contents of this chapter have been submitted to:
Schühle, D. T.; Polášek, M.; Lukeš, I.; Chauvin, T.; Tóth, E.; Schatz, J.; Hanefeld, U.; Peters, J. A.
Dalton Transactions.

Introduction

Magnetic resonance imaging (MRI) is one of the most powerful techniques in medical diagnostics. Usually, the water ^{1}H-signal is detected and the contrast is generated by differences in proton density and longitudinal (T_1) or transverse (T_2) relaxation time. To enhance the contrast in T_1-weighted images, mainly gadolinium(III) based contrast agents (CAs) are administered prior to the examination.[1-6] To avoid the release of the toxic free lanthanide ion, strong chelators such as 1,4,7,10-tetracarboxymethyl-1,4,7,10-tetraazacyclododecane (DOTA) and derivatives thereof are used. The contrast that can be achieved with a certain amount of CA depends on the choice of the ligand because that determines its physico-chemical properties and its distribution in the patient.

Good performance of the contrast agent per mmol Gd is desirable i.e. the millimolar longitudinal proton relaxivity (r_1) of the contrast agent has to be as high as possible. The two commonly used ways to optimize the relaxivity are to increase the rotational correlation time (τ_R) of the CA and to optimize the residence time of a water molecule directly bound to the metal center (τ_M) to 20 - 40 ns (at 60 MHz and 25 °C).

Recently, we have shown that calix[4]arenes are versatile building blocks in the design of MRI CAs.[7-10] They allow the introduction of four chelating groups on the *upper rim*, enable further functionalization at the *lower rim* and they turned out to be very rigid, which has a beneficial effect on the value of τ_R, and thus the relaxivity.[7] The rigidity is mainly due to the densely arranged chelators on the calixarene that leads to hindered rotation within the molecule. The previously studied **1** (see Figure 5.1) showed micelle formation and interaction with human serum albumin (HSA). Both effects result in a significant increase of the molecular volume, which is reflected in a longer τ_R and, therefore, in a higher relaxivity.

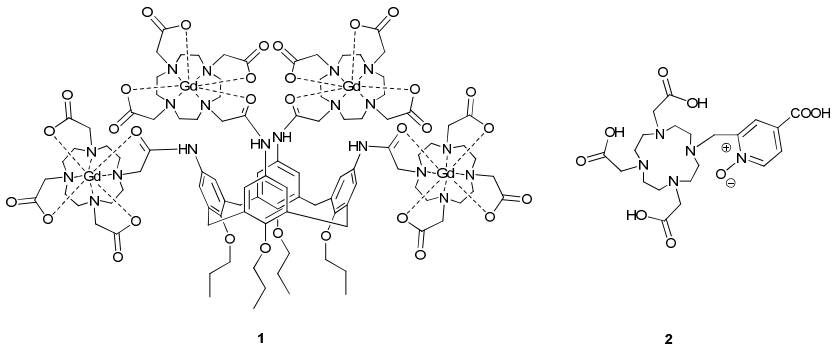

1 **2**

Figure 5.1. Structures of calixarene **1** and PyNox **2**.

The relaxivity of **1** is limited mainly by its long τ_M.[7] Therefore, we now decided to replace the DOTA moieties in **1** by chelator **2** (Figure 5.1). The Gd(III) complex of the parent **2** has a τ_M of 34 ns at 25 ºC and therefore, is optimal in this respect.[11-13] The rigid pyridine moiety, the presence of the carboxylic acid group attached to the pyridine ring and the possibility to convert this group into an amide with partial double bond character makes **2** a good ligand for conjugation to other molecules. First attempts to increase the relaxivity of systems based on **2** by increasing τ_R were to couple it to PAMAM-dendrimers.[14] The unexpectedly small increase in relaxivity of those conjugates was attributed to local motions in the rather flexible dendrimer core that reduce the effective rotational correlation time.

In this paper, we describe the synthesis of **3** along with the evaluation of its relaxometric properties.

Results and Discussion

Synthesis

Conjugate **3** was obtained from starting materials described before.[13,15] As previously observed during the synthesis of compound **1**, the crucial step is the amide bond formation of tetraaminocalix[4]arene **4** and the carboxy functionalised chelator.[7]

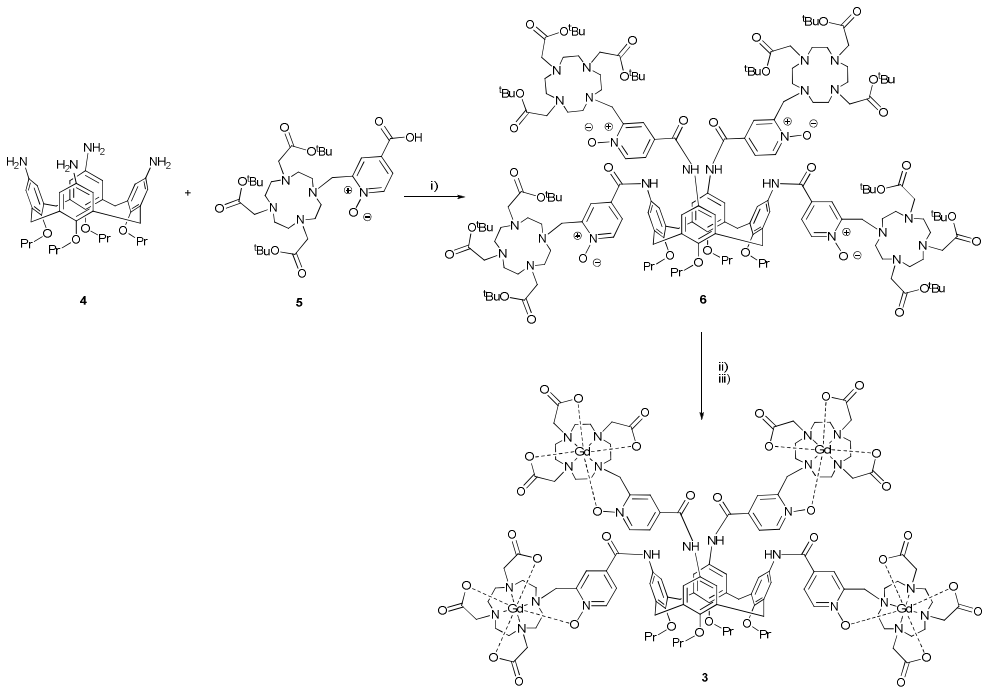

Scheme 5.1. Preparation of **3**: (i) TBTU, MeCN, 3d, rt; (ii) TFA/DCM 50:50, overnight, rt; (iii) $GdCl_3 \cdot 6H_2O$, NaOH, H_2O, pH 7, 1 d, rt.

The reaction was performed using six equivalents of **5** as its Hünig's base (DIPEA) salt and *O*-(benzotriazol-1-yl)-*N*,*N*,*N'*,*N'*-tetramethyluronium tetrafluoroborate (TBTU) at room temperature. After three days the conversion was complete as monitored by HPLC. The reaction mixture contained only **6** and low molecular weight compounds that were removed by ultrafiltration. The mixture was dissolved in a methanolic NH_4OAc buffer to break ion pairs between the chelator and hydroxybenzotriazole (HOBt) and subjected to continuous ultrafiltration first with this buffer and then with pure methanol. A smooth deprotection of the *tert*-butyl ester groups by TFA and subsequent complexation of the unpurified intermediate dodecaacid with an excess of $GdCl_3 \cdot 6H_2O$ gave **3**, which was purified by ultrafiltration after complexation of the excess of Gd(III) with EDTA.

Aggregation

Previously, we have shown that above the critical micelle concentration (*cmc*) of 0.21 mM, calix[4]arene **1** forms micelles with a radius of 2.2 nm in aqueous solution.[7] Dynamic light scattering (DLS) on a 3.7 mM sample of **3** at 25 °C (see Figure 5.2) illustrates that also this compound self-aggregates. The presence of two peaks in the DLS spectra shows that there are two different aggregates present with hydrodynamic radii of 8.2 and 85.0 nm. Increase of temperature to 50 ºC did not result in significant changes indicating that these aggregates are very stable. It needs to be stressed that the intensity weighted DLS spectra depicted in Figure 5.2 do not reflect the quantitative composition of the solution. Particles that are a factor of 10 larger than others scatter light approximately one million times more than the smaller aggregates.[16] This means that **3** is almost exclusively present as small, 8.2 nm micelles with only traces of larger aggregates. The narrow size distribution for the small aggregates is an indication that they are spherical micelles. This shape was confirmed by cryo-TEM (data not shown). There is no evidence of larger aggregates in the cryo-TEM, which is another indication that the concentration of these larger aggregates is negligible.

The *cmc* of the micelles was determined with the use of relaxometric NMR measurements.[17] This method makes use of the increase in relaxivity of Gd-complexes upon aggregation due to increase of τ_R. Therefore, the paramagnetic relaxation rate (R_1) was measured as a function of the concentration of Gd (c_{Gd}) in **3**. In the absence of self aggregation, a plot of R_1 versus c_{Gd} should be a straight line. If there is self aggregation, R_1 is a sum of two linear relations, starting at the *cmc*.

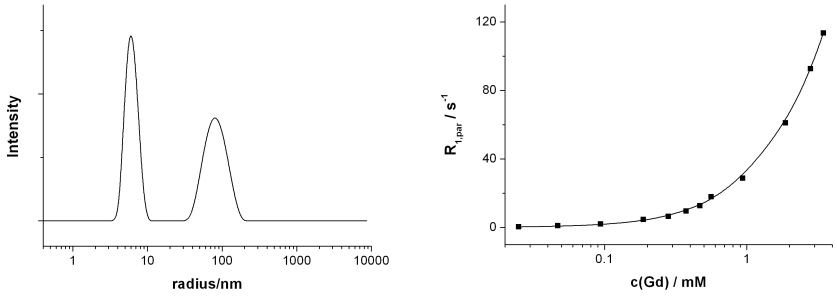

Figure 5.2. DLS (3.7 mM, 25 ºC) (left) and relaxometric ^{1}H NMR measurements of **3** (25 ºC, 20 MHz) (right). The line indicates the results form the fitting of the experimental data with Equations 5.1 and 5.2.

$$\frac{1}{T_1} = \frac{1}{T_{1obs}} - \frac{1}{T_{1dia}} = R_1 = 4cmc \cdot r_1^{n.a} + (c_{Gd} - 4cmc) \cdot r_1^{a} \quad 5.1$$

$$R_1 = c_{Gd} \cdot r_1^{n.a} \quad 5.2$$

Above the *cmc*, Equation 5.1 describes R_1 as a function of the concentration of Gd (c_{Gd}), the relaxivity of the monomer ($r_1^{n.a.}$) and the aggregates (r_1^{a}) as well as the *cmc*. Equation 5.2 describes R_1 as a function of c_{Gd} below the *cmc*.

The value of $r_1^{n.a.}$ was determined to be 17.1 $s^{-1}mM^{-1}$ using an independent measurement of the relaxivity of a sample well below the *cmc* (6.25 μM). The data from the relaxometric measurements as a function of c_{Gd} at 25 ºC (Figure 5.2), were fitted using Equations 5.1 and 5.2 keeping $r_1^{n.a.}$ fixed to 17.1 $s^{-1}mM^{-1}$. The best-fit value for the *cmc* is 35±5 μM and that for r_1^{a} 33.5±0.5 $s^{-1}mM^{-1}$ at 25 ºC and 20 MHz. It should be noted that only one *cmc* was observed, which once again indicates that the larger aggregates detected in the DLS are present in negligible amounts.

At 37 ºC, a strictly linear dependence of R_1 on the concentration was found for values of c_{Gd} between 0.025 mM and 3.70 mM. This indicates that the *cmc* is even smaller at higher temperatures; which is typical for noncharged surfactants.

The lower *cmc* of **3** compared to **1** as well as the presence of a very small fraction of an additional type of larger aggregates suggests that stronger hydrophobic interactions exist among the chelates **3**. This can be attributed to the relatively large hydrophobic part in this compound due to the presence of the pyridine-*N*-oxide moieties. In addition, this may give rise to a different shape of the monomer and thus to different geometries of the aggregates.

Water exchange

The most suitable technique to asses the water exchange kinetics is variable temperature ^{17}O NMR. From chemical shifts (ω), longitudinal (T_1) and transverse (T_2) relaxation times of the water ^{17}O resonance, the reduced parameters ($\Delta\omega_r$, T_{1r}, T_{2r}) can be calculated by using the mole fraction of the Gd-bound water (P_m) and the corresponding parameters of a reference sample (ω_A, T_{1A}, T_{2A}).[19]

$$\Delta\omega_r = \frac{1}{P_m}(\omega - \omega_A) \tag{5.3}$$

$$\frac{1}{T_{1r}} = \frac{1}{P_m}\left[\frac{1}{T_1} - \frac{1}{T_{1A}}\right] \tag{5.4}$$

$$\frac{1}{T_{2r}} = \frac{1}{P_m}\left[\frac{1}{T_2} - \frac{1}{T_{2A}}\right] \tag{5.5}$$

The measurements were performed at 7.05 T and at relatively high concentration (91.7 mM Gd corresponding to 22.9 mM **3**). At this high concentration, the contribution of monomeric **3** can be neglected and the data are representative for micellar **3**.

The almost constant value found for $\Delta\omega_r$ and the fact that T_{2r} has no maximum in the studied temperature range means that **3** is in the fast exchange regime for all temperatures.

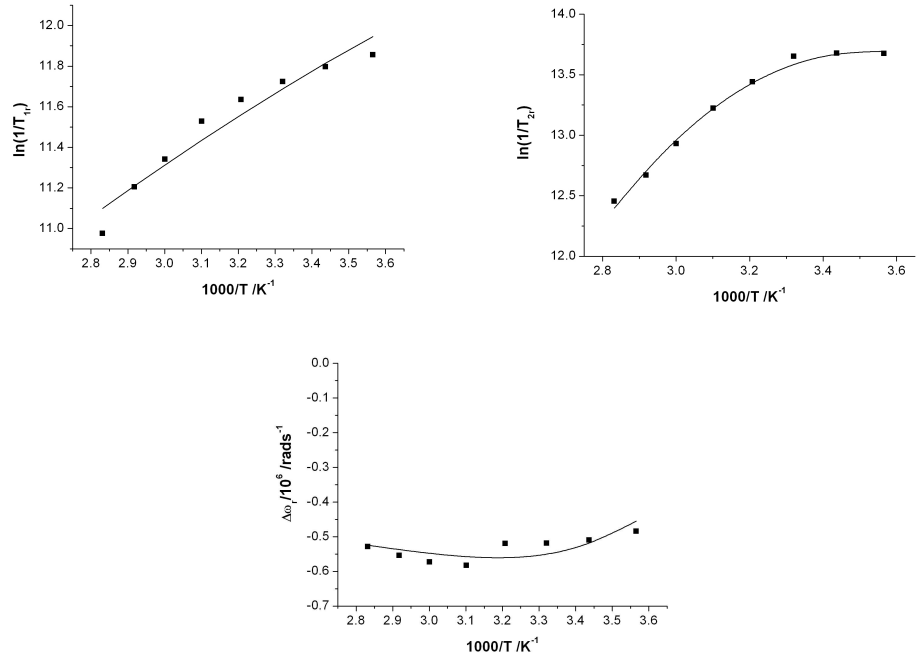

Figure 5.3. Temperature dependence of reduced longitudinal (T_{1r}) and transversal (T_{2r}) relaxation times and angular frequency ($\Delta\omega_r$) of a 22.9 mM aqueous solution of **3** at 7.05 T (curves represent results from the fittings, see Experimental).

The best fit-values obtained from a fitting of the experimental data with the appropriate equations of the temperature dependence of these reduced parameters are compiled in Table 5.1.[18] The curves in Figure 5.3 are calculated with these values. The parameters describing the water exchange kinetics, τ_R and its activation enthalpy $\Delta H^{\neq}$ are in the expected range for conjugates with **2**.[11] The slightly longer τ_M found for **3** can be attributed to the fact that the conversion of the carboxylic acid to an amide has an effect on the electron density in the aromatic ring and therefore also on the oxygen atom coordinated to the metal center. Similar effects were observed for PAMAM conjugates with **2**.[14] The best-fit values for the rotational dynamics are in the expected range for aggregates of this type and the electronic parameters, namely the mean square zero-field splitting energy (Δ^2) and its rotational correlation time (τ_v^{298}), are almost identical to those found for the parent system **2**.[11,12]

Table 5.1. Parameters obtained from simultaneous fitting of the variable temperature ^{17}O NMR data of **3**.

$\Delta H^{\neq}$ [kJmol^{-1}]	38.4 ± 2.8
τ_M^{298} [ns]	72.7 ± 9.9
τ_R^{298} [ps]	754 ± 20
E_R [kJmol^{-1}]	9.64 ± 0.72
Δ^2 [10^{20} s^{-1}]	0.46 ± 0.04
τ_v^{298} [ps]	2.70 ± 0.20
A/ħ [10^6 rads^{-1}]	-3.32 ± 0.13

Relaxivity

Nuclear magnetic relaxation dispersion (NMRD) is a widely used technique in MRI research. The relaxivity r_1 as a function of the magnetic field (B) or the proton Larmor frequency ($\upsilon(^1H)$) is called NMRD profile. From these profiles, important parameters such as mainly the electronic parameters as well as τ_R can be obtained by fitting them with the appropriate equations.[18]

Owing to the very low *cmc* of **3**, it was not possible to measure NMRD profiles of monomeric **3**. An NMRD profile of micellar **3** was acquired at 925 μM concentration (Figure 5.4). It shows a peak around 20 to 40 MHz which is typical for large, slowly

tumbling systems. The relaxivity of **3** (31.2 $s^{-1}mM^{-1}$ per Gd^{3+} and 125 $s^{-1}mM^{-1}$ per molecule at 25 ºC and 20 MHz) is about twice of that of conjugates with generation 4 PAMAM dendrimers (16 $s^{-1}mmol^{-1}$ for G4-Gd-**2**) and is even more superior to the generation 1 analogue (G1-Gd-**2**).[14] This can only be caused by either a higher τ_R due to aggregation or higher internal rigidity.

To gain more insight into the reasons for the enhanced relaxivity of micellar **3** compared to its PAMAM analogues, the NMRD profile was analysed with the Solomon-Bloembergen-Morgan theory, extended by the Lipari-Szabo approach, for the inner sphere contribution and the Freed equations for the outer sphere contribution.[18,19] In the Lipari-Szabo approach, τ_R of slowly tumbling molecules is described by two different and independent tumbling times that contribute to the overall motion: a fast local (τ_l) and a slower global (τ_g) correlation time.[1] The extent to which they contribute to τ_R is expressed by an order parameter S^2 with S^2=1 for a perfectly rigid system (τ_l is negligible) and S^2=0 for flexible compounds where internal motions fully dominate the rotational dynamics. To limit the number of parameters involved in the fitting, the parameters that describe the water exchange kinetics were fixed to the values found by ^{17}O NMR (Table 5.1). A simultaneous fit of the ^{17}O and NMRD data was not possible which might be ascribed to different aggregation behaviours at the different concentrations needed for the measurements. A good fit for the NMRD profile was obtained for the values listed in Table 5.2. For comparison, previously published data for **1** and for PAMAM conjugates of **2** are included in Table 5.2.

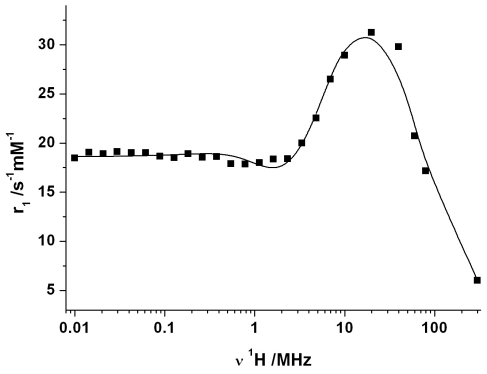

Figure 5.4. NMRD profile of a 925 μM solution of **3** at 25 ºC. The curve indicates the results from the fitting.

In comparison to micellar **1**, not only τ_M is much more favourable, but also the overall rotational dynamics is improved. This is due to the larger radius of the spherical micelles formed by **3** (8.2 nm compared to 2.2 nm for **1**). The rather small value for τ_l indicates a fast internal motion within the micelles and therefore, a loss in rigidity compared to **1**. The order parameter S^2 shows that the contribution of internal motion to the overall rotational dynamics is significant and that the rotations of the chelates around the connection point to the calixarene are not hindered effectively. The larger distance between the metal ion and the platform leads to more flexibility due to rotations and/or vibrations. This can be rationalized by the additional bonds between the metal and the calixarene core that increase the distance between the bulky chelates and therefore, decrease the steric repulsions between them. The electronic parameters follow the trend observed for Gd-**2** and the PAMAM conjugates. For G4-Gd-**2**, we assume a similar radius as found for other PAMAM dendrimers conjugated with DOTA based chelators of about 6 nm, whereas the generation 1 analogue measures around 2 nm.[20] Micellar **3** measures 8.2 nm, which makes it the largest particle studied up to now for conjugates with **2**. Upon an increase of size, generally Δ^2 descreases whereas τ_v increases.[21]

Table 5.2. Relaxometric parameters for selected Gd(III) chelates (underlined values were fixed during the fittings).

	1[a]	Gd-**2**[b]	G1-Gd-**2**[c]	G4-Gd-**2**[c]	**3**
τ_M^{298} [ns]	1200 ± 120[d]	34 ± 0.1	<u>55.5</u>	55.5 ± 2	<u>72.7</u>[d]
τ_R^{298} [ps]	1802 ± 110[e]	93 ± 13	τ_g = 570 ± 30	τ_g = 1040 ± 100	τ_g = 2621 ± 196[e]
			τ_l = 190 ± 13	τ_l = 213 ± 6	τ_l = 163 ± 52[e]
S^2	-	-	0.35 ± 0.03	0.38 ± 0.03	0.44 ± 0.03[e]
Δ^2 [10^{20} s^{-1}]	0.051 ± 0.006[e]	0.90 ± 0.11	0.105 ± 0.006	0.083 ± 0.002	0.042 ± 0.003[e]
τ_v^{298} [ps]	61.9 ± 2.2[e]	4.7 ± 0.6	49 ± 2	56 ± 1	95 ± 4[e]
r_1 [$s^{-1}mM^{-1}$][f]	18.3[g]	5.7	11.0	15.6	31.2
Density of relax. [$(g/l)^{-1}s^{-1}$][f]	26.0[g]	8.7	13.5	17.7	39.2

[a] values adopted from Ref[7];

[b] see Ref[11]; values obtained by a simultaneous fit of ^{17}O and NMRD data;

[c] see Ref[14]; values obtained by a simultaneous fit of ^{17}O and NMRD data;

[d] values obtained by a fit of ^{17}O data;

[e] values obtained by a fit of NMRD data of the micellar compound at 25 ºC;

[f] At 25 ºC and 20 MHz;

[g] At 37 ºC and 20 MHz.

The order parameter S^2 for the micellar **3** is in the same range as that found for the PAMAM conjugates of **2**.[14] This means that the internal motions in **3** and the dendrimers contribute to about the same extent to the overall rotational dynamics and that there is no rigidification within **3**. To confirm that τ_g is the main factor causing the two fold enhanced relaxivity of the micellar **3** with respect to that for the generation 4 dendrimer, a simulation was performed. All parameters for **3** were kept at the values mentioned in Table 5.2 with the exception of τ_g, which was changed to the value found for G4-Gd-**2**. The simulated relaxivity at 20 MHz and 25 °C is 18.2 $s^{-1}mmol^{-1}$, which is very close to the value observed for G4-Gd-**2** (15.6 $s^{-1}mmol^{-1}$) confirming that the increase of relaxivity for micellar **3** is indeed due to its larger size.

For molecular imaging applications, the molar relaxivity, r_1 is not always the most appropriate parameter to express the efficiency of a CA. It is often more important to know the payload of Gd that can be delivered per mass unit of CA. Therefore, the *density of relaxivity* was introduced, which is defined as the relaxation rate enhancement by a unity mass of the CA.[22] It is calculated by dividing the relaxivity per particle by its molecular weight. Micellar **3** has a *density of relaxivity* of 39.2 $(g/l)^{-1}s^{-1}$ at 20 MHz and 25 °C. This is significantly higher than that of the benchmark metallostar (32.3 $(g/l)^{-1}s^{-1}$) which has one of the highest *densities of relaxivity* reported so far.[22] The higher *density of relaxivity* of **3** can be attributed to both optimized τ_M and rotational motions that even compensate the fact that the metallostar has two inner sphere water molecules.

Interaction with Bovine Serum Albumin

As shown in previous studies on lanthanide binding calixarenes, this class of compounds is able to interact with albumins.[7,23,24] Therefore, binding studies with **3** and bovine serum albumin (BSA) were performed.[23] The increase of τ_R upon binding of **3** to albumin leads to an increase in r_1. A sample of **3** with a concentration well below the *cmc* (6.25 μM) was titrated with BSA at 37 ºC and 20 MHz. The peptide concentration (c_{BSA}) was varied between 0.1 and 2.0 mM (Figure 5.5). The relaxivity shows a stepwise increase in relaxivity upon an increase of the BSA concentration. A sample with a four times higher concentration of **3** showed a similar behaviour (data not shown). In both cases, no plateau

in the relaxivity was reached indicating that the binding is rather weak, as was also observed for **1**.[7] The stepwise increase of r_1 upon an increase of the protein concentration might be rationalized by binding of **3** to different binding sites in BSA, probably on the surface of the protein.

Due to the weak binding, it was not possible to determine accurate binding constants of **3** to BSA. For practical applications, the observed relaxivity ($r_{1,obs}$) of the solution, which is defined as the relaxivity of **3** in the presence of the albumin after correction for the diamagnetic contribution of the protein is of much greater relevance.[25] For many albumin targeted CAs, r_1 is rather high but due to relatively weak binding, $r_{1,obs}$ is in the range of 16 to 28 $s^{-1}mM^{-1}$ for solutions containing the physiological albumin concentration (0.67 mM).[25] As shown in Figure 5.5, between 0.6 mM and 0.8 mM BSA concentration, the relaxivity of a 6.25 μM solution of **3** under these conditions has an $r_{1,obs}$ of around 26 $s^{-1}mM^{-1}$, per gadolinium, which corresponds to a relaxivity of 104 $s^{-1}mM^{-1}$ per mM **3** and per BSA binding site. The observed relaxivity could be further enhanced by shifting the equilibrium to the BSA-bound form. This is demonstrated by the fact that at high c_{BSA}, a relaxivity of 40.8 $s^{-1}mM^{-1}$ (per mM **3** 163.2 $s^{-1}mM^{-1}$) was observed.

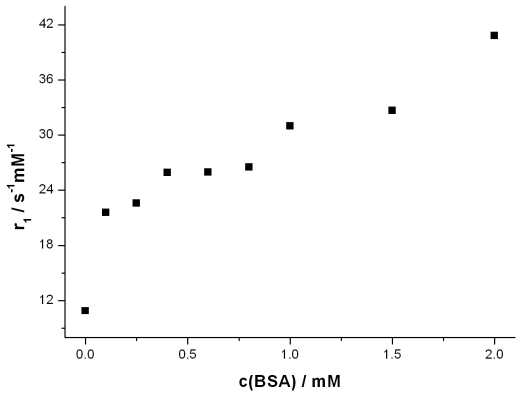

Figure 5.5. Relaxometric BSA titration of a 6.25 μM solution of **3** (37 ºC, 20 MHz).

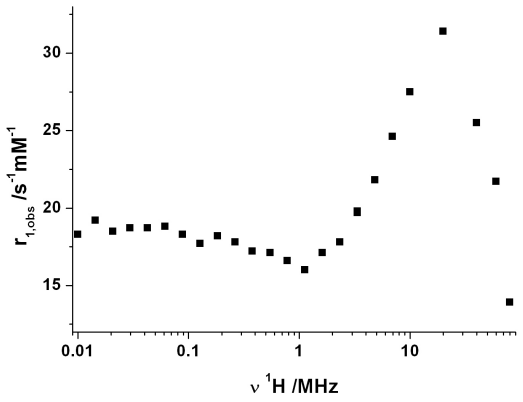

Figure 5.6. NMRD profile of a 6.25 μM solution of **3** in the presence of 0.6 mM BSA at 37 ºC.

To obtain more information about the relaxivity of **3** under *in vivo* conditions, an NMRD measurement of **3** was performed in the presence of 0.6 mM albumin (Figure 5.6). The rather narrow peak at around 20 MHz is a strong indication for the formation of slowly tumbling BSA adducts. Therefore, **3** has potential as an MRI contrast agent for application in angiography.

Conclusions

The compound presented in this study is a promising candidate for MRI applications. Its self-aggregation in water results in spherical micelles that appear already at low concentration (<25 μM at 37 °C). Thanks to an almost optimal value of τ_M, **3** exhibits good relaxivities both in monomeric and aggregated form as well as in the presence of BSA. The high relaxivities of the supramolecular species are due to their large sizes and not to an intramolecular rigidification. With this compound, a relaxivity of more than 163 $s^{-1}mM^{-1}$ per calixarene molecule could be achieved. The density of relaxivity at 20 MHz and 25 °C of this compound is extremely high (39.2 $(g/l)^{-1}s^{-1}$), which opens up possiblities to use similar compounds in the molecular imaging of, for example, receptors on cell surfaces.

Experimental

Compounds **2** and **4** were readily available following literature procedures.[11,15] All other chemicals were of commercial grade and were used without further purification. The NMR spectra were acquired on a Varian Inova-300 spectrometer.

Sample preparation

Compound **3** was dissolved in water containing approximatelly 0.5% of ^{17}O-enriched water and *tert*-butanol as internal standard. The gadolinium concentration was determined by bulk magnetic susceptibility (BMS) measurements using acidified water containing a small amount of *tert*-butanol as external internal standard.[26] All further measurements were performed using this solution (91.7 mM Gd, 22.9 mM **3**) as a stock solution.

Methods

^{17}O NMR. These measurements were performed on a Varian Inova-300 spectrometer (40.7 MHz). T_1 relaxation times were measured by the standard inversion recovery pulse sequence. T_2 relaxation times were determined by the Carr-Purcell-Meiboom-Gill spin echo pulse sequence. No frequency lock was used and the samples were not spun. The chemical shifts (in ppm) were corrected for the BMS by using a reference of acidified water having *tert*-butanol as internal standard. To ensure temperature equilibration, the samples were kept in the probe for at least 10 minutes prior to the measurements.

^{1}H NMRD. The ^{1}H NMRD profiles were recorded on a Stelar Smartracer FFC fast-field-cycling relaxometer covering magnetic fields from $2.35 \cdot 10^{-4}$ to 0.25 T, which corresponds to a proton Larmor frequency range of 0.01-10 MHz. The relaxivity at higher fields was recorded using a Bruker WP80 with the Spinmaster Smartracer PC-NMR console at variable field from 20 MHz to 80 MHz. The temperature was controlled by a VTC90 temperature control unit and fixed by a gas flow. The temperature was determined according to previous calibration with a Pt resistance temperature probe. All samples were

kept in the probe for at least 10 minutes to equilibrate the temperature prior to the measurment.

Fittings of NMR data. All fittings were performed using the Micromath Scientist program with the least-square procedure and the commonly used equation set.[19,21] For some of the parameters describing the NMRD profiles, commonly accepted values were used such as for the distance between Gd(III) and a proton of coordinated water (r_{GdH}) 3.1 Å and the distance of the closest approach of an outer sphere water proton to Gd(III) 3.5 Å. The activation energy for the electronic rotational correlation time (E_v) was fixed at 1 kJmol^{-1} and the parameter determining the spin rotation contribution (δ_{gL}) at 0.021.[19] The diffusion coefficient and its activation energy were fixed to the values of pure water.[27]

DLS. Dynamic light scattering (DLS) was performed on a Zetasizer NanoZs, Malvern, UK instrument. The samples measured prior to filtration through a 0.2 μm syringe filter showed identical spectra than after filtration.

Synthesis

5,11,17,23-Tetrakis-(*tert*-butyl-DO3A-py$^{No\text{-}C}$-acetamidyl)-25,26,27,28-tetrapropoxy-calix[4]arene (6)

In an inert atmosphere, the DIPEA salt of *tert*-butyl-DO3A-py$^{No\text{-}C}$-carboxylic acid· (**5**) (292 mg, 367 μmol) and TBTU (162 mg, 367 μmol) were stirred in anhydrous MeCN (8 ml) for 1 h. This was then added to a solution of 5,11,17,23-tetraamino-25,26,27,28-tetrapropoxy-calix[4]arene (**4**) (40 mg, 61.3 μmol) in anhydrous MeCN (20 ml). After stirring the mixture for 3 d at ambient temperature, the solvent was removed and the product was purified by ultrafiltration over a 1 kDa membrane using continuous elution with a 0.05 M NH_4OAc solution in MeOH followed by pure methanol. After evaporation of the solvent, the product could be obtained as a fluffy slightly yellow powder by lyophilisation from benzene (176.3 mg, 54.4 μmol, 89%).

^{1}H NMR (300 MHz, MeOD-d_4, 55 ˚C, TMS): δ = 1.06 (12 H, t, *J* = 7.4 Hz, CH_3), 1.40, 1.46 (72 and 36 H, 2 s, *tert*-Bu), 2.01 (8 H, sext, *J* = 7.4 Hz, CH_2-CH_3), 2.81 – 3.02 (64 H, m, N-CH_2-CH_2), 3.26 (4 H, d, *J* = 13.2 Hz, ArCH_2Ar), 3.36, 3.43 (32 H, 2 br s, N-CH_2-CO), 3.96 (8 H, t, *J* = 7.4 Hz, OCH_2CH$_2$), 4.60 (4 H, d, *J* = 13.2 Hz, ArCH_2Ar), 7.18 (8 H,

s, Ar-H), 7.80 (4 H, br m, Ar-H), 8.30 (4H, d, *J* = 6.9 Hz, Ar-H), 8.34 (4H, br s, Ar-H). ^{13}C NMR (75 MHz, MeOD-d_4, 55 ˚C, TMS): δ = 9.63 ($CH_2\mathit{C}H_3$), 23.24 ($\mathit{C}H_2CH_3$), 27.34 ($OC(\mathit{C}H_3)_3$), 31.13 ($Ar\mathit{C}H_2Ar$), 46.27, 50.39, 50.90, 53.75 ($N\mathit{C}H_2\mathit{C}H_2N$, $N\mathit{C}H_2COO$), 77.09 ($O\mathit{C}H_2CH_2$), 81.37, 81.48 ($O\mathit{C}(CH_3)_3$), 118.58, 121.05, 121.59, 132.24, 135.20, 143.79, 148.94, 154.00, 160.35 (Ar-C), 171.40, 171.53 (*C*OtBu), 178.99 (*C*ONH). ESI-MS: calc.: *m/z* = 1660.08 $(M+2K)^{2+}$, found: 1659.97.

5,11,17,23-Tetrakis-(DO3A-py$^{No\text{-}C}$-acetamidyl)-25,26,27,28-tetrapropoxy-calix[4]arene

5,11,17,23-Tetrakis-(*tert*-butyl-DO3A-py$^{No\text{-}C}$-acetamidyl)-25,26,27,28-tetrapropoxy-calix[4]arene (**6**) (99.0 mg, 30.5 μmol) was dissolved in a mixture of TFA/DCM 50:50 (6 ml). After stirring overnight, the solvents were evaporated and the product was lyophilized from water to give the title compound (113.8 mg) as its TFA salt. The compound was not purified since TFA as well as inorganic impurities can easily be removed after the complexation with Gd^{3+} by ultrafiltration.

^{1}H NMR (300 MHz, D_2O, 90 ˚C): δ = 1.57 (12 H, t, *J* = 7.0 Hz, $C\mathit{H}_3$), 2.47 (8 H, sext, *J* = 7.0 Hz, $C\mathit{H}_2$-CH_3), 3.81 – 4.99 (112 H, m, N-$C\mathit{H}_2$-$C\mathit{H}_2$, $ArC\mathit{H}_2Ar$, N-$C\mathit{H}_2$-CO, $OC\mathit{H}_2CH_2$), 7.68 (8 H, s, Ar-H), 8.37 (4 H, d, *J* = 6.3 Hz, Ar-H), 8.62 (4H, s, Ar-H), 8.87 (4H, d, *J* = 6.3 Hz, Ar-H). ^{13}C NMR (75 MHz, D_2O, 90 ˚C): δ = 10.9 ($CH_2\mathit{C}H_3$), 23.86 ($\mathit{C}H_2CH_3$), 31.70 ($Ar\mathit{C}H_2Ar$), 50.91, 51.12, 53.52, 55.04, 55.70 ($N\mathit{C}H_2\mathit{C}H_2N$, $N\mathit{C}H_2COO$), 77.62 ($O\mathit{C}H_2CH$), 117.24 (quart, *J* = 293 Hz, $F_3\mathit{C}COO$), 122.12, 126.41, 128.62, 132.47, 135.06, 141.21, 154.99 (Ar-C), 162.86 (quart, *J* = 34.8 Hz, $F_3C\mathit{C}OO$), 171.70 (*C*ONH). ESI-MS: calc.: *m/z* = 857.93 $(M+3H)^{3+}$, found: 858.23.

5,11,17,23-Tetrakis-(DO3A-py$^{No\text{-}C}$-acetamidyl)-25,26,27,28-tetrapropoxy-calix[4]arene Gd-complex (3)

5,11,17,23-Tetrakis-(DO3A-py$^{No\text{-}C}$-acetamidyl)-25,26,27,28-tetrapropoxy-calix[4]arene (88.8 mg of the crude compound) was dissolved in water (20 ml) and $GdCl_3 \cdot 6H_2O$ (51.4 mg, 138 μmol) was added. The pH was slowly adjusted to 7 using aqueous NaOH and the solution was stirred for 1 d. EDTA (40 mg, 138 μmol) was added and the pH kept between 5.5 and 7.5. After stirring for further 3 h, the Gd^{3+}-complex was purified by ultrafiltration (500 Da membrane, solvent: water) and obtained after lyophilisation as a yellow powder (45.0 mg, ca. 60% yield). ESI-MS: calc.: *m/z* = 1085.42 $(M+3Na)^{3+}$, found: 1085.25.

References

1 Tóth, É.; Merbach; A. E. *The Chemistry of Contrast Agents in Medical Magnetic Resonance Imaging*, Wiley, New York, **2001**.

2 Caravan, P. *Chem. Soc. Rev.*, **2006**, *35*, 512.

3 Caravan, P.; Ellison, J. J.; McMurry, T. J.; Lauffer, R. B. *Chem. Rev.*, **1999**, *99*, 2293.

4 Aime, S.; Fasano, M.; Terreno, E. *Chem. Soc. Rev.*, **1998**, *27*, 19.

5 Aime, S.; Crich, S. G.; Gianolio, E.; Giovenzana, G.; Tei, L.; Terreno, E. *Coord. Chem. Rev.*, **2006**, *250*, 1562.

6 Bottrill, M.; Kwok L.; Long, N. J. *Chem. Soc. Rev.*, **2006**, *35*, 557.

7 Schühle, D.T.; Schatz, J.; Laurent, S.; Vander Elst, L; Muller, R. N.; Stuart, M. C. A.; Peters, J. A. *Chem. Eur. J.*, **2009**, *15*, 3290.

8 Mandolini, L.; Ungaro, R. *Calixarenes in Action*, Imperial College Press, London, **2000**.

9 Vicens, J.; Harrowfield, J.; Baklouti, L. *Calixarenes in the Nanoworld*, Springer, Dordrecht, **2007**.

10 Vicens, J.; Böhmer, V. *Calixarenes, a Versatile Class of Macrocyclic Compounds*, Kluwer, Dordrecht, **1991**.

11 Polášek, M.; Rudovský, J; Hermann, P.; Lukeš, I.; Vander Elst, L.; Muller, R. N. *Chem. Commun.*, **2004**, 2602.

12 Polášek, M.; Šedinová, M.; Kotek, J.; Vander Elst, L.; Muller, R.N.; Hermann, P.; Lukeš, I. *Inorg. Chem.*, **2009**, *48*, 455.

13 Polášek, M.; Kotek, J.; Hermann, P.; Císařová, I.; Binnemans, K.; Lukeš, I. *Inorg. Chem.*, **2009**, *48*, 466.

14 Polášek, M.; Hermann, P.; Peters, J. P.; Geraldes, C. F. G. C.; Lukeš, I. *in preparation*.

15 Klimentová, J.; Vojtísek, P. *J. Mol. Struct.*, **2007**, *826*, 48.

16 Lindner, P.; Zemb, T. *Neutrons, X-rays and Light: Scattering Methods Applied to Soft Condensed Matter*, Elsevier, Amsterdam, **2002**.

17 André, J. P.; Tóth, É.; Fischer, H.; Seelig, A.; Mäcke, H. R.; Merbach, A. E. *Chem. Eur. J.*, **1999**, *5*, 2977.

18 Powell, D. H.; Dhubhghaill, O. M. N.; Pubanz, D.; Helm, L.; Lebedev, Y. S.; Schlaepfer, W.; Merbach, A. E. *J. Am. Chem. Soc.*, **1996**, *118*, 9333.

19 Gaëlle, N. M.; Tóth, É.; Eisenwiener, K.; Mäcke, H. R.; Merbach, A. E. *J. Biol. Inorg. Chem.*, **2002**, *7*, 757.

20 Kobayashi, H.; Brechbiel, M. W. *Adv. Drug Deliv. Reviews*, **2005**, *57*, 2271.

21 Helm, L. *Prog. Nucl. Magn. Res. Spectrosc.*, **2006**, *49*, 45.

22 Livramento, J. B.; Tóth, É.; Sour, A.; Borel, A.; Merbach, A. E.; Ruloff R. *Angew. Chem. Int. Ed.*, **2005**, *117*, 1504.

23 Bryant, Jr, L. H.; Yordanov, A. T.; Linnoila, J. J.; Brechbiel, M. W.; Frank, J. A. *Angew. Chem. Int. Ed.*, **2000**, *39*, 1641.

24 Aime, S., Barge, A.; Botta, M.; Casnati, A.; Fragai, M.; Luchinat, C.; Ungaro, R. *Angew. Chem. Int. Ed.*, **2001**, *40*, 4737.

25 Dumas, S.; Troughton, J. S.; Cloutier, N. J.; Chasse, J. M.; McMurry, T. J.; Caravan, P. *Austr. J. Chem.*, **2008**, *61*, 682.

26 Corsi, D. M.; Platas-Iglesias, C.; van Bekkum, H.; Peters, J. A. *Magn. Reson. Chem.*, **2001**, *39*, 723.

27 Vander Elst, L.; Sessoye, A.; Laurent, S.; Muller, R. N. *Helv. Chim. Acta*, **2005**, *88*, 574.

Calix[4]arene based paramagnetic liposomes as MRI contrast agents

6

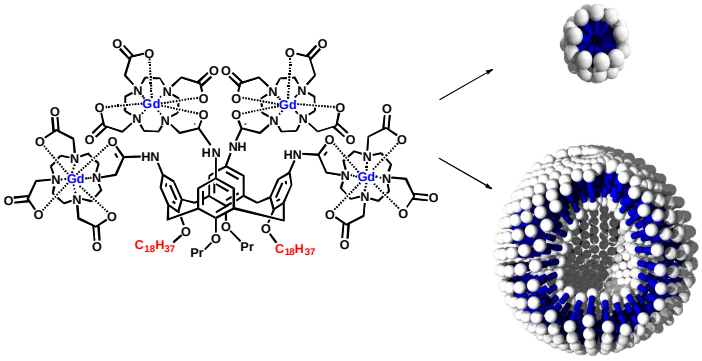

Introduction

Magnetic resonance imaging (MRI) is one of the most important imaging techniques in medical diagnostics. It makes use of the differences in proton densities and of longitudinal and transversal relaxation times (T_1 and T_2, respectively) of water protons in different tissues.[1-6] The resolution of this technique is high but in general, it is not very sensitive. Therefore, contrast agents can be administered to increase the differences in T_1 and T_2 relaxation times of neighboring tissues, which leads to a better contrast. The quality of T_1-weighted images can be enhanced by Gd(III)-complexes. They are applied since the paramagnetic metal accelerates the relaxation times of water protons in its proximity very efficiently.[1-3] Free Gd(III) is toxic and therefore, complexes that are considered to be applied *in vivo* need to exhibit both high kinetic and thermodynamic stability. In order to achieve high stability of the complexes, mainly diethylenetriaminepentaacetic acid (DTPA) and 1,4,7,10-tetra(carboxymethyl)-1,4,7,10-tetraazacyclododecane (DOTA) and their derivatives are in use.[1] Especially DTPA-bisamides are suspected of releasing the metal ion *in vivo* and of being a probable cause of Nephrogenic System Fibrosis (NSF).[7]

In general, high complex stability and small amounts of CA needed for the examination are desirable. Two ways to decrease the amount of CA can be deduced from Equation 6.1. T_1-Contrast agents act by shortening the observed longitudinal relaxation time of water in the tissue ($T_{1,obs}$), which results in a bright spot in the MR image. Since the diamagnetic relaxation time ($T_{1,dia}$) is an intrinsic property of the tissue under observation, the contrast needs to be generated by either enlarging the relaxivity (r_1) or the concentration of the Gd complex ($[Gd]$). The relaxivity is a property of the complex itself and can be modified by adjusting the rotational correlation time (τ_R), the average water residence lifetime at the metal center (τ_M) and the electronic parameters (τ_v, Δ^2). The local concentration of contrast agent in the body can be controlled by introducing e.g. targeting functions that deliver it specifically to the site of interest.

$$\frac{1}{T_{1,obs}} = \frac{1}{T_{1,dia}} + r_1[Gd] \tag{6.1}$$

Probably the simplest way to increase the relaxivity is through τ_R. The larger a particle is, the slower it tumbles. This means that τ_R gets longer thus resulting in an enhanced relaxivity compared to a smaller particle with similar electronic and water exchange parameters. Covalent attachment of chelators to large particles is a synthetically rather demanding approach. Self-assembly in water is an alternative and more straightforward method that leads to relatively large particles starting from small monomers just by dissolution. Therefore, for example micelles or liposomes are interesting targets in MR research.[8,9] They have the additional advantage that due to their size, they are able to diffuse through the leaky vasculature into the tumor and accumulate there by enhanced permeability and retention (EPR). The extent to which this occurs depends strongly on the size of the aggregates and is optimal for particles with a radius of about 50 – 100 nm.[9] Liposomes can be prepared in defined sizes and thus, are widely used as for example drug carriers or imaging agents.[9-11] The attachment of targeting vectors to their surface can enhance the tumor uptake even further.[12] A widely used formulation of paramagnetic liposomes consists of different kinds of lipids, cholesterol (to enhance their stability), PEGylated lipids (to increase the average lifetime in blood) and DTPA-bistearylamide (DTPA-BSA).[13] As mentioned before, DTPA-bisamides are considered to have possible toxic effects due to their comparably low stability and therefore, there is a need to replace compounds based on this moiety by stable chelators with preferably a higher relaxivity.

A factor limiting the relaxivity of paramagnetic liposomes is the slow diffusion of water molecules across the lipid bilayer.[14] Gd(III) that is entrapped inside the liposomes has a significantly quenched relaxivity due to the limited amount of water molecules that can be influenced by the metal ion. Thus, besides the usual optimizations of τ_R and τ_M, the relaxivity of such liposomes can be enhanced by accelerating the water diffusion through the bilayer. This can be achieved by, for example, inclusion of unsaturated lipid chains into the bilayer, which destructs the order within the layer and thus, accelerates the diffusion of water through it.[14]

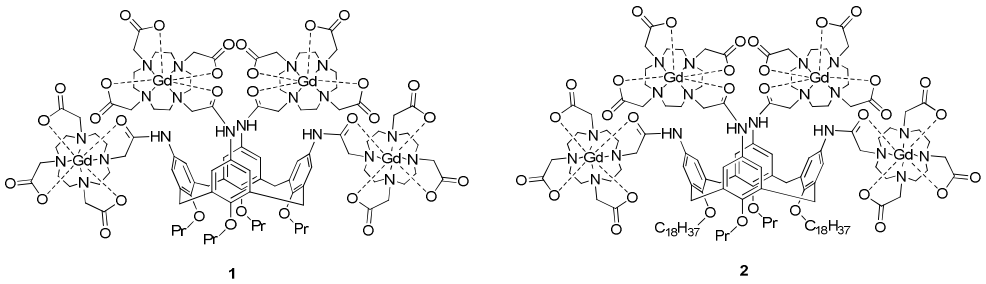

Figure 6.1. Schematic representation of the surfactants discussed.

Recently, we showed that the calix[4]arene based DOTA-monoamide **1** has good relaxivity and the tendency to aggregate in water.[15] The finding that **1** forms micelles in aqueous solution with a critical micelle concentration (*cmc*) of 0.21 mM inspired us to test whether the inclusion of the slightly modified paramagnetic calix[4]arene **2** into the liposomal bilayer is possible. Calixarenes are able to transport metal ions and anions through liposomal bilayers.[16] Transport of the non-charged water molecules through the hydrophobic membrane appears to be easier than that of ions. An increased diffusion of water through the membrane will lead to an enhanced relaxivity of calixarene containing paramagnetic liposomes. In this study, the inclusion of **2** into liposomal bilayers along with its effect on the morphology of the aggregates is investigated.

Results and Discussion

Synthesis

Alkylation of **3** with octadecyl bromide using NaH as a base yielded the tetraalkylated calixarene **4** in the *cone*-conformation (see Scheme 6.1). Tetranitro calixarene **5a** was obtained as a slightly yellow resinous solid by subsequent ipso-nitration with fuming nitric acid in a 1:1 mixture of glacial acetic acid and dichloromethane. The reduction of the four nitro-groups was achieved with hydrazine as a reductant in a boiling methanol/THF mixture using a catalytic amount of Raney-nickel. Amide coupling of calix[4]arene derivative **5b** with *tert*-butyl-DOTA-monoacid using EDC and a stoichiometric amount of 1-

hydroxybenzotriazole (HOBt) resulted in the corresponding conjugate. Purification was achieved by ultrafiltration over a 1 kDa membrane. Compared to the synthesis of **1**, longer reaction times and a larger excess of *tert*-butyl-DOTA-monoacid had to be used for full conversion. This might be caused by self-aggregation of **2** and the resulting steric crowding around the aniline groups. Cleavage of the protective *tert*-butyl esters was achieved by stirring the ester in a 1:1-mixture of TFA/DCM at ambient temperature overnight. The complexation of the lanthanide was performed by portionwise addition of $GdCl_3 \cdot 6H_2O$ to an aqueous solution of the free ligand adjusting the pH to 4 – 4.5 after each addition of the salt. The excess of the Gd salt and other inorganic salts formed during the complexation were removed by ultrafiltration. The yield of the deprotection/complexation was only 64% since small amounts of **2** passed the membrane used for the ultrafiltration.

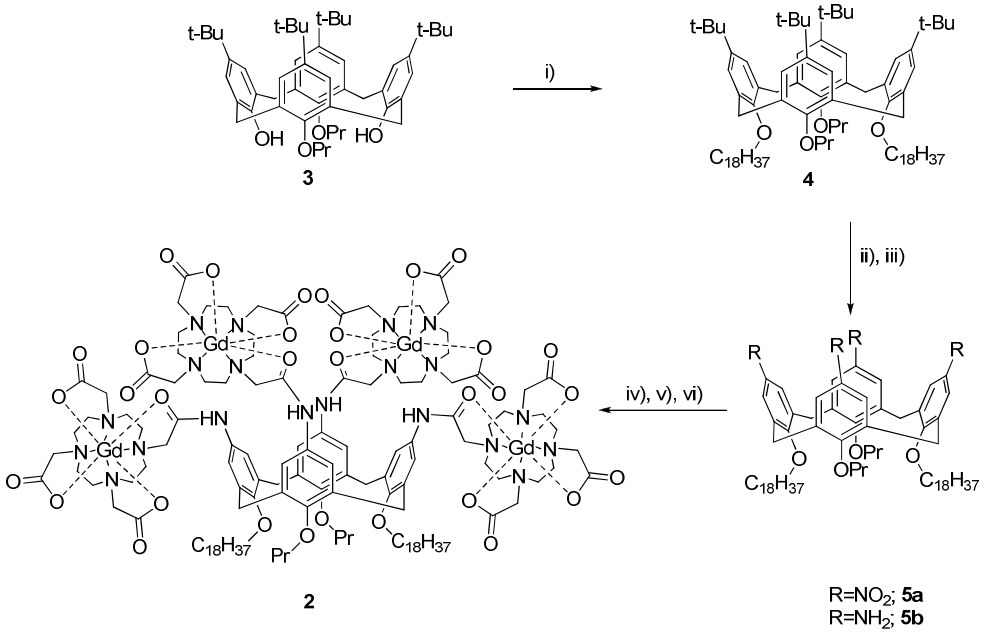

Scheme 6.1. i) $C_{18}H_{37}$-Br, NaH, DMF, 24 h, rt, 48% ii) HNO_3, HOAc, DCM, 2.5 h, rt, 96%, iii) $N_2H_4 \cdot H_2O$, Raney-Ni, THF/MeOH, 2 h, reflux, 86%, iv) *tert*-butyl-DOTA-monoacid, EDC, HOBt, DIPEA, DMF, 9 d, rt, 66%, v) TFA/DCM 50:50, overnight, rt, vi) $GdCl_3 \cdot 6H_2O$, 64% over 2 steps.

Self-Aggregation

As shown previously, calix[4]arene **1** aggregates in aqueous solution.[15] Therefore, dynamic light scattering (DLS) was performed on an aqueous solution containing 0.185 mmol of **2** (Figure 6.2). Two different kinds of aggregates with radii of 4.9 nm and 170 nm were found in solution. The formation of larger aggregates was not observed in the case of **1** whereas it was detected on a different, non-charged calixarene-DOTA analogue (see Chapter 5 of this thesis). Changes in the aggregation behaviour can be attributed to the different size and shape of the various calixarenes: larger monomers lead to the formation of larger aggregates. The DLS spectra (Figure 6.2) do not reflect the quantitative composition of the solution. The intensity of such intensity-weighted spectra is proportional to the square of the volume of the particles. This means that spherical particles that are ten times larger than others scatter light by a factor of one million more. Therefore, the aggregates with a radius of 4.9 nm represent the main component in the solution. This is also reflected in the cryo-TEM image of an aqueous solution of **2** (Figure 6.2). Whereas the small aggregates are well visible, there is no evidence of any larger one.

Upon self-aggregation, τ_R is increasing and thus, the relaxivity of a solution containing micelles is increased compared to a solution below the critical micelle concentration (*cmc*) with only monomers present.[8] This can be used to determine the *cmc* of self-aggregating paramagnetic compounds of this type.[8] The *cmc* of **2** is so low, that it could not be determined by relaxometric measurements since the relaxivity of the solution did not change upon dilution of the samples.[17] In general, it is difficult or even impossible to determine such low *cmc* values also with other experimental techniques such as surface tension measurement, fluorescence spectroscopy or isothermal titration calorimetry (ITC).

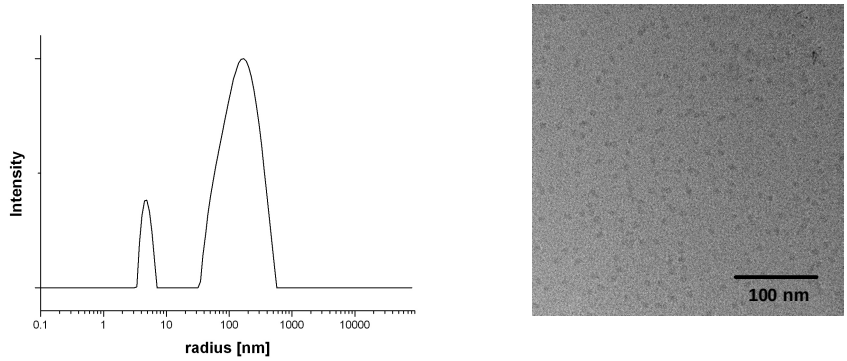

Figure 6.2. Dynamic light scattering (DLS) at 25 °C and cryo-TEM image of a 185 μM solution of **2**.

To get an insight into the parameters governing the relaxivity of **2**, relaxometric NMR measurements were performed. Nuclear magnetic relaxation dispersion (NMRD) is a powerful technique to characterize MRI contrast agents. The field dependence of the relaxivity (NMRD profile) gives important information on the extent to which the different parameters such as τ_v, Δ^2, τ_R and τ_M govern the overall relaxivity. To evaluate these parameters, an NMRD profile of a 400 μM solution of **2** was measured (see Figure 6.3). Since the *cmc* of **2** is very low, the contribution of the monomer on the relaxivity can be neglected, and therefore, the NMRD profile measured is that of the aggregated system.

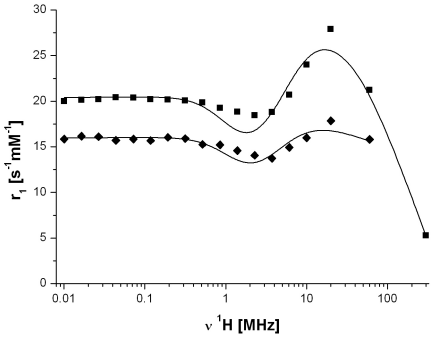

Figure 6.3. ^{1}H NMRD profiles of **1** (diamonds, see Chapter 4) and of **2** (squares, 400 μM) at 37 °C (lines indicate the results from the fittings).

The NMRD profile of the micellar **2** was fitted with a set of equations based on the Solomon-Bloembergen-Morgan theory for the inner sphere contribution and those of Freed for the outer sphere.[18] The diffusion coefficient was fixed to the value of pure water.[19] The results are compiled in Table 6.1. For comparison, the previously reported values for **1** are included in this table.[15]

The average water residence life time at 310 K (τ_M^{310}) of **2** is somewhat shorter than that found for **1**, which possibly is due to a slightly higher steric strain around the Gd-bound water molecules in the former micelles. The values of the parameters governing the electronic relaxation (τ_v and Δ^2) are, within the accuracy, identical for **1** and **2**. Simulations of NMRD profiles with varying τ_M and τ_R values, while keeping the other parameters fixed at the best-fit values of **1,** demonstrate that the higher relaxivity of **2**, as compared to that of **1**, can be mainly attributed to the relatively high value of τ_R for **2**.

Fitting of the NMRD profiles with the Lipari-Szabo approach gave similar results.[17] This model separates τ_R in a short local (τ_l) and a longer global (τ_g) rotational correlation time. The extent to which those correlation times contribute to the overall rotational correlation time is expressed by the order factor S^2. If internal motions fully dominate the rotational dynamics, S^2 is zero, if internal motions are negligible, S^2 is one. The best-fit value of S^2 was always equal to 1, which is a strong indication that the micelles formed by **2** are highly rigid. This is in line with the results obtained for the micellar **1**.[15]

Table 6.1. Parameters obtained from fitting of the ^{1}H NMRD profile of the micellar **2** (400 μM) at 37 ºC along with the parameters found for the micellar **1**.[15]

	1[a]	**2**
τ_M^{310} [ns]	720 ± 72	490 ± 46
τ_R^{310} [ns]	1.21 ± 0.11	2.47 ± 0.60
τ_v^{310} [ps]	60.9 ± 2.3	59.0 ± 3.5
Δ^2 [10^{18} s^{-1}]	5.10 ± 0.60	5.37 ± 0.20

[a] see Ref. 15.

According to the Debye-Stokes-Einstein equation, τ_R of a spherical particle is proportional to r_0^3 (r_0 is the effective radius of a particle). If the micelles in both cases could be considered spherical, an 11-fold increase of τ_R would be expected going from **1** to **2** from the DLS data, which is not in agreement with the results of the fittings (see above). This discrepancy suggests that either the particles are not spherical or that the Lipari-Szabo approach is not adequate in the present case. In a recent study on PAMAM dendrimers loaded with chelates on their surface, a significant deviation of the values of τ_g from those expected based on the size of the particles was found.[20] This was attributed to the fact that the Lipari-Szabo model that was used to obtain τ_g is not sufficient to discribe the motions within a large particle. These motions cannot simply be separated into overall global motions of the whole molecule and fast motions of the chelate around the connecting bonds to the dendrimer core. For example, motions of compartments relative to each other are not considered in the Lipari-Szabo model. The micelles formed by **2** are even larger than the generation four PAMAM conjugates described in this paper, so the motions may be even more complex.

Liposome formulations

Liposomes are normally prepared starting from a mixture of lipids and cholesterol, which is dissolved in either pure chloroform or a chloroform/methanol mixture. Then the solvents are evaporated to create a thin film of the lipids. Upon resuspension in an aqueous buffer and treatment with ultrasound, this film is broken into multilamellar aggregates. Only after extrusion of these aggregates through filters with appropriate sizes, spherical and rather monodisperse liposomes are obtained.[21] This procedure opens the possibility to include lipophilic compounds into the bilayer at several stages of the preparation: a) the formation of the lipid film, b) the extrusion and c) after the formation of liposomes. The influence of the formulation method on the loading of the liposomes with **2** as well as the effect of the loading method on the morphology of the aggregates is investigated here.

Probably the simplest method for inclusion of paramagnetic compounds into the liposomal bilayer is to mix all components before the lipid film is made. This has been done, for example, in the formulation of paramagnetic liposomes containing DTPA-BSA.[13]

In this way, a relatively homogeneous mix within the film is achieved. Three different kinds of liposomes with varying amounts of **2** present during the formulation (1.5 mol%, 5 mol% and 10 mol%) were prepared. It should be noted that the amount of gadolinium in the bilayer is four times higher than that of **2** since **2** contains four Gd-atoms. Therefore, Gd-loadings close to liposomes bearing DTPA-BSA (ca. 20 mol%) can be achieved with relatively small amounts of **2**.[13] DLS measurements revealed that in all cases, aggregates with a rather narrow size distribution having a polydispersity index (PDI) < 0.1 were obtained after extrusions through polycarbonate filters with diameters of first 200 nm and then 100 nm. The formulation with 10 mol% **2**, resulted in a suspension containing liposomes and additional aggregates with an average radius of 4.9 nm as shown by DLS (data not shown). This is most probably due to not included micellar **2**. For this reason, no further characterization of this system was performed.

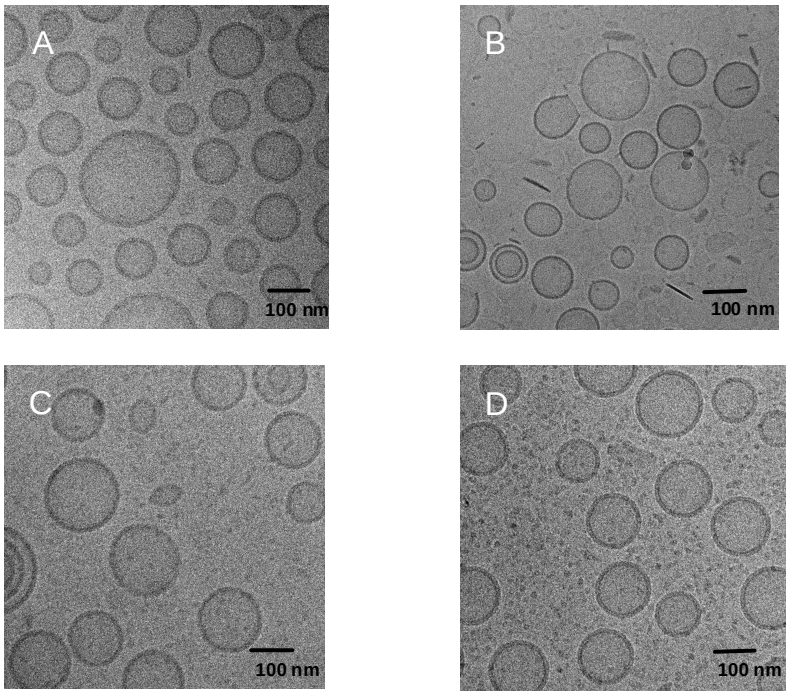

Figure 6.4. Liposomes with 0 mol% of **2** (A), 5 mol% **2** present during the lipid film preparation (B) 8.8 mol% **2** present during the extrusions (C) and 8.8 mol% **2** added after the liposome formation (D).

In the cryo-TEM images of samples containing liposomes with **2** present during the lipid film preparation, spherical liposomes accompanied by disk-like micelles (bicelles) are visible (Figure 6.4 B). The fraction of the bicelles is increasing with increasing concentration of **2**. This surfactant is incorporated into the bilayer leading to a destruction of the vesicles due to bicelle formation. The formation of bicelles in DSPC-based liposomes was already described before.[22] A possible explanation is that **2** itself forms small spherical aggregates and therefore, is able to induce a high curvature in aggregates. This is needed on the edges of the bicelles since a bilayer cannot expose its hydrophobic interior to the surrounding water. To cap this end, a surfactant is required that can form such a high curvature.

To the best of our knowledge, there is just one publication dealing with the formation of paramagnetic bicelles.[23] The relaxivity of these bicelles is significantly higher than the relaxivity of liposomes. This can be attributed to the fact that bicelles do not entrap water in their interior and that all hydrophilic chelators are oriented towards the bulk water surrounding the bicelles. Therefore, there is no quenching effect of the relaxivity due to slow diffusion of water through the bilayer between inside and outside as in the case of liposomes. The fate of paramagnetic bicelles *in vivo* remains to be exploited.

The surfactant **2** was also added in later stages of the preparation. During the extrusion process, the multilamellar aggregates are mechanically broken and reformed to finally yield spherical vesicles with a size that is determined by the filter used for the extrusion. This breaking and reformation is a dynamic process and therefore, it allows the incorporation of surfactants into the bilayer. This was explored by addition of 8.8 mol% **2** to a resuspended lipid film with the composition DSPC/DSPE-PEG2000-OMe/cholesterol 56.8:37.2:6 (for cryo-TEM of the blank see Figure 6.4 A). The extrusion was performed well above the expected phase transition temperature (T_m) at 65 °C and the suspension was stored for 2 days at 65 °C to ensure equilibration. As depicted in Figure 6.4, the shape of the vesicles obtained in this way is spherical and only a negligible amount of bicelles is formed. Some micelles are visible in the cryo-TEM images. This is probably due to the presence of **2**, which is not incorporated in the liposomes.

The incorporation of **2** into already existing liposomes turned out to be difficult. The surfactant **2** was dissolved in EtOH/H_2O 2:1 and added to a liposome suspension. A

significant amount of micellar **2** is present in suspension as illustrated by cryo-TEM (Figure 6.4 D). This means that a majority of **2** was not included using this method.

Since the first attempts to include **2** into liposomal bilayers by addition of the calixarene before the extrusion were most successfull, this process was optimized. To accelerate the inclusion, the extrusion was performed at 85 °C. The calixarene was directly dissolved in a suspension containing DSPC/DSPE-PEG2000-OMe/cholesterol 56.8:37.2:6 in order to give the inclusion some more driving force. Whereas **2** is already aggregated into micelles in aqueous solution, it is amorphous in the lyophilized powder obtained from the complex synthesis. Therefore, when the solid calixarene is treated with a suspension containing the resuspended lipid film, hydrophobic interactions do not need to be first broken and then reformed during the incorporation.

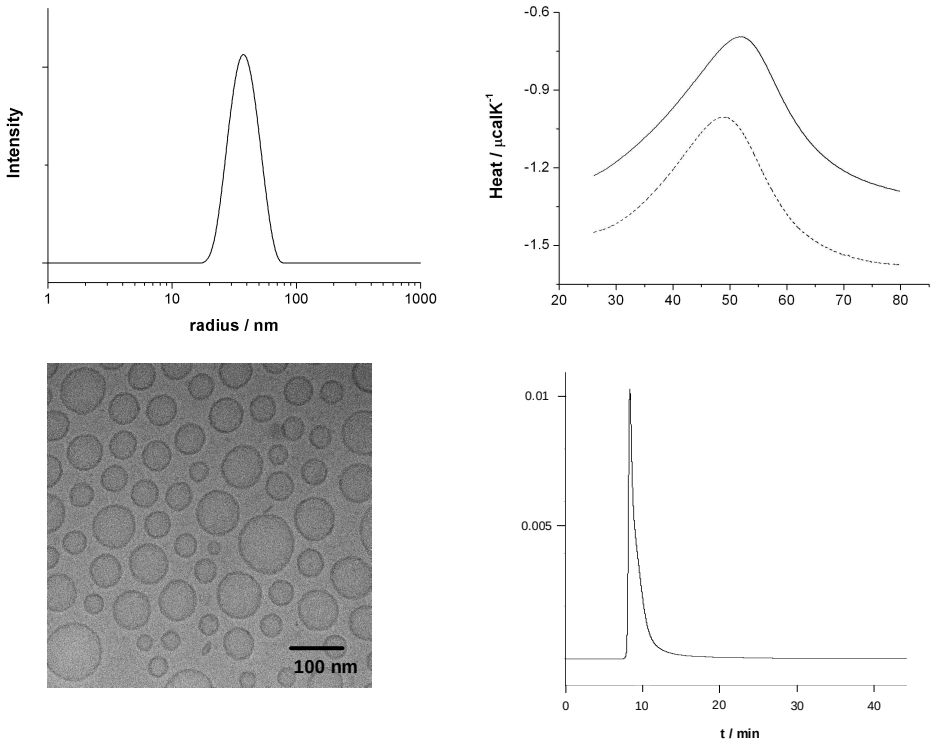

Figure 6.5. Characterisation of the liposome formulation with 8.8 mol% **2** present during the extrusion: DLS spectra at 25 °C (top left), DSC heating trace of a blank liposome formulation (solid line) and of the liposomes (dashed line, top right), cryo-TEM (down left) and SEC (down right).

The DLS of the system obtained (see Figure 6.5) shows vesicles with an average radius of 39.0 nm and a narrow size distribution (PDI < 0.1). To check whether **2** is really incorporated into the lipid bilayer, DSC measurements were performed to determine the phase transition temperature (T_m) of the vesicles (Figure 6.5). The blank vesicles without calixarene have a T_m of 51.6 °C, whereas there is a shift of about 3 °C in the case of the paramagnetic liposomes (T_m = 48.4 °C) containing 8.8 mol% of **2**. Since the micellar **2** has no phase transition in the observed temperature range, the shift of T_m is direct evidence for incorporation of **2** into the bilayer. The cryo-TEM is almost identical to that of a suspension prepared in the absence of any calixarene. The fact that no micellar **2** can be observed means that the inclusion of **2** into the liposomes is close to quantitative as is also illustrated by SEC (retention time of the micellar **2**: 34.1 min).

NMR characterization of the calixarene based liposomes

Further characterization of the paramagnetic liposomes was performed by relaxometric NMR measurements. Especially the temperature dependence of NMRD profiles gives important information on the effect of the water diffusion through the lipid bilayer on the relaxivity. Strijkers et al. have shown that above the phase transition temperature of the lipid bilayer, DSPC based paramagnetic liposomes with DTPA-BSA included in the bilayer have about the same relaxivity as DOPC based analoga that do not have a phase transition in the observed temperature range from 25 to 60 °C.[13] They ascribe this to the fast diffusion of water through lipid membranes above the phase transition. Upon decrease of temperature, the DOPC based liposomes have a gradual decrease in relaxivity due to an increase of τ_M. By contrast, the relaxivity of suspensions of DSPC based liposomes show a steep decrease in relaxivity at T_m. This is caused by an efficient slowing down of the diffusion of water molecules through the bilayer leading to quenching of the relaxivity contribution originating from the Gd atoms inside the vesicles. The local maxima around 20 MHz in the NMRD profiles of the presently studied system, liposomes containing **2** (see Figure 6.6), are significantly higher than those of the previously studied systems (about a

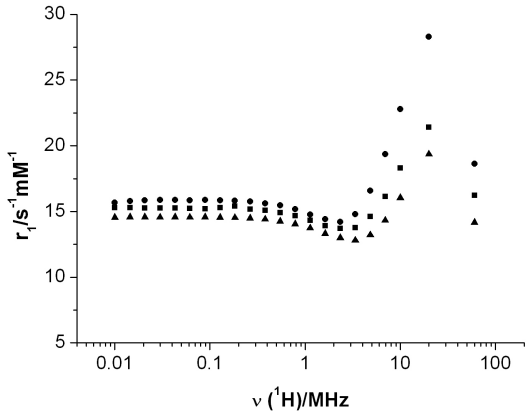

Figure 6.6. NMRD profiles of liposomes containing 8.8 mol% **2** at 25 °C (triangles), 37 °C (squares) and 55 °C (circles).

factor 3 at 37 ºC). [13] This can be rationalized by either a relatively fast diffusion of water through the bilayer of the liposomes already below T_m or by a location of most of the Gd ions on the outer surface of the liposomes. Since the extrusion was performed at 85 °C, which is well above the phase transition, we think that even if the calixarene is originally oriented outside the bilayer, there should be a flip-flop mechanism leading to about equal amounts of **2** on the inner and outer surfaces of the bilayer of the resulting liposomes.

We conclude that because of the presence of **2,** the permeability for water of the liposomal bilayers is relatively large. Two possible explanations can be envisaged for the effect of 2 on the permeability: (i) it forms channels through the bilayer that allow water molecules to cross it or (ii) the calixarene molecules disturb the packing of the lipids in the bilayer.[14] It should be noted that the channels formed by the calixarenes are highly hydrophobic, which may not be favorable for fast water transport. Anyway, both possible mechanisms would result in relatively fast water diffusion through the liposome membranes and, therefore, enhanced relaxivities already below the phase transition temperature. As illustrated by Figure 6.6, there is only a minor temperature effect on the relaxivity at low Larmor frequencies (< 3 MHz), which is surprising in view of the strong temperature dependence of the relaxivity at higher frequencies. This indicates that at lower frequencies,

the increase in relaxivity with temperature due to the increased permeability and τ_M is counteracted by a decrease due to another effect. Most likely, increased local motions result in a decrease of the rotational correlation time, τ_R, with temperature, resulting in a decreasing contribution to the over all relaxivity. Fittings of the NMRD profiles were not attempted, because so far, there is no adequate model for the relaxivity of liposomes with paramagnetic chelates incorporated in the membrane.

Conclusions

The synthesis of the amphiphilic calixarene **2** is presented here. This compound has promising properties as an MRI CA. In water, it forms micelles with a radius of 4.9 nm above a very low *cmc*. Those aggregates have enhanced relaxivity (27.9 $s^{-1}mM^{-1}$ at 20 MHz and 37 °C) compared to the aggregated model calixarene **1** (17.8 $s^{-1}mM^{-1}$ at 20 MHz and 37 °C) due to their larger size. Incorporation into the bilayer of liposomes was investigated using three different methods of inclusion. Mixing **2** with the corresponding lipids and cholesterol prior to the lipid film formation leads to a significant formation of bicelles. Preparation by addition of **2** to pre-formed liposomes is not efficient, but addition of **2** prior to extrusion at 85 °C leads to almost quantitative incorporation of the surfactant into the walls of the vesicles. Calixarene **2** accelerates the diffusion of water through the lipid bilayer below its phase transition temperature. This results in relatively high relaxivities (21.2 $s^{-1}mM^{-1}$ at 20 MHz and 37 °C) for these paramagnetic liposomes. The high relaxivity per Gd and the high content of metal ions inside the lipid bilayer means that the relaxivity per liposome is high. Therefore, this system has potential in molecular imaging and it may be of interest in the design of multimodality probes, since the cavity inside the liposomes is available for a second modality.

Experimental

Materials. All reagents and anhydrous solvents used during the synthesis were of commercial quality. 5,11,17,23-Tetra-(*tert*-butyl)-25,27-dihydroxy-26,28-dipropoxy-calix [4]arene and tris-1,4,7-*tert*-butoxycarbonylmethyl-10-carboxymethyl-1,4,7,10-tetraazacy clododecane were synthesised as described in the literature.[24,25] For the formulation of the liposomes, cholesterol (Avanti polar Inc., Alabaster, AL, USA), DSPC (1,2-distearoyl-*sn*-glycero-3-phosphocholine) and DSPE-PEG2000-OMe (1,2-distearoyl-*sn*-glycero-3-phosphoethanolamine-*N*-[methoxy(polyethyleneglycol)-2000]) (Lipoid AG, Cham, Switzerland) were used without further purification.

Methods

DLS. Dynamic light scattering (DLS) was performed on a Zetasizer NanoZs, Malvern, UK instrument.

Cryo-TEM. A few microliters solution were placed on a quantifoil 3.5/1 holey carbon/coated grid (Quantifoil micro tools GmbH, Jena, Germany). The grids were automatically blotted and vitrified using the vitrobot (FEI, Eindhoven, The Netherlands). Frozen hydrated specimen were observed with a Gatan cryo-stage (Model 626, Gatan, Pleasanton, CA) in a Philips CM10 cryo/electron microscope (Philips, Eindhoven, The Netherlands) operating at 100 keV. Images were recorded under low-dose conditions with a slow scan CCD camera (Gatan, Pleasanton, CA).

NMR. The ^{1}H NMRD profiles were recorded on a Stelar Smartracer FFC fast-field-cycling relaxometer covering magnetic fields from $2.35 \cdot 10^{-4}$ to 0.25 T, which corresponds to a proton Larmor frequency range of 0.01-10 MHz. The temperature was controlled by a VTC90 temperature control unit and fixed by a gas flow. The temperature was determined according to previous calibration with a Pt resistance temperature probe. The longitudinal relaxation times at 20 and 60 MHz were recorded on Bruker Minispec relaxometers (mq20 and mq60). All samples were kept in the probe for at least 10 minutes to equilibrate the temperature prior to the measurment.

Determination of the Gd concentration. The pH of the solution used for the NMRD measurements was adjusted to 1 and the sample heated for 1 h. The concentration was determined by measuring the relaxation rate of this solution at 10 MHz and 25 °C. From this and the previously determined relaxivity of the Gd aquoion under the same conditions (17.75 $s^{-1}mM^{-1}$), the concentration was calculated.

Fittings. For the fittings, the established equations were used.[17,18] The least-squares fit of the ^{1}H NMRD data were performed by the MicroMath program Scientist.

SEC. Size exclusion chromatography was performed on a Waters Ultrahydrogel 1000 column at a flow of 0.6 ml/min and 25 °C. Elution was achieved in the standard HEPES buffer. The fractions were detected at 254 nm.

Preparation of liposomes

a) Addition of 2 before the lipidic film preparation. DSPC, DSPE-PEG2000-OMe, cholesterol and **2** were dissolved in a mixture of chloroform (2 mL) and methanol (2 mL). Two formulations were prepared with a total amount of compounds of 50 μmol and with the following ratios: DSPC/DSPE-PEG2000-OMe/cholesterol/1 2.42/0.2/1.32/0.06 (containing 1.5 mol% **2**) and a second formulation: 2.28/0.2/1.32/0.2 (containing 5 mol% **2**).

The solutions were vacuum-dried to get a thin lipidic film. The film was then hydrated and broken with a HEPES/NaCl buffer (10 mM, 135 mM NaCl, pH=7.4), resulting in a suspension of multi-lamellar layers of lipids. This mixture was extruded through polycarbonate membrane filters with a porosity of 200 nm (10 times) and 100 nm (10 times), using a Lipofast extruder (Avestin, Canada). The temperature during the extrusion was set at 55˚C. The extruded solutions were ultra-centrifuged for 1.5 h at 4˚C on an ultracentrifuge (Beckman L7, rotor 50Ti, 40Krpm, 266000 g). The pellet was separated from the supernatants and washed with 0.5 mL of a fresh buffer solution.

b) Addition of 2 during the extrusion. DSPC (52.1 mg, 66.0 μmol), DSPE-PEG2000-OMe (19.27, 7 μmol), and cholesterol (16.68 mg, 43.15 μmol) were dissolved in chloroform (3 ml). After evaporation of the solvent, the film was resuspended in HEPES buffer (3 ml). After addition of **2** (12.04 mg, 3.72 μmol) dissolved in 100 μl of buffer to 1

ml of this suspension, the mixture was extruded at 65 °C first through a 200 nm filter (11 times) and then through a 100 nm filter (11 times). Prior to the characterization, the suspension was stored at 65 °C for 2 days.

c) Incorporation of 2 into existing liposomes. A solution of **2** (12.23 mg, 3.78 μmol) in a 2:1 mixture of EtOH/HEPES buffer 2:1 (36 μl) was added to 0.8 ml of the suspension described in b) at 65 °C and immediately vortexed. Prior to the characterization, the suspension was stored at 65 °C for 2 days.

d) Optimization of the addition of 2 during the extrusion. DSPC (104 mg, 132 μmol), DSPE-PEG2000-OMe (38.54, 14 μmol), and cholesterol (33.36 mg, 86.3 μmol) were dissolved in chloroform (6 ml). After evaporation of the solvent, the film was resuspended in HEPES buffer (6 ml). Calixarene **2** (36.3 mg, 11.2 μmol) was dissolved in 3 ml of this suspension, the mixture was extruded at 85 °C first through a 200 nm filter (13 times) and then through a 100 nm filter (13 times).

Synthesis

5,11,17,23-Tetra(*tert*-butyl)-25,27-dioctadecoxy-26,28-dipropoxy-calix[4]arene (4)

A suspension of 5,11,17,23-tetra-(*tert*-butyl)-25,27-dihydroxy-26,28-dipropoxy-calix[4]-arene (1.00 g, 1.36 mmol) and NaH (0.82 g, 20.5 mmol, 60% in mineral oil) in DMF (20 ml) was stirred for 30 min at rt and 1-bromo-octadecane (1.00 g, 2.99 mmol) was added. After 24 h, 2 M HCl was carefully added until no further precipitation occurred. The product was extracted with $CHCl_3$ and the aqueous phase washed with $CHCl_3$. The organic phases were combined, dried over Na_2SO_4 and then the solvent was removed. The residue was treated with MeOH and the crude product was filtered off. The pure product (0.80 g, 0.65 mmol, 48%) was obtained by column chromatography (silica gel, hexane)

^{1}H NMR (400 MHz, $CDCl_3$, 25 ˚C, TMS): δ = 0.88 (6 H, t, *J* = 7.1 Hz, C*H*$_3$), 0.99 (6 H, t, *J* = 7.6 Hz, C*H*$_3$), 1.08 (36 H, s, tert-Bu), 1.26 – 1.38 (60 H, m, $CH_2CH_2CH_2$, $CH_2CH_2CH_3$), 1.98 – 2.08 (8 H, m, OCH_2CH_2), 3.10 (4 H, d, *J* = 12.5 Hz, $ArCH_2Ar$), 3.81 (4 H, t, *J* = 7.6 Hz, OCH_2CH_2), 3.84 (4 H, t, *J* = 7.6 Hz, OCH_2CH_2), 4.41 (4 H, d, *J* = 12.5 Hz, $ArCH_2Ar$), 6.77 (8 H, s, Ar-H). ^{13}C NMR (400 MHz, $CDCl_3$, 25 ˚C): δ = 10.36, 14.13 ($OCH_2CH_2CH_3$), 22.70, 23.34, 26.26, 29.37, 29.67, 29.72, 29.76, 29.91, 30.27, 31.07 ($CH_2CH_2CH_2$,

$CH_2CH_2CH_3$), 31.46 (Ar-CH_2-Ar), 31.94, 33.79 ($CH_2CH_2CH_2$), 75.38, 77.97 (OCH_2CH_2), 124.84, 133.84, 144.09, 153.72, 1543.76 (Ar-C). IR (KBr) $\tilde{\upsilon}$ (cm^{-1}): 2960 (s), 2921 (s), 2851 (s) (C-H), 1482 (m) (Ar-C-H), 1387 (s), 1362 (s),1301 (m), 1248 (m), 12020 (s), 1125 (m), 1070 (m), 1045 (m), 1014 (m), 969 (m), 870 (m), 721 (m). Elem. analysis: calc.: C,83.43%; H, 11.40%. Found: C, 83.41%; H, 11.36%. MS (Maldi, DHB): calc.: *m/z* = 1237.1 ($C_{86}H_{140}O_4$, $M+H)^+$, found: 1237.1. mp: 62 – 63 ºC.

5,11,17,23-Tetranitro-25,27-dioctadecoxy-26,28-dipropoxy-calix[4]arene (5a)

To a solution of 5,11,17,23-tetra-(*tert*-butyl)-25,27-dioctadecoxy-26,28-dipropoxy-calix[4]-arene (**4**) (2.01 g, 1.62 mmol) in DCM (17.5 ml) and glacial acetic acid (17.5 ml) was added fuming nitric acid (5.8 ml) at 0 ºC. The violet solution was stirred for 2.5 h at room temperature until it turned orange. Water was added, the phases separated and the aqueous layer was extracted twice with DCM. The combined organic phases were washed with water and dried over Na_2SO_4. After evaporation of the solvent, the remaining oil was treated with MeOH in an ultrasonic bath and the MeOH was decanted. This procedure was repeated once and the remaining oil was dried in vacuo for 3 h to yield **5a** (1.86 g, 1.56 mmol, 96% mmol).

An analytically pure sample could be obtained by column chromatography (silica gel, DCM/MeOH 50:1).

^{1}H NMR (400 MHz, $CDCl_3$, 25 ˚C, TMS): δ = 0.88 (6 H, t, *J* = 6.4 Hz, C*H*$_3$), 1.04 (6 H, t, *J* = 7.4 Hz, C*H*$_3$), 1.25 – 1.37 (60 H, m, $CH_2CH_2CH_2$, $CH_2CH_2CH_3$), 1.87 – 1.93 (8 H, m, OCH_2CH_2), 3.41 (4 H, d, *J* = 14.0 Hz, ArC*H*$_2$Ar), 3.94 (4 H, t, *J* = 7.6 Hz, OCH_2CH_2), 4.00 (4 H, t, *J* = 7.6 Hz, OCH_2CH_2), 4.52 (4 H, d, *J* = 14.0 Hz, ArC*H*$_2$Ar), 7.54 (4 H, s, Ar-H), 7.60 (4 H, s, Ar-H). ^{13}C NMR (400 MHz, $CDCl_3$, 25 ˚C): δ = 10.12, 14.09 (*C*H3), 22.67, 23.27, 25.94, 29.34, 29.63, 29.69, 30.11 ($CH_2CH_2CH_2$, $CH_2CH_2CH_3$), 31.11 (Ar-CH_2-Ar), 31.90 ($CH_2CH_2CH_2$), 76.22, 77.70 (OCH_2CH_2), 123.92, 124.02, 135.30, 135.47, 142.83, 161.58, 161.73 (Ar-C). IR (KBr) $\tilde{\upsilon}$ (cm^{-1}): 2924 (s), 2852 (s) (C-H), 1586 (m) (Ar-C-H), 1526 (s) (N=O), 1458 (m) (Ar-C-H), 1347 (s), 1301 (m), 1262 (m), 1210 (m), 1094 (m), 993 (m), 959 (m), 901 (m), 806 (w), 770 (w), 745 (m). Elem. analysis: calc.: C,70.44%; H, 8.78%, N, 4.69%. Found: C, 70.20%; H, 8.93%; N, 4.68%. MS (Maldi, DHB): calc.: *m/z* = 1193.8 ($C_{70}H_{105}N_4O_{12}$, $M+H)^+$, found: 1193.9.

5,11,17,23-Tetraamino-25,27-dioctadecoxy-26,28-dipropoxy-calix[4]arene (5b)

To a solution of 5,11,17,23-tetranitro-25,27-dioctadecoxy-26,28-dipropoxy-calix[4]arene (**5a**) (1.18 g, 0.99 mmol) and $N_2H_4 \cdot H_2O$ (5.6 ml) in THF (40 ml) and MeOH (20 ml), Raney nickel was added and the suspension stirred at reflux for two hours. The hot mixture was filtered over celite and allowed to cool to rt. DCM and 1 M NaOH were added and the phases separated. The organic phase was dried over Na_2SO_4. After evaporation of the solvent the solid was dried in vacuo for 3 h to yield **5b** (0.92 g, 0.85 mmol, 86% mmol).

^{1}H NMR (400 MHz, $CDCl_3$, 25 ˚C, TMS): δ = 0.88 (6 H, t, *J* = 6.1 Hz, C*H*$_3$), 0.95 (6 H, t, *J* = 7.4 Hz, C*H*$_3$), 1.26 – 1.33 (60 H, m, $CH_2CH_2CH_2$, $CH_2CH_2CH_3$), 1.83 – 1.89 (8 H, m, OCH_2CH_2), 2.91 (4 H, d, *J* = 13.2 Hz, ArC*H*$_2$Ar), 3.17 (8 H, br s, N-*H*), 3.70 – 3.77 (8 H, m, OC*H*$_2$CH$_2$), 4.31 (4 H, d, J = 13.2 Hz, ArC*H*$_2$Ar), 6.04 (4 H, s, Ar-H), 6.06 (4 H, s, Ar-H). ^{13}C NMR (400 MHz, $CDCl_3$, 25 ˚C, TMS): δ = 10.42, 14.13 (*C*H$_3$), 22.70, 23.17, 26.30, 29.38, 29.68, 29.74, 29.86, 29.88, 30.15 ($CH_2CH_2CH_2$, $CH_2CH_2CH_3$), 31.17 (Ar-*C*H$_2$-Ar), 31.94 ($CH_2CH_2CH_2$), 75.08, 77.24 (OCH_2CH_2), 115.78, 135.65, 135.71, 140.24, 150.10, 150.13 (Ar-C). Elem. analysis: calc. ($C_{70}H_{112}N_4O_{12}$ + 0.5 THF): C,77.93%; H, 10.54%, N, 5.05%. Found: C, 77.78%; H, 10.65%; N, 4.79%. ESI-MS: calc.: *m/z* = 1073.9 $(C_{70}H_{112}N_4O_{12}, M+H)^+$, found: 1073.9.

5,11,17,23-Tetrakis(tris-4,7,10-*tert*-butoxycarbonylmethyl-1,4,7,10-tetrazacyclododec-1-yl-acetamidyl)-25,27-dioctadecoxy-26,28-dipropoxy-calix[4]arene

Under inert atmosphere, a suspension of tris-1,4,7-*tert*-butoxycarbonylmethyl-10-carboxymethyl-1,4,7,10-tetrazacyclododecane (1.55 g, 2.71 mmol), $DIPEA_{abs.}$ (1.3 mL), HOBt (370 mg, 2.71 mmol) and EDC (520 mg, 2.71 mmol) in $DMF_{abs.}$ (20 ml) was stirred for 0.5 h at ambient temperature. A solution of 5,11,17,23-tetraamino-25,27-dioctadecoxy-26,28-dipropoxy-calix[4]arene (**5b**) (350 mg, 326 µmol) in $THF_{abs.}$ (3ml) was added. After 2 d stirring at rt, another portion of tris-1,4,7-tert-butoxycarbonylmethyl-10-carboxy-methyl-1,4,7,10-tetrazacyclododecane (388 mg, 678 µmol) was activated with HOBt (93 mg, 6.88 mmol), EDC (130 mg, 0.68 mmol) and $DIPEA_{abs.}$ (0.33 ml) in $DMF_{abs.}$ and added to the mixture. After 3 d, EDC (0.50 g, 2.61 mmol) and $DIPEA_{abs.}$ were added and the reaction was continued for another 4 d. Thereafter, the solvent was removed in high vacuo, and the residue purified by ultrafiltration using a membrane with a cut-off of 1 kDa. The solvent was changed from a 0.05 M NH_4HCOO buffer in MeOH to pure MeOH. After evaporation of the solvent, the residue was freeze-dried from benzene to yield a slightly

brown powder of the conjugate (710 mg, 216 µmol, 66%). No ^{13}C-NMR data could be obtained because the compound decomposes during the long measurements.

^{1}H NMR (400 MHz, dmso-d_6, 100 ˚C, TMS): δ = 0.88 (6 H, t, *J* = 6.4 Hz, C*H*$_3$), 0.98 (6 H, t, *J* = 7.2 Hz, C*H*$_3$), 1.28 (60 H, m, $CH_2CH_2CH_2$, $CH_2CH_2CH_3$), 1.42, 1.47 (108 H, 2 s, tert-Bu), 1.81 – 1.87 (8 H, m, OCH_2CH_2), 2.26 – 2.97 (64 H, m, N-C*H*$_2$-C*H*$_2$), 3.04 (4 H, d, *J* = 13.2 Hz, ArC*H*$_2$Ar), 3.16, 3.18 (32 H, 2 s, N-C*H*$_2$-CO), 3.80 (4 H, t, *J* = 7.2 Hz, OC*H*$_2$CH$_2$), 3.88 (4 H, t, J = 6.8 Hz, OC*H*$_2$CH$_2$), 4.38 (4 H, d, *J* = 13.2 Hz, ArC*H*$_2$Ar), 6.67 (4 H, br. s, Ar-H), 6.67 (4 H, br. s, Ar-H), 10.02 (4 H, br. s, NH). ESI-MS: calc.: *m/z* = 1098.11 $(C_{182}H_{312}N_{20}O_{32}+3H)^{3+}$, found 1098.45.

5,11,17,23-Tetrakis(tris-4,7,10-carboxymethyl-1,4,7,10-tetrazacyclododec-1-yl-acetamidyl)-25,27-dioctadecoxy-26,28-dipropoxy-calix[4]arene

5,11,17,23-Tetrakis(tris-4,7,10-*tert*-butoxycarbonylmethyl-1,4,7,10-tetrazacyclododec-1-yl-acetamidyl)-25,27-dioctadecoxy-26,28-dipropoxy-calix[4]arene (500 mg, 155 µmol) was dissolved in DCM/TFA 50:50 (20 ml) and stirred overnight. After the liquids were removed, the crude product was lyophilized from water to yield the title compound as its TFA salt (556 mg). The compound was not purified further since the TFA as well as inorganic impurities can easily be removed after complexation by ultrafiltration. The NMR spectra were recorded in the presence of pyridine in order to obtain better spectra.

^{1}H NMR (400 MHz, dmso-d_6, 100 ˚C, TMS): δ = 0.90 (6 H, t, *J* = 7.5 Hz, C*H*$_3$), 0.99 (6 H, t, *J* = 7.5 Hz, C*H*$_3$), 1.26 - 1.48 (60 H, m, $CH_2CH_2CH_2$, $CH_2CH_2CH_3$), 1.89 (8 H, sext, *J* = 7.2 Hz, OCH_2CH_2), 2.93 – 3.16 (64 H, m, N-C*H*$_2$-C*H*$_2$, 4 H, ArC*H*$_2$Ar), 3.59- 3.67 (32 H, br s, N-C*H*$_2$-CO), 3.81 (4 H, t, *J* = 7.2 Hz, OC*H*$_2$CH$_2$), 3.92 (4 H, t, *J* = 7.2 Hz, OC*H*$_2$CH$_2$), 4.40 (4 H, d, *J* = 12.6 Hz, ArC*H*$_2$Ar), 6.97 (4 H, br. s, Ar-H), 7.12 (4 H, br. s, Ar-H), 9.66 (2 H, br. s, NH), 9.77 (2 H, br. s, NH). ESI-MS: calc.: *m/z* = 873.53 $(C_{134}H_{216}N_{20}O_{32}+3H)^{3+}$, found 873.88.

5,11,17,23-Tetrakis(tris-4,7,10-carboxymethyl-1,4,7,10-tetrazacyclododec-1-yl-acetamidyl)-25,27-dioctadecoxy-26,28-dipropoxy-calix[4]arene Gd-complex (2)

5,11,17,23-Tetrakis(tris-4,7,10-carboxymethyl-1,4,7,10-tetrazacyclododec-1-yl-acetamidyl)-25,27-dioctadecoxy-26,28-dipropoxy-calix[4]arene (500 mg) as obtained above was dissolved in water and $GdCl_3 \cdot 6H_2O$ (326 mg, 860 µmol) was added in small portions. After each addition, the pH was adjusted to 4 to 4.5 using aqueous NaOH during which a solid precipitated. As soon as this solid was dissolved again, a new portion of

$GdCl_3 \cdot 6H_2O$ was added and the procedure repeated. After complete addition, the solution was stirred overnight. The Gd(III)-complex was purified by ultrafiltration (1 kDa membrane, solvent: water) and obtained after lyophilisation as a white powder (296 mg, 64% yield).

ESI-MS: calc.: m/z = 1641.10 $(C_{134}H_{204}Gd_4N_{20}O_{32}+2Na)^{2+}$, found 1640.80.

References

1 Tóth, É.; Merbach; A. E. *The Chemistry of Contrast Agents in Medical Magnetic Resonance Imaging*, Wiley, New York, **2001**.

2 Caravan, P. *Chem. Soc. Rev.*, **2006**, *35*, 512.

3 Caravan, P.; Ellison, J. J.; McMurry, T. J.; Lauffer, R. B. *Chem. Rev.*, **1999**, *99*, 2293.

4 Aime, S.; Fasano, M.; Terreno, E. *Chem. Soc. Rev.*, **1998**, *27*, 19.

5 Aime, S.; Crich, S. G.; Gianolio, E.; Giovenzana, G.; Tei, L.; Terreno, E. *Coord. Chem. Rev.*, **2006**, *250*, 1562.

6 Bottrill, M.; Kwok L.; Long, N. J. *Chem. Soc. Rev.*, **2006**, *35*, 557.

7 Rofsky, N. M.; Sherry, A. D.; Lenkinski, R. E. *Radiology*, **2008**, *247*, 3, 608.

8 André, J. P.; Tóth, É.; Fischer, H.; Seelig, A.; Mäcke, H. R.; Merbach, A. E. *Chem. Eur. J.* **1999**, *5*, 2977.

9 Mulder, W. J. M.; Strijkers, G. J.; van Tilborg, G. A. F.; Griffioen, A. W.; Nicolay, K. *NMR Biomed.*, **2006**, *19*, 142.

10 Terreno, E.; Castelli, D. D.; Cabella, C.; Dastrù, W.; Sanino, A.; Stancanello, J.; Tei, L.; Aime, S. *Chem. Biodiv.* **2008**, *5*, 1901.

11 Allen, T. M.; Cullis, P. R. *Science*, **2004**, ***303***, 1818.

12 Mulder, W. J. M.; Strijkers, G. J.; Griffioen, A. W.; van Bloois, L.; Molema, G.; Storm, G.; Koning, G. A.; Nicolay, K. *Bioconj. Chem.*, **2004**, *15*, 799.

13 Strijkers, G. J.; Mulder, W. J. M.; van Heeswijk, R. B.; Frederik, P. M.; Bomans, P.; Magusin, P. C. M. M.; Nicolay, K. *MAGMA*, **2005**, *18*, 186.

14 Laurent, S.; vander Elst, L.; Thirifays, C.; Muller, R. N. *Eur. Biophys. J.*, **2008**, *37*, 1007.

15 Schühle, D.T.; Schatz, J.; Laurent, S.; Vander Elst, L; Muller, R. N.; Stuart, M. C. A.; Peters, J. A. *Chem. Eur. J.*, **2009**, *15*, 3290.

16 Iqbal, K. S. J; Cragg, P. J. *J. Chem. Soc., Dalton Trans.* **2007**, 26 and references therein.

17 Gaëlle, M. N.; Tóth, É.; Eisenwiener, K.-P.; Mäcke, H. R.; Merbach, A. E. *J. Biol. Inorg. Chem.* **2002**, *7*, 757.

18 Powell, D. H.; Ni Dhubhghaill, O. M.; Pubanz, D.; Helm, L.; Lebedev, Y. S.; Schlaepfer, W.; Merbach, A. E. *J. Am. Chem. Soc.* **1996**, *118*, 9333.

19 Vander Elst, L.; Sessoye, A.; Laurent, S.; Muller, R. N. *Helv. Chim. Acta*. **2005**, *88*, 574.

20 Polášek, M.; Hermann, P.; Peters, J. A.; Geraldes, C. F. G. C.; Lukeš, I. *Bioconj. Chem.*, *in press*.

21 Torchilin, V.; Weissig, V. *Liposomes*, Oxford University Press, New York, **2003**.

22 Johansson, E.; Engvall, C.; Arfvidsson, M.; Lundahl, P.; Edwards, K. *Biophys. Chem.*, **2005**, *113*, 183.

23 Gløgård, C.; Stensrud, G.; Klaveness, J. *Int. J. Pharma.*, **2003**, *253*, 39.

24 Aarons, R. J.; Notta, J. K.; Meloni, M. M.; Feng, J.; Vidyasagar, R.; Narvainen, J.; Allan, S.; Spencer, N.; Kauppinen, R. A.; Snaith, J. S.; Faulkner, S. *Chem. Commun.* **2006**, 909.

25 Iwamoto, J.; Araki, K.; Shinkai, S. *J. Org. Chem.*, **1991**, *56*, 4955.

Summary

Since their emergence in synthetic and supramolecular chemistry, calixarenes have found broad application in for example physics, biology, and medicine. In general, calixarenes are used either as synthetic platforms and/or as hydrophobic baskets that can interact with apolar guests. In Chapter 1 of this thesis, a short overview of the biological applications of metal binding calixarenes is given, ranging from artificial ion channels, enzyme mimics and inhibitors to agents for medical imaging and radiotherapy.

Deprotonation of imidazolium salts to *N*-heterocyclic carbenes is often a decisive step in modern catalytic reactions. Those carbenes can either act as catalyst, for example in umpolung reactions or as ligands in metal catalysed reactions. Therefore, the H/D exchange of the C^2–proton of 15 imidazolium substituted calix[4]arenes and 11 non-macrocyclic model compounds in methanol/water 97:3 at 25 °C is investigated in Chapter 2. The influence of the counter ion, substitution directly on the imidazolium unit or on the prearranging calixarene backbone was studied. Some trends can be seen comparing the exchange rates: salts bearing aromatic units directly attached to the imidazole units show accelerated exchange compared to alkyl analogues. The angle between the imidazolium and the aryl ring is relevant for the electronic stabilisation of the intermediate carbene. Counterions have an influence on the kinetic acidity but no trend is obvious. Anion binding as well as solvation might play a role. Substituents on the calixarene backbone in proximity of the exchangable protons can either accelerate or suppress the exchange.

As illustrated in Chapter 1, calixarenes can act as artificial cation transporters. Often, the low selectivity towards a particular alkaline metal ion is a limiting factor in such ion channel mimics. Chapter 3 deals with a way to enhance the sodium selectivity of calix[4]arene amides. Their interaction with alkaline metal cations has been evaluated through extracting aqueous solutions of Li-, Na- and K-picrates with solutions of calix[4]arene amides in CH_2Cl_2. Electron withdrawing groups on the *upper rim* of the calix[4]arene scaffold were found to have a negative effect on the absolute amount of metal ions extracted. The decreased extraction ability is accompanied by a higher selectivity towards sodium cations.

In medical diagnosis by magnetic resonance imaging, Gd^{3+}-containing compounds are used as T_1 contrast agents. Strong complexation of the metal ion by large and rigid ligand

systems is a prerequisite for the design of highly efficient contrast agents. In Chapter 4, the preparation of an amphiphilic conjugate of a calix[4]arene with four Gd-DOTA chelates is described. Its relevant properties for application as MRI contrast agent were investigated by NMR, DLS and cryo-TEM. The compound aggregates in water exhibiting a critical micelle concentration (*cmc*) of 0.21 mM (or 0.84 mM with respect to Gd) at 37 ºC. The relaxivity of the aggregates at 37 °C and 20 MHz (18.3 $s^{-1}mM^{-1}$) is about twice that of the monomer. Nuclear magnetic relaxation dispersion (NMRD) profiles show the relaxivity of the monomer to be almost independent of the magnetic field strength up to 60 MHz. At higher concentrations, the NMRD profiles exhibit a maximum at about 20 MHz, which is typical for high molecular volumes. The average water residence lifetime is 1.20 μs at 25 °C as determined by ^{17}O NMR. The rotational correlation time of the monomer (390 ns at 37 °C) is very close to the optimal value that was predicted for high-field contrast agents. Monomer as well as micelles turned out to be very rigid systems with negligible local contributions to the overall rotational dynamics. The binding to human serum albumin (HSA) is significant (K_A=1.2·10^3 M^{-1}) and the relaxivity of the HSA-adduct at 20 MHz is 24.6 $s^{-1}mM^{-1}$.

The factor limiting the relaxivity of the model compound presented in Chapter 4 is the slow exchange between metal bound water and the bulk. Therefore, in Chapter 5 a pyridine-*N*-oxide functionalized DOTA analogue is conjugated to a calix[4]arene and the corresponding Gd-complex was evaluated with respect to its suitability as MRI contrast agent. The compound forms spherical micelles in water with a *cmc* of 35 μM and a radius of 8.2 nm. The relaxivity of these aggregates is 31.2 $s^{-1}mM^{-1}$ at 25 ºC and 20 MHz, which corresponds to a molecular relaxivity of 125 $s^{-1}mM^{-1}$. The high relaxivity is mainly caused by the short average residence time of a water molecule bound to the metal τ_M (72.7 ns) and the size of the micelles. The interaction with bovine serum albumin (BSA) was studied and the observed relaxivity was up to 40.8 $s^{-1}mM^{-1}$ (163.2 $s^{-1}mM^{-1}$ per binding site) at 20 MHz and 37 ºC in the presence of 2.0 mM protein.

The self-aggregation of the potential magnetic resonance angiography agents presented in Chapters 4 and 5 was the inspiration to investigate whether similar systems can be incorporated into the bilayer of liposomes. The calixarene presented in Chapter 6 exhibits two aliphatic chains that were attached to facilitate its incorporation into the bilayer. This

compound forms micelles below a very low *cmc* with a radius of 4.9 nm. The enhanced relaxivity (27.9 $s^{-1}mM^{-1}$ at 20 MHz and 37 °C) of these micelles compared to those formed by the model compound characterised in Chapter 4 can be rationalized by the larger size of the micelles.

For efficient tumor uptake, particles with a radius of about 50 nm are desirable. Liposomes of this size are discribed in this chapter and methods to load them with the amphiphilic calixarene are exploited. When the surfactant is present during the preparation of the lipid film, a significant fraction of bicelles was obtained besides the liposomes. The incorporation into existing liposomes is rather ineffictive whereas the addition of the surfactant prior to the extrusion leads to spherical liposomes and practically quantitative incorporation of 8.8 mol% calixarene. This means that a relatively high Gd loading of the liposomes can be achieved rather easily. The calixarene facilitates water diffusion through the lipid bilayer resulting in an almost three times enhanced relaxivity at 20 MHz and 37 °C compared to common paramagnetic liposomes. Those vesicles are promising canditates for molecular imaging applications of tumours due to their high relaxivity per particle.

Samenvatting

Sinds hun opkomst in synthetische en supramoleculaire chemie hebben calixarenen brede toepassing gevonden in bijvoorbeeld fysica, biologie, en medische wetenschappen. Over het algemeen worden calixarenen gebruikt ofwel als synthetisch platform en/of als hydrofobe mandvormige verbinding voor interactie met apolaire gastmolekulen. In hoofdstuk 1 van dit proefschrift wordt een kort overzicht gegeven van biologische toepassingen van metaal-bindende calixarenen, variërend van kunstmatige ionkanalen, enzym "mimics" en inhibitoren tot medische imaging en radiotherapie.

Deprotonering van imidazoliumzouten tot *N*-heterocyclische carbenen is dikwijls een beslissende reactiestap in moderne katalytische reacties. Die carbenen kunnen ofwel als katalysator dienen in, bijvoorbeeld ‘umpolung’ reacties of als liganden in metaal-gekatalyseerde reacties. Daarom wordt in hoofdstuk 2 de H/D uitwisseling van het C^2 proton van 15 imidazolium gesubstitueerde calix[4]arenen en 11 niet-macrocyclische modelverbindingen in water/metanol 97:3 bij 25 °C onderzocht. De invloed van het tegenion en van substitutie direct op het imidazoliniumion of op het calixareenskelet, dat voorgevormd wordt, werden bestudeerd. Bij vergelijking van de uitwisselingssnelheden werden enige trends zichtbaar: zouten met aromatische groepen, die direct aan de imidazooleenheid zijn gebonden, vertonen een versnelde uitwisseling ten opzichte van hun alkylanaloga. De hoek tussen de imidazolium- en de arylringen is van belang voor de electronische stabilisatie van het intermediaire carbeen. Tegenionen hebben invloed op de kinetische activiteit, maar daarin was geen duidelijke trend te onderscheiden. Zowel anionbinding als solvatatie spelen hierbij mogelijk een rol. Substituenten aan het calixareenskelet in de buurt van de uitwisselbare protonen kunnen de uitwisseling zowel versnellen als vertragen.

Zoals weergegeven in hoofdstuk 1, kunnen calixarenen als kunstmatige kationtransporteur fungeren. Dikwijls is een lage selectiviteit voor een bepaald alkalimetaalion de limiterende factor in dergelijke ionkanaal "mimics". Hoofdstuk 3 handelt over een manier om de natriumselectiviteit van calix[4]arenen te verhogen. Hun interactie met alkalikationen is geëvalueerd door extracties van waterige oplossingen van Li-, Na- en K-pikraten met oplossingen van calixareenamiden in CH_2Cl_2. Electronenzuigende groepen op de "*upper rim*" van het calixareenskelet bleken een negatief effect op de absolute

hoeveelheid metaalionen, die geëxtraheerd wordt, te hebben. Het afgenomen extraherend vermogen gaat vergezeld van een hogere selectiviteit voor natriumkationen.

In medische diagnose met MRI (Magnetic Resonance Imaging) worden Gd^{3+}-houdende verbindingen als contrastreagens gebruikt. Een sterke complexering van het metaalion in grote en starre ligandsystemen is een voorwaarde voor het verkrijgen van een efficiënt contrastreagens. In hoofdstuk 4 wordt de bereiding van een amfifiel conjugaat van een calix[4]areen met vier Gd-DOTA chelaten beschreven. De eigenschappen relevant voor zijn toepassing als MRI contrastreagens werden met NMR, DLS en cryo-TEM onderzocht. De verbinding aggregeert in water en heeft daarin bij 37 °C een kritische micelconcentratie (*cmc*) van 0,21 mM (of 0,84 met betrekking tot Gd). De "relaxivity" van de aggregaten bij 37 °C en 20 MHz (18,3 $s^{-1}mM^{-1}$) is ongeveer twee keer zo groot als die van het monomeer. "Nuclear Magnetic Relaxation Dispersion" (NMRD) profielen laten zien dat de "relaxivity" van het monomeer tot 60 MHz bijna onafhankelijk van de magnetische veldsterkte is. Bij hogere concentraties vertonen de NMRD profielen een maximum bij ongeveer 20 MHz, hetgeen karakteristiek is voor grote moleculaire volumes. De gemiddelde verblijftijd van een watermolecuul in de eerste coordinatiesfeer van Gd^{3+}, zoals bepaald met ^{17}O NMR, is 1,20 μs bij 25 °C. De rotatiecorrelatietijd van het monomeer (390 ns bij 37 °C) is vlakbij de voor hoog-veld contrastreagentia voorspelde optimale waarde, Zowel monomeer als micellen bleken erg starre systemen te zijn met verwaarloosbare lokale bijdragen aan de overall rotatiedynamiek. De binding aan menselijk serumalbumine (HSA) is aanzienlijk (K_A = $1{,}2 \cdot 10^3$ M^{-1}) en de "relaxivity" van het HSA-adduct bij 20 MHz is 24,6 $s^{-1}mM^{-1}$.

De factor, die de "relaxivity" van de in hoofdstuk 4 besproken verbinding limiteert is de langzame uitwisseling van water tussen de metaalion-gecoordineerde toestand en de bulk. Daarom wordt in hoofdstuk 5 een pyridine-*N*-oxide gefunctionaliseerd DOTA-analogon geconjugeerd met een calix[4]areen. Het corresponderende Gd-complex werd geëvalueerd met betrekking tot zijn geschiktheid als MRI contrastreagens. Het complex vormt bolvormige micellen met een *cmc* van 35 μM en een straal van 8,2 nm. De "relaxivity" van deze aggregaten is 31,2 $s^{-1}mM^{-1}$ bij 25 °C en 20 MHz, hetgeen overeenkomt met een moleculaire "relaxivity" van 125 $s^{-1}mM^{-1}$. De hoge "relaxivity" wordt voornamelijk veroorzaakt door de korte verblijftijd van het watermolecuul in de metaal-gebonden toestand (τ_M = 72,7 ns) en door de grootte van de micellen. De interactie met

runder serumalbumine (BSA) werd bestudeerd en de waargenomen "relaxivity" in aanwezigheid van 2,0 mM eiwit was tot 40,8 $s^{-1}mM^{-1}$ (163,2 $s^{-1}mM^{-1}$ per bindings site) bij 37 °C en 20 MHz.

Geïnspireerd door de in hoofdstukken 4 en 5 gepresenteerde zelf-aggregatie van potentiële "magnetic resonance angiography" (MRA) reagentia werd vervolgens onderzocht of soortgelijke systemen ingebouwd kunnen worden in de dubbellaag van liposomen. Het in hoofdstuk 6 gepresenteerde calixareen heeft twee alifatische ketens die werden aangebracht om zijn inbouw in de dubbellaag te vergemakkelijken. Deze verbinding vormt micellen met een straal van 4,9 nm en het systeem heeft een erg lage *cmc*. De hoge "relaxivity" (27,9 $s^{-1}mM^{-1}$ bij 20 MHz en 37 °C) van deze micellen ten opzichte van die van de modelverbinding beschreven in hoofdstuk 4 kan worden toegeschreven aan de grotere omvang van de micellen.

Deeltjes met een straal van ongeveer 50 nm zijn gewenst voor een efficiëntere tumoropname. De bereiding van liposomen van deze grootte is beschreven in dit hoofdstuk, evenals methoden om ze te laden met het amfifiele calixareen. Als deze oppervlakteactieve stof aanwezig is tijdens de bereiding van de lipidefilm, wordt naast de liposomen een aanzienlijke fractie bicellen verkregen. De inbouw van calixaren in reeds bestaande liposomen is tamelijk ineffectief, maar toevoeging ervan voor de extrusie leidt tot sferische liposomen en een vrijwel kwantitatieve inbouw van 8,8% calixareen. Dit betekent dat een relatief hoge Gd-belading van liposomen tamelijk makkelijk bereikt kan worden. Het calixarene bevordert de diffusie van water door de lipidedubbellaag, hetgeen resulteert in een verhoging van de "relaxivity" bij 20 MHz en 37 °C met bijna een factor 3 ten opzichte van die van de gebruikelijke paramagnetische liposomen. Omdat ze een hoge "relaxivity" per deeltje hebben, zijn deze liposomen veelbelovend voor toepassing in "molecular imaging" van tumoren.

List of Publications

Publications

1. Second-Order Nonlinear Optical Properties of the Ag(111)/Electrolyte Interface in the Presence of Self-Assembled Monolayers Containing Conjugated π-Systems. I. α-Functionalized Terthiophene Films on Ag(111).
   Santos, E.; Schühle, D. T.; Jones, H.; Schmickler, W.
   Langmuir, **2005**, *21*, 6406-6421.

2. Synthesis of 1,2,2a,3-Tetrahydro-1,4,7b-triazacyclopenta[cd]indenes.
   Schmid, S.; Schühle, D.; Steinberger, S.; Xin, Z.; Austel, V.
   Synthesis, **2005**, *18*, 3107-3118.

3. A Short and Convenient Synthesis of 3-Aminomethyl-5-imino-8-nitro-2,3-dihydroimidazo[1,2-a]pyridines.
   Schmid, S.; Schühle, D.; Austel, V.
   Synthesis, **2006**, *12*, 2031-2038.

4. Kinetic Acidity of Supramolecular Imidazolium Salts - Effects of Substituent, Preorientation, and Counterion on H/D Exchange Rates.
   Fahlbusch, T.; Frank, M.; Schatz, J.; Schühle, D. T.
   Journal of Organic Chemistry, **2006**, *71*, 1688-1691.

5. Thiophenes and their Benzo Derivatives: Applications.
   Brendgen, T.; Schatz, J.; Schühle, D. T.
   Comprehensive Heterocyclic Chemistry – III, Volume 3, Chapter 3.12., Eds. Katritzky, A.; Ramsden, Ch.; Scriven, E. F. V.; Taylor, R. J. K.; Jones, G. **2008**, 931-974.

6. Information Transfer in Calix[4]arenes: Influence of Upper Rim Substitution on Alkaline Metal Complexation at the Lower Rim.
Schühle, D. T.; Klimosch, S.; Schatz, J.
Tetrahedron Letters, **2008**, *49*, 5800-5803.

7. Metathesis in Pure Water Mediated by Supramolecular Additives.
Brendgen, T.; Fahlbusch, T.; Frank, M.; Schühle, D. T.; Seßler, M.; Schatz, J.
Advanced Synthesis and Catalysis, **2009**, *351*, 303-307.

8. Calix[4]arenes as Molecular Platforms for MRI Contrast Agents.
Schühle, D. T.; Schatz, J.; Laurent, S.; Vander Elst, L.; Muller, R. N.; Stuart M. C. A.; Peters, J. A.
Chemistry – A European Journal, **2009**, *15*, 3290.

9. Densely packed Gd(III)-chelates with fast water exchange on a calix[4]arene scaffold: a potential MRI contrast agent.
Schühle, D. T.; Polášek, M.; Lukeš, I.; Chauvin, T.; Tóth, E.; Schatz, J.; Hanefeld, U.; Peters, J. A.
Submitted to Dalton Transactions.

10. Biological Applications of Metal Binding Calixarenes.
Schühle, D. T.; Peters, J. A.; Schatz, J.
Invited for publication in Chemical Reviews.

Oral presentations

1. Calix[4]arenes as versatile building blocks in the design of MRI contrast agents
   Design&Synthesis, Structure&Reactivity and Biomolecular Chemistry, Lunteren, The Netherlands, October 30, 2007.

2. Calixarenes and their use in catalysis, molecular recognition and as MRI contrast agents
   Institute of Inorganic Chemistry, Charles University, Prague, Czech Republic, November 5, 2007.

3. Calixarenes as versatile building blocks in the design of MRI contrast agents with potential high field application
   Meeting COST D38 ("Metal-based systems for molecular imaging") working group "Magnetic Resonance Imaging Probes", Orléans, France, February 29, 2008.

4. Calixarenes as versatile building blocks in the design of MRI contrast agents
   Imagination 2008, Leiden, April 25, 2008.

5. Calixarenes as versatile building blocks in the design of MRI contrast agents
   Molecular Imaging, Magnetic Resonance, and Intermodality Contrast Agent Research, 11th bi-annual conference, Valencia, Spain, May 23, 2008.

6. Calix[4]arene based model compounds towards enhanced MRI contrast agents
   Meeting COST D38 ("Metal-based systems for molecular imaging") working group "Magnetic Resonance Imaging Probes", Delft, February 20, 2009.

7. Calix[4]arene based model compounds towards enhanced MRI contrast agents, Annual workshop COST D38 ("Metal-based systems for molecular imaging"), Warsaw, April 26, 2009.

Posters

1. Novel modular calix[4]arene-based magnetic resonance imaging (MRI) contrast agents
   Schühle, D.; Hanefeld, U.; Peters, J.A.; Schatz, J.
   8th International Conference on Calixarene Chemistry, Prague/Czech Republic, June 25 – 29, 2005.

2. Calix[4]arene als Plattformen für neue hochmolekulare Kontrastmittel für die Kernspintomographie
   Schühle, D.; Hanefeld, U.; Peters, J.A.; Schatz, J.
   ORCHEM 2006, Bad Nauheim/Germany, September 7 – 9, 2006.

3. Towards MRI contrast agents for higher fields
   Schühle, D.; Hanefeld, U.; Schatz, J.; Peters, J.A.
   Imagination 2007, Rotterdam, March 14, 2007.
4. Octreotide carrying liposomes for molecular recognition of somatostatin receptors
   Abou, D.; Schühle, D.; Peters, J.A; Wolterbeek, H.T.; Koning, G.; Krijger, G.
   Imagination 2007, Rotterdam, March 14, 2007.

5. Towards MRI contrast agents for higher fields
   Schühle, D.; Hanefeld, U.; Schatz, J.; Peters, J.A.
   Annual workshop COST D38 ("Metal-based systems for molecular imaging"), Eindhoven, May 4 – 5, 2007.

6. Towards magnetic resonance contrast agents for higher fields
   Schühle, D.; Hanefeld, U.; Schatz, J.; Peters, J.A.
   Annual workshop COST D38 ("Metal-based systems for molecular imaging"), Lisbon, Portugal, April 27 – 29, 2008.

7. Modular Magnetic Resonance Imaging Contrast Agents Based on the Calix[4]arene Core
   Schühle, D.T.; Peters, J.A.
   Design&Synthesis, Structure&Reactivity and Biomolecular Chemistry, Lunteren, The Netherlands, October 20 – 22, 2008.

8. Modular Magnetic Resonance Imaging Contrast Agents Based on the Calix[4]arene Core
   Schühle, D.T.; Peters, J.A.
   Biotechnical Sciences Delft Leiden Congress, Delft, The Netherlands, October 29, 2008.

9. Somatostatin receptor targeted liposomes for MRI/SPECT dual imaging probes
   D. Abou, D.; Schühle, J. A. Peter, H. T. Wolterbeek,
   Meeting COST D38 ("Metal-based systems for molecular imaging") working group "Magnetic Resonance Imaging Probes", Delft , The Netherlands, February 20, 2009.

10. Calix[4]arene Based Model Compounds Towards Enhanced MRI Contrast Agents
    Schühle, D.T.; Djanashvili, K.; Peters, J.A.
    Gratama Workshop 2009, Delft, The Netherlands, September 14 – 15, 2009.

Acknowledgements

At the end of my unforgettable PhD studies, it is time to think back. Having worked in two different groups and countries was a challenge. Here is the place to express my gratitude to all those people who made it possible that I could develop as a scientist and as a person, and who made it a very precious experience to me to do a PhD.

First of all, my heartfelt thanks to my supervisor Joop Peters: Joop, it was a pleasure to work under your guidance and to learn from you. You were essential for this thesis and for a great working atmosphere. Thank you for the time you have invested in me, for your support in business and private matters, your honest feedbacks, your humorous view on everything, your funny emails, for making me do things that are ‘good for my cv’ and for having left many footsteps in my personality. I am proud to have you as a mentor and example.

Thanks are also due to Jürgen Schatz, my promoter and teacher in calixarene chemistry. It was a great time in Ulm where you have given me the scientific basis to start independent research. I would like to thank you for your scientific advices, for having developed the idea for this project and for giving me the opportunity to do a part of my work abroad. And of course, thanks for all the nice time in- and outside the lab.

My promoter Roger Sheldon is gratefully acknowledged for giving me the chance to work in BOC, the funny conversations and remarks and the interesting discussions about my propositions.

Prof. V. Austel and Prof. G. Maas are gratefully acknowledged for having taught me the beauty of organic chemistry.

Thomas, my dear school, university, house and lab mate: together, we have gone through quite some good and challenging times. Thank you for being a loyal friend and support.

I would like to thank all the members of the Institute Organic Chemistry I in Ulm for the good time there. Special thanks go to Christine, Goga, Holger and Stefan for being good colleagues and even better friends. You have made my time in Ulm very precious to me by being there and who you are.

Antonia, thanks for your company from the very first day on in the ‘Ionenlotto’ course.

Kristina, the time we have spent together at the TU and at conferences gave me the chance to learn a lot about science from you. More importantly, you became an indispensable friend and advisor to me. Thank you for all the valuable help in my projects and in the making of this thesis, for the precious discussions about science, life and nonsense and for enriching my life in Delft with your humor and warmth.

It was a pleasure to be a part of BOC thanks to the people who are or have been working there. Thanks to everybody from the 'lab upstairs' for the very pleasant mood in the lab and all the nice coffee breaks. My special thanks go to Mieke van der Kooij and Mieke Jacobs for all their help that was by far not limited to administration. Thanks are due to Prof. van Bekkum for the thorough corrections of my thesis.

Maria, Monica, Frank, Florian, Jeroen, Milos and Thomas C., apart the work, we have spent quite some free time together. You made the evenings with you rush by and my stay in Delft very pleasant. Many thanks also to you, Ulf, for your helpful scientific advices, the funny and informative chats and the introduction into the Dutch culture.

Special thanks go to SAS group for the good time that we had together, inside and outside the E-CAST. Aurélie, Patrick and Job, thanks for your scientific advices and your help with all kinds of measurement and computer problems.

Thanks to all my collaborators: the groups in Prague, Mons and Orléans, Marc from Groningen, and Diane, Bert and Martijn from Delft. Roy, it was great to have your support in the lab during the final stage of this thesis.

The COST D38 family of lanthanide chemists is gratefully acknowledged for the unforgettable meetings with excellent science and very nice people. Carlos Geraldes, it is amazing how you've always made sure that I ended up in good company during all the conference dinners. Your guided city tours were always highlights during the conference.

At the end, I would like to extend my gratitude to those people who did not directly contribute to my scientific achievements. Hebs and Maren, thanks for staying so close despite the geographical distance. My old friends from Hochdorf and surroundings, I am honored how natural it feels to still be a part of you whenever I am at home.

Last but not least, will ich den beiden Menschen danken, die es mir möglich machen, meine Träume zu leben. Mama und Papa, danke für eure bedingungslose Unterstützung und dafür, daß ihr mir nach wie vor das Gefühl gebt, bei euch ‚daheim' zu sein.

Curriculum Vitae

Daniel Schühle was born on August 15, 1978 in Biberach an der Riß (Germany). He obtained his secondary school diploma in 1998 at the Wieland-Gymnasium in the same town and did his military service in the following months. Between 1999 and 2004, he studied chemistry at the University of Ulm (Germany) graduating with the thesis entitled 'Towards ditopic receptors: functionalised calix[4]arenes and their behaviour towards complexation of alkaline metal ions'. This work was performed under supervison of Prof. J. Schatz. For his diploma, he was awarded the Dr. Barbara Mez-Starck award in the year of his graduation. Then, he started his PhD studies at the University of Ulm and spent half a year in the Applied Organic Chemistry and Catalysis group at the Delft University of Technology as a Marie-Curie fellow under supervision of Dr. J. A. Peters. During this stay, he started a collaboration resulting in his second stay in Delft in the Biocatalysis and Organic Chemistry group starting in November 2006 to accomplish his PhD thesis in the field of MRI contrast agents while taking advantage of his calixarene expertise.